Lysophospholipases as Mediators of Bioactive Lipid Metabolism and Signaling

By

James Anthony Wepy

Dissertation

Submitted to the Faculty of the

Graduate School of Vanderbilt University

in partial fulfillment of the requirements

for the degree of

DOCTOR OF PHILOSOPHY

in

Chemistry

January 31, 2019

Nashville, Tennessee

Approved:
Lawrence J. Marnett, Ph.D.
Gary A. Sulikowski, Ph.D.
Brian O. Bachmann, Ph.D.
Alan R. Brash, Ph.D.

DEDICATION

To my loving and supportive family,
whom always stood by me, no matter the distance

ACKNOWLEDGEMENTS

Graduate school has been a challenging and fulfilling experience since starting at Vanderbilt University in 2013, and I owe the inspiration I felt during those challenges and my resulting successes to my mentor, Lawrence J. Marnett. I would first like to thank Larry for his support, encouragement, and patience during my graduate training. Larry has never been discouraging and has always provided all the resources necessary to follow up on my ideas – good and not so good. Larry's support has enabled me to become a confident, successful, and excited scientist, and joining his lab continues to be one of the best decisions I have made.

I would also like to thank my thesis committee, Gary Sulikowski, Brian Bachmann, Alan Brash, and Alex Brown. All of these accomplished scientists have shaped my dissertation and graduate project over the past five years and have guided my professional development. Specifically, Alex Brown was instrumental in my submission of a successful fellowship application, encouraging me through disappointing reviews and offering a positive and optimistic outlook when it would have been far easier to quit. Carol Rouzer has also acted as an honorary committee member to me during my time in Larry's lab, helping to develop my communication skills as a scientist and always being available to lend a red pen. Anne Lara has made graduating from Vanderbilt a realistic goal, always helping to pull some strings and make sure I was able to schedule my committee meetings at the last minute.

I have also been privileged to work with a number of great scientists as colleagues and labmates throughout my time at Vanderbilt. James Galligan has been a second mentor to me, teaching me techniques and how to think, calling me out on my mistakes, and motivating me through the tough stretches of failures during graduate school; but most of all valuing my

scientific opinions and being a great friend. Will Beavers has also been a helpful role model throughout graduate school, offering guidance and advice when I needed help and encouraging me to share a drink when I (and he) needed a break. Michelle Mitchener and Brenda Crews have basically been parents to me while in Larry's lab (even after Michelle graduated), making sure I had what I needed for my experiments and that I was properly registered or scheduling my exams before I missed every deadline. Phil Kingsley, Orrette Wauchope, Michael Goodman, Joseph Manna, Shu Xu, Jeannie Camarillo, Jashim Uddin, and Kebreab Ghebreselasie have also been there for me throughout graduate school, as friends, colleagues, and mentors, and helped to bring out the enjoyable aspects of graduate school over the struggles.

Scientifically, I again would like to thank everyone mentioned, in addition to the Vanderbilt High-Throughput Screening Core Facility, the Vanderbilt Antibody and Protein Resource, the VMC Flow Cytometry Shared Resource, and the Vanderbilt Mass Spectrometry Research Center and Proteomics Core, for all of the collaborations, support, teamwork, and assistance over the past few years. This work could not have been completed without the help of my peers, labmates, and the resources at Vanderbilt University. I would also like to thank my sources of funding, the National Institutes of Health Grants CA089450 and T32-ES007028, the Hancock Jr. Memorial Cancer Center Fund, and the National Institute of General Medical Sciences Fellowship, Ruth L. Kirschstein National Research Service Award (5F31GM120879-02), for making this work possible and for supporting the research of Larry Marnett and the rest of his laboratory.

Outside of the lab, I have had lifelong support from my family. My mother, Christine Wepy, has offered continued inspiration since I was born. She has been behind me every step of the way, teaching the value of diligence and perseverance, but also when to step out of the lab or

the classroom. She taught me to look for reasons to celebrate, and with her support I have been able to achieve plenty of them. My grandparents, Louis and Donna, were just as much my parents and gave me just as much support. When my mom stood behind me, my grandma stood in front of me as a force to be reckoned with. My grandpa taught me the value of being dependable, with advice to make the best of any situation, rides and tire changes in the middle of the night, and a breakfast of champions every morning. My siblings, Alexa and Joey, have been my greatest friends and bandmates. Our music has inspired my work at every step. My Aunt and Godmother Jen has supported me as another parent when I needed guidance, and an older sister when I needed assurance. My Aunt Doris taught me how to act as a functioning adult, with table manners, professionalism, and the proper way to hold a wine glass. My entire family has been there for me throughout my life and never stopped telling me how proud I have been making them.

Finally, the newest member of my family, my wife, Cindy, has been my partner throughout my time in graduate school, and I could not have come this far without her. We have supported each other over the past 5.5 years over 1,104 miles and never once considered giving up. Since the day I met her, she has inspired me to be my best self. She has given me some of the best days of my life, and taught me as much as I have learned over all 21 grades of my education. Throughout our relationship, we have learned a lot from each other – I taught her to value her accomplishments and take breaks when earned, and she taught me to set at least three alarms when I need to get somewhere on time. Being with her has made me a better man, and finally living with her was the encouragement I needed to finish this Dissertation project.

TABLE OF CONTENTS

LIST OF TABLES

LIST OF FIGURES

LIST OF ABBREVIATIONS

2-AG	2-arachidonoylglycerol
AA	arachidonic acid
*a*AA	alkynylarachidonic acid
ABHD	α/β-hydrolase domain
ACN	acetonitrile
AEA	*N*-arachidonoyl ethanolamide
*a*FA	alkynylfatty acid
*a*LA	alkynyllinoleic acid
*a*PA	alkynylpalmitic acid
BSA	bovine serum albumin
CES1	carboxylesterase 1
COX	cyclooxygenase
DKO	double knockout
DMSO	dimethyl sulfoxide
DNA	deoxyribonucleic acid
DTT	dithiothreitol
EC_{50}	effective concentration at 50% maximum response
EDTA	ethylenediaminetetraacetic acid
FA	fatty acid
FAAH	fatty acid amide hydrolase
FBS	fetal bovine serum
GAP-43	growth-associated protein 43

GPCR	G protein-coupled receptor
IC_{50}	inhibitory concentration at 50% maximum response
IP3	inositol 1,4,5-triphosphate
LPA	lysophosphatidic acid
LPC	lysophosphatidylcholine
LPE	lysophosphatidylethanolamine
LPG	lysophosphatidylglycerol
LPI	lysophosphatidylinositol
LPS	lysophosphatidylserine
LYPLA1	lysophospholipase A1
LYPLA2	lysophospholipase A2
LysoPL	lysophospholipids
MAGL	monoacylglycerol lipase
MAPK	mitogen-activated protein kinase
MRM	multiple reaction monitoring
mRNA	micro ribonucleic acid
MS	mass spectrometry
MS/MS	tandem mass spectrometry
NAPE	N-arachidonoylphosphatidylethanolamine
NSAID	non-steroidal anti-inflammatory drugs
PAGE	polyacrylamide gel electrophoresis
PFB	pentafluorobenzyl
PE	phosphatidylethanolamine

PG	prostaglandin
PG-EA	prostaglandin ethanolamine
PG-G	prostaglandin glyceryl ester
PG-SA	prostaglandin serinol amide
PI	phosphatidylinositol
PLA	phospholipase A
PLC	phospholipase C
PLD	phospholipase D
PMSF	phenylmethylsulfonyl fluoride
PTM	post-translational modification
PPT1	palmitoyl protein thioesterase 1
RNA	ribonucleic acid
SDS	sodium dodecyl sulfate
SILAC	stable-isotope labeling of amino acids in cell culture
siRNA	small interfering ribonucleic acid
SRM	selected reaction monitoring
TAMRA	tetramethylrhodamine
WT	wild-type

1

Introduction

1.1 Cyclooxygenase Metabolism of Endocannabinoids

The Endocannabinoid System

Endocannabinoids are bioactive lipids that induce a plethora of physiological effects upon binding to cannabinoid receptors (1-3). Their name is derived from the *Cannabis sativa* plant, extracts of which have been used medicinally for their analgesic and anxiolytic effects since before recorded history (4,5). The pharmacoactive compounds in these extracts, cannabinoids, were first discovered as ligands for the cannabinoid receptors, followed by the endogenous ligands, appropriately termed "endocannabinoids". Although endocannabinoids derive their name from the exogenous cannabinoid receptor ligands, it is actually the cannabis plants that have hijacked the identity of endocannabinoids. Through cultivation by humans, the plants co-evolved to induce pleasant pharmacoactive effects through their natural products that mimic our own endocannabinoid signaling system.

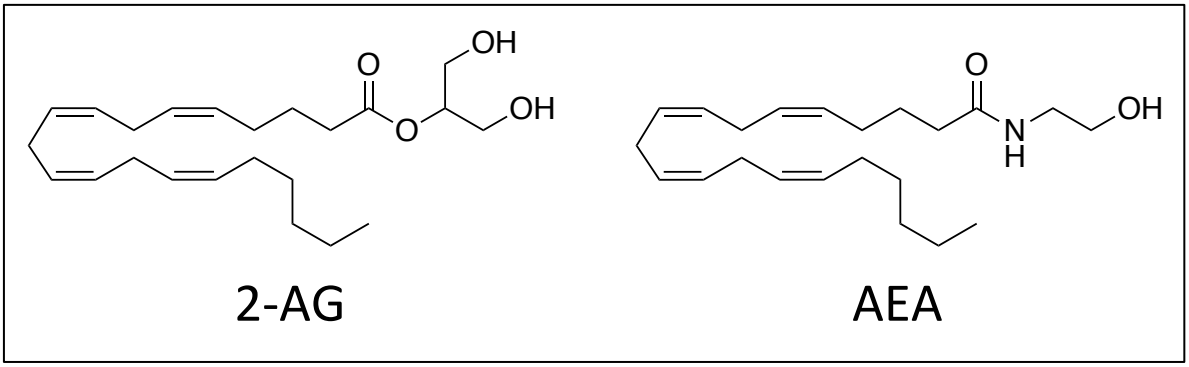

Figure 1.1: Structures of the endocannabinoids, 2-AG and AEA.

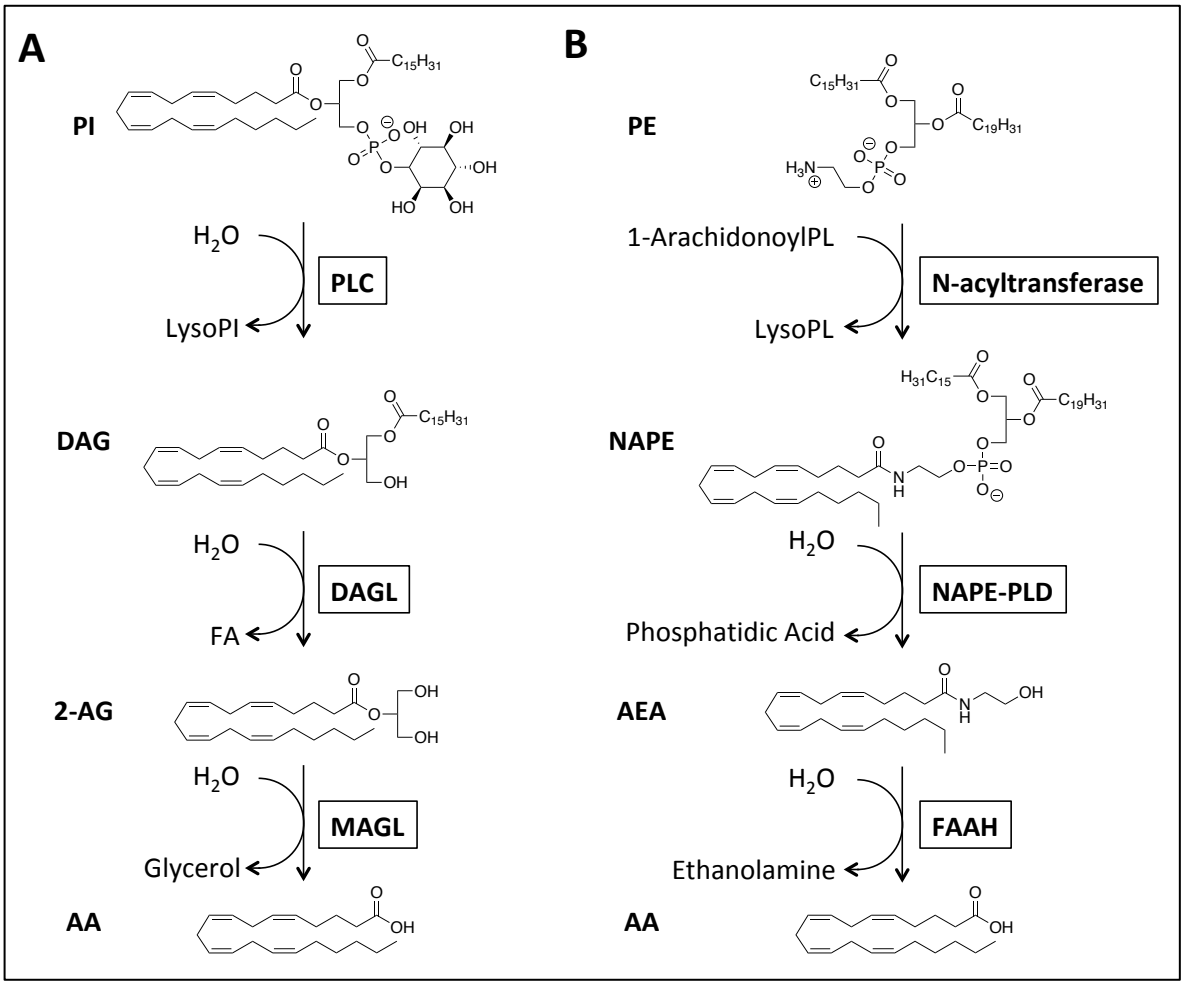

Figure 1.2: Biosynthesis of endocannabinoids (6). (A) Generation of 2-AG from PIs. (B) Generation of AEA from phosphatidylethanolamines.

The most well-characterized endocannabinoids are 2-arachidonoylglycerol (AG) and N-arachidonoylethanolamine (AEA) (Figure 1.1), which are derivatives of the polyunsaturated fatty acid (FA), arachidonic acid (AA). 2-AG and AEA are generated in cells through a variety of biochemical pathways involving multiple hydrolysis reactions of phospholipids from the lipid bilayer (Figure 1.2). In the case of 2-AG, it is thought that phosphatidylinositols (PI) containing AA are the primary source of the endocannabinoid, following hydrolysis by phospholipase C (PLC) and diacylglycerol lipase (6-8). Specifically, upon extracellular stimuli such as a ligand binding to a G protein-coupled receptor (GPCR), PLC is activated and able to metabolize its

lipid substrates. In the case of PI 4,5-bisphosphate, PLC hydrolyzes the glycerol side of the phosphate bond to release important messengers of cell signaling processes, inositol 1,4,5-triphosphate (IP3) and diacylglycerols, which activate the IP3 receptor to mobilize calcium into the cell and recruit protein kinase C, respectively. Diacylglycerols are then hydrolyzed at the sn1-position by diacylglycerol lipase to generate 2-AG (Figure 1.2A). Alternatively, 2-AG can be generated by various other biosynthetic pathways. For example, phospholipase A (PLA) 1 hydrolyzes AA-containing PIs to generate sn2-substituted arachidonoyl lysophophatidylinositols. These are then hydrolyzed by lysophospholipase C at the glycerol side of the phosphate bond to generate 2-AG.

In the case of AEA, generation of the endocannabinoids begins with phosphatidylethanolamines (PE) (6,9-12). First, the Ca^{2+}-dependent N-acyltransferase enzymes transfer AA from phospholipids to the amine of a PE substrate to form N-arachidonoylphosphatidylethanolamine (NAPE). These N-acyltransferases are specific toward sn1-arachidonoyl phosoholipids, which only constitute about 0.5% of brain phospholipids (11). It is thought that the low prevalence of these sn1-arachidonoyl-substituted phospholipids are a contributing factor to low AEA levels in cells. The generation of these sn1-arachidonoyl lipids is a subject of interest because unsaturated fatty acids are usually present at the sn2-position of glycerophosphate headgroups. However, in physiological settings, acyl migration from the sn2- to the sn1-position readily occurs, suggesting a possible source for these unconventional lipid substrates (13). NAPE-phospholipase D (PLD) then hydrolyzes the ethanolamine side of the phosphate bond to generate AEA and a phosphatidic acid (Figure 1.2B). Alternatively, like 2-AG, AEA can be generated from NAPE by various other hydrolysis reactions. For example, phospholipases can first remove the acyl moieties from the glyceryl backbone to yield a

glycerylphospho-N-arachidonoylethanolamine, which is then hydrolyzed by the phosphodiesterase, GDE1, to yield AEA (6).

As mentioned, 2-AG and AEA action is mediated by binding to the cannabinoid receptors, CB1 and CB2, as ligands. These GPCRs are expressed in different tissue, with CB_1 mainly present in the central nervous system, and CB_2 mainly found in immune cells and other peripheral tissue (14,15). Each receptor induces specific effects and has different binding affinities for endocannabinoid ligands (16). AEA has a high affinity for both CB_1 and CB_2, though a higher affinity for CB_1, but acts only as a partial agonist for the receptors (17,18). Interestingly, because of this high affinity and low intrinsic effect on CB_2, AEA actually attenuates the effect of other complete CB_2 agonists, such as 2-AG. In contrast to AEA, 2-AG has a slightly lower binding affinity to the CB_1 and CB_2 receptors, but acts as a complete agonist (19). Both CB_1 and CB_2 receptors are involved in a huge range of physiological effects, including cognition, memory, anxiety, appetite, emesis, analgesia, motor function, sensory, autonomic and neuroendocrine responses, etc., which are ligand- and location-dependent (20).

The physiological effects induced by the endocannabinoids are primarily modulated through cellular metabolism, most commonly by hydrolysis (21,22). Both 2-AG and AEA are relatively unstable in the presence of hydrolyzing enzymes, with 2-AG being primarily hydrolyzed by monoacylglycerol lipase (MAGL) to generate AA and glycerol (23,24), and AEA being primarily hydrolyzed by fatty acid amide hydrolase (FAAH) to generate AA and ethanolamine (25-27). However, multiple other enzymes have been shown to metabolize the endocannabinoids. For example, the α/β hydrolase domain (ABHD) proteins, ABHD6 and ABHD12, have been attributed with a significant portion of 2-AG hydrolysis in cells (28). Furthermore, alternative metabolic pathways exist, namely oxidation, with both

endocannabinoids being rapidly oxidized by a variety of oxygenases in cells (29).

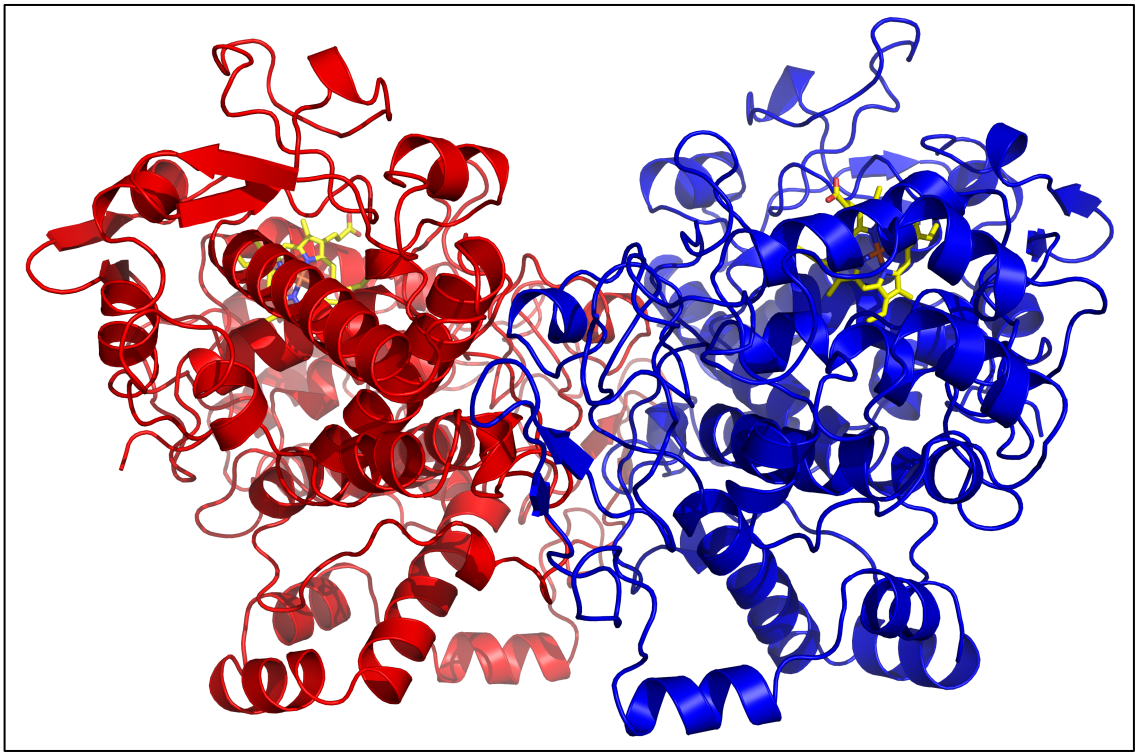

Figure 1.3: Crystal structure of COX-2 heterodimer, with each monomer subunit highlighted in red or blue.

Cyclooxygenase Mechanism and Activity

Cyclooxygenases (COXs), originally named prostaglandin (PG)-endoperoxide synthases, are membrane-embedded proteins responsible for the oxygenation of polyunsaturated FAs, specifically AA (the hydrolysis product of the endocannabinoids), to generate a series of eicosanoid metabolites (30-33). Structurally, COXs are homodimers comprised of two equivalent subunits, as depicted in Figure 1.3, each with three distinct domains.

First, the epidermal growth factor-like domain, located at the dimer interface (residues 34-72), is relatively uncharacterized, though it is thought to stabilize the structure of the protein and potentially allow for communication between each monomer (34,35). Second, at the base of

the protein (residues 73-116) is the membrane-binding domain, acting as an anchor for the protein to embed itself into the membrane. This region also acts as an entrance for its substrates, typically found in a lipid bilayer, to enter the catalytic domain. Finally, the catalytic domain, made up of the remaining residues, contains two distinct active sites that enable the oxygenation of its lipid substrates after binding a heme cofactor (36). This domain contains the peroxidase active site, in which heme iron oxidation to a ferryl-oxo complex enables the activation of Tyr385 by its oxidation to a tyrosyl radical. The tyrosyl radical accesses the second COX active site, where it abstracts the 13-pro(*S*) hydrogen atom from an AA substrate molecule, initiating the cyclooxygenation reaction to form a PG product, specifically PGG_2 (Figure 1.4). The hydroperoxy endoperoxide PGG_2 is then rapidly reduced to the alcohol PGH_2, the source of a range of various PG species (30-32). Interestingly, because the heme cofactor only binds to one of the monomers, COXs are actually functional heterodimers (37-39). The monomer in which the heme is bound is catalytically active, whereas the second monomer acts as an allosteric site to regulate the activity of the active monomer.

The two COX enzymes, COX-1 and COX-2, are 60% identical and share similar rates of oxygenation of AA (33). While the basic function of COX-1 and COX-2 is to generate prostaglandins, key differences between the two enzymes differentiate the functional effects of their activity. COX-1 is constitutively expressed almost ubiquitously throughout all tissues and is thought to maintain homeostatic levels of PGs (40-42). In contrast, COX-2 is induced by a variety of inflammatory stimuli, including lipopolysaccharides, cytokines, and growth factors (43,44).

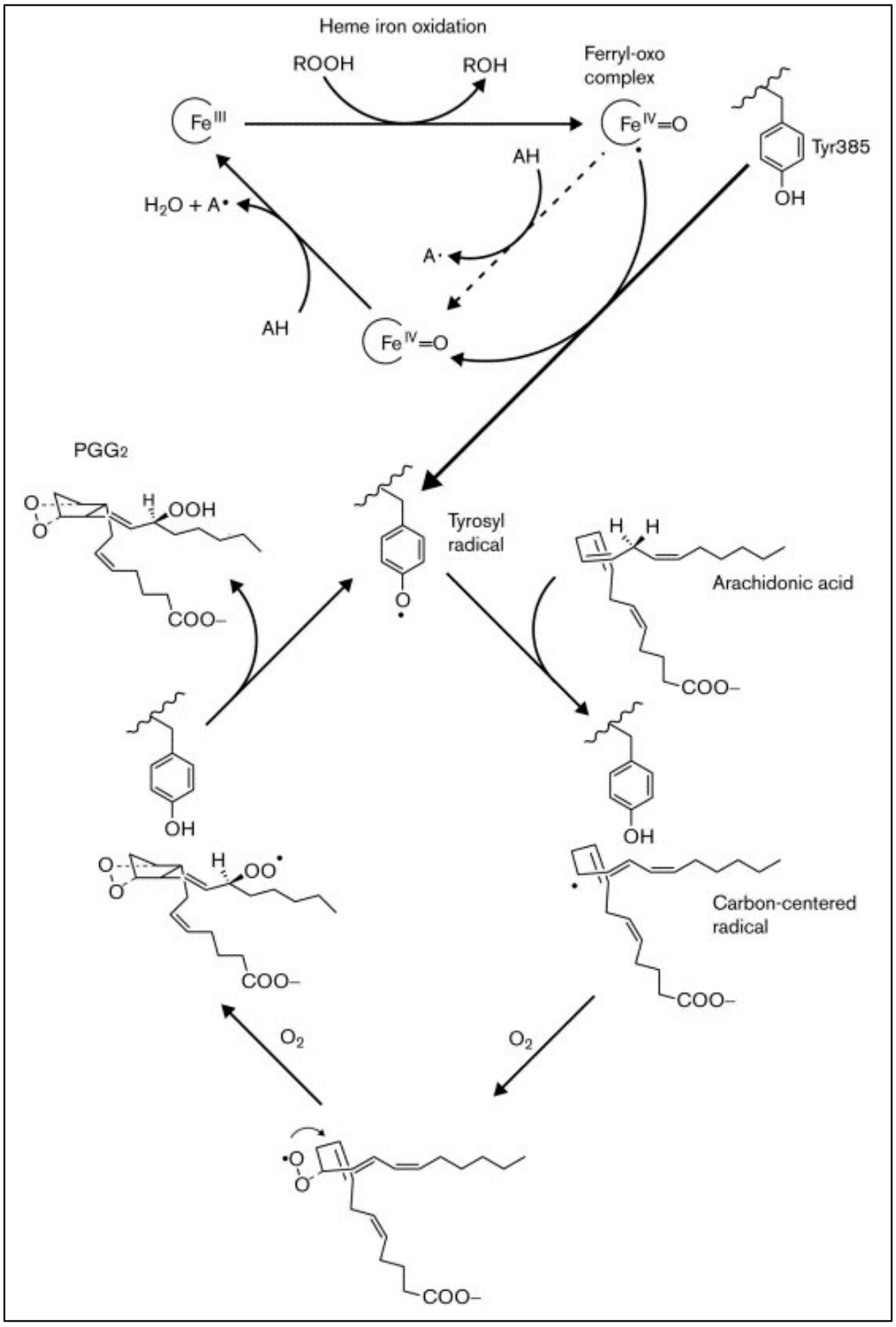

Figure 1.4: Mechanism of COX-2 activation and catalysis. A hydroperoxide oxidizes the heme prosthetic group to a ferryl-oxo derivative that can be reduced in the first step of the peroxidase catalytic cycle or can oxidize Tyr385 to a tyrosyl radical (upper half of figure). The tyrosyl radical then oxidizes the 13-pro(S) hydrogen of arachidonic acid to initiate the cyclooxygenase catalytic cycle. Reprinted with permission from Elsevier (36).

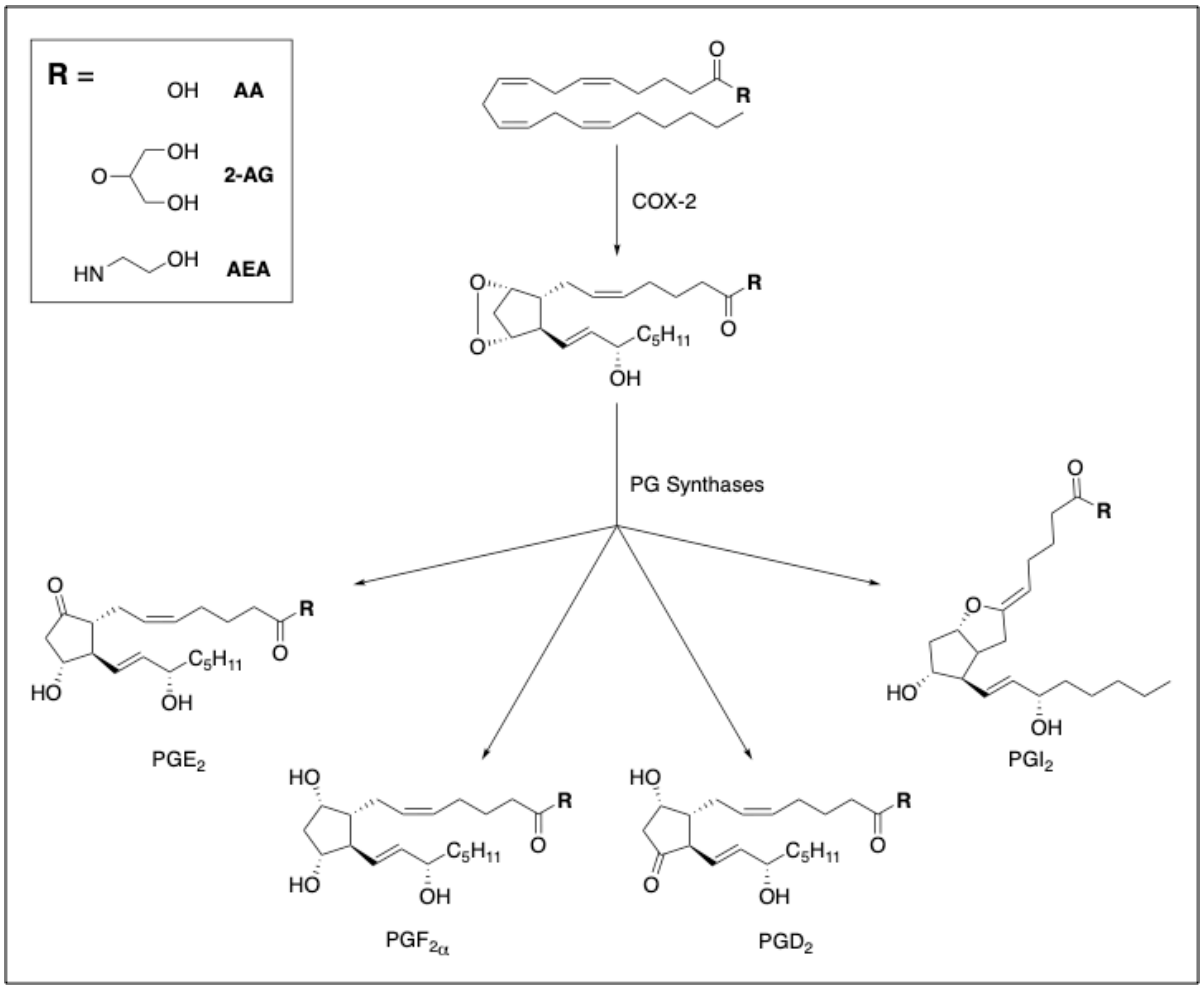

Figure 1.5: Generation of various PG, PG-G, and PG-EA derivatives following COX-2 oxygenation of AA-containing substrates.

In addition to differences in expression, the two enzymes differ in the size of their active sites, with COX-2 having a slightly larger cavity than COX-1 by about 80 $Å^3$ (45). This key difference between the two enzymes allows for COX-2 to display more promiscuous activity, as it is able to fit larger substrates into its active site. Specifically, COX-2 can accommodate the endocannabinoids, 2-AG and AEA, in active conformations, whereas COX-1 displays much lower activity toward the endocannabinoids (46-48). Accordingly, COX-2 is able to oxygenate 2-AG and AEA to form the ester and amide derivatives of PGs, PG glyceryl esters (PG-Gs) and PG ethanolamines (PG-EAs), respectively (Figure 1.5).

Eicosanoid Products of COX-2 Oxygenations

COX-2 oxygenates AA, AEA, and 2-AG to generate PGH_2, PGH_2-EA, and PGH_2-G, respectively, which are then converted to multiple different prostanoid products by a variety of PG synthase enzymes (Figure 1.5) (49). Each PG species acts as a ligand for specific GPCRs to induce a variety of well-characterized, tissue-dependent effects, namely inflammatory responses and nociception (50,51). Furthermore, initial studies have demonstrated multiple biological roles for the PG-EA and PG-G derivatives. PG-EAs, such as PGE_2-EA and $PGF_{2\alpha}$-EA, have been shown to exert similar functions to their free PG counterparts, inducing both pro- and anti-inflammatory effects through GPCR signaling (52-54). PG-Gs have demonstrated some contrasting effects to their free PG counterparts, and have been implicated in mediating calcium mobilization and inflammatory responses (55-58). Interestingly, these effects were not mediated through canonical PG receptors, and, the $P2Y_6$ receptor remains the only known unique receptor of PG-Gs, specifically PGE_2-G, in cells (59). Furthermore, PGE_2-G is a surprisingly potent ligand for the $P2Y_6$ receptor, with an effective concentration at half of the maximum response (EC_{50}) of ~1 pM, whereas PGE_2 displayed no activity toward the receptor. These results suggest PG-Gs can be extremely pharmacoactive ligands with unique biological roles, though low physiological concentrations and poor stability limit the potential of biochemical studies.

COX-2 has been shown to oxygenate AA, AEA, and 2-AG at roughly equivalent rates, but drastically lower levels of AEA accordingly reduce PG-EA generation (46,60). AA is only present at about 10-fold higher levels than 2-AG in macrophages; however, PG levels in these cells exceed those of PG-Gs by roughly 1000-fold (61). One possible explanation for the low physiological concentrations of PG-Gs is modulation of COX-2 activity toward 2-AG by competitive and allosteric modulators (62). AA itself has been shown to significantly reduce

COX-2 activity by binding in its allosteric site to completely inhibit 2-AG oxygenation, as well as more typical competitive mechanisms of inhibition. Recently, non-canonical lipids, such as 13(S)-methylarachidonate, have been demonstrated to positively mediate 2-AG oxygenation by COX-2, suggesting a potential pharmacological strategy of increasing PG-G levels in cells (39). Another possible explanation for low PG-G levels is their hydrolytic instability (55). PG-Gs added exogenously to rat plasma were shown to be completely metabolized within 5 min, which is thought to be due to the presence of various esterases hydrolyzing the glycerol ester to release free PGs (63-65). As part of this dissertation, we have identified and validated a major serine hydrolase responsible for the hydrolysis of PG-Gs across multiple human cancer cells (66).

1.2 PG-G Hydrolysis

PG-G Hydrolytic Instability

Establishing the physiological relevance of PG-Gs in vivo has been a significant challenge due to their enzymatic hydrolysis to PGs (55). PG-Gs are hydrolyzed in vitro by MAGL (63,67), ABHD6 (68), ABHD12 (68), carboxylesterase-1 (CES1), and palmitoyl-protein thioesterase-1 (PPT1) (69). CES1 and PPT1 have been shown to metabolize PG-Gs in human THP1 cells (69). CES1, a xenobiotic-metabolizing enzyme that is expressed in high amounts in the liver, hydrolyzes a wide array of substrates, ranging from ester and amide-containing xenobiotics (70), to long chain FA esters and thioesters (71), and cholesteryl esters from lipid droplets (71,72). Similarly, PPT1, a lysosomal hydrolase, has multiple substrates; it appears predominantly responsible for the depalmitoylation of a number of proteins as well as hydrolysis

of palmitoyl-CoA and palmitoyl thioglucoside (73,74). Consistent with the wide substrate specificity exhibited by CES1 and PPT1, both enzymes are capable of hydrolyzing PG-Gs and 2-AG (65,69,75). In THP1 monocytes, the hydrolysis of 2-AG is almost entirely attributed to CES1, with minor involvement of PPT1 (65,69,75). Kinetic analysis of both enzymes showed greater catalytic turnover for 2-AG than for PG-Gs, with both enzymes exhibiting almost twofold more activity for 2-AG than for PG-Gs (65). As none of these enzymes robustly hydrolyzed PG-Gs preferentially over endocannabinoids and other substrates, we aimed to identify the major PG-G hydrolase responsible for their rapid metabolism.

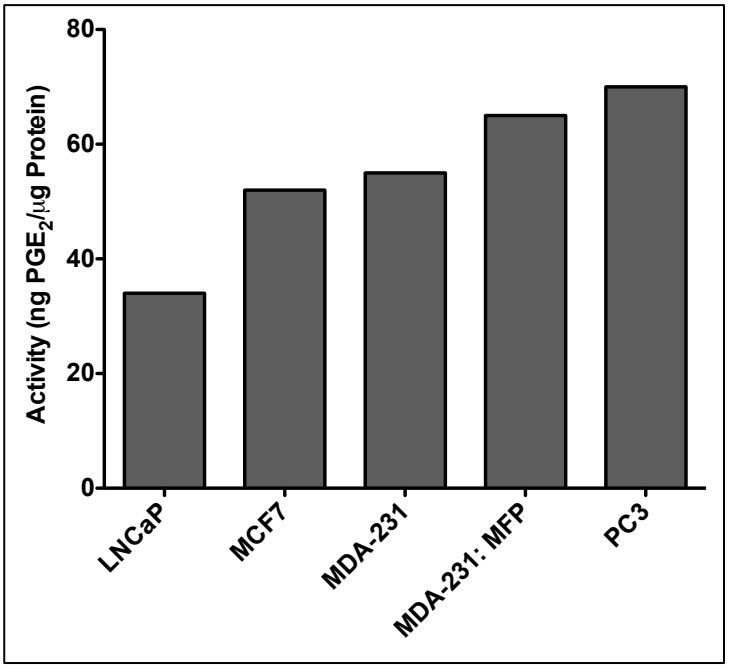

Figure 1.6: PGE_2-G hydrolase activities in human cancer cells. Hydrolytic activity was determined by quantifying hydrolyzed PGE_2 following exogenous addition of PGE_2-G to various cell lysates containing equivalent amounts of protein.

Identification of LYPLA2 as a PGE_2-G Hydrolase in Cancer Cells

Nomura et al. recently profiled serine hydrolases in a series of human cancer cell lines

(76,77). The serine hydrolase proteome was enriched by covalently labeling the enzymes with fluorophosphonate molecules bound to biotin followed by avidin chromatography. The purified serine hydrolases were identified by multidimensional liquid chromatography mass spectrometry-based proteomic analysis of tryptic digests. Spectral counting, revealed the relative levels of serine hydrolase activities across a number of aggressive and non-aggressive cancer cell types (76,77). Utilizing the cancer cell types investigated in these serine hydrolase inventories, PGE_2-G hydrolysis by the cytosolic fractions of two breast cancer cell lines, MDA-MB-231 and MCF7, and two prostate cancer cell lines, PC3 and LNCaP was quantified (Figure 1.6) (66). These studies demonstrate that LNCaP cells exhibited the lowest hydrolytic activity, while PC3 cells displayed the highest rate of PGE_2-G hydrolysis. By comparing the PGE_2-G hydrolytic activity across the cell lines to published inventories of over 60 cytosolic serine hydrolases and their levels of expression in each cell line (76,77), one enzyme, LYPLA2, correlated across all data sets and was identified as a potential PG-G hydrolase.

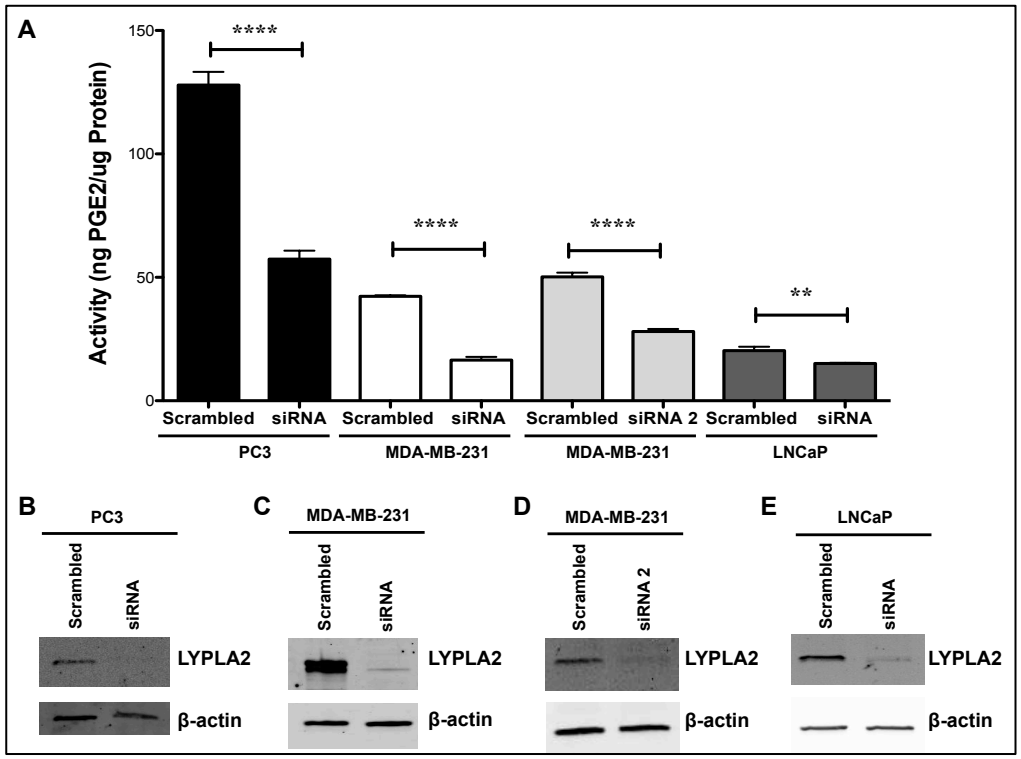

Figure 1.7: LYPLA2 siRNA knockdown in PC3, MDA-MB-231, and LNCaP cells. (A) PGE_2-G hydrolytic activity of cytosol obtained from PC3, MDA-MB-231, and LNCaP control (scrambled) or LYPLA2-deficient (siRNA) cells. Western blot analysis of LYPLA2 in control (scrambled) and LYPLA2-depleted (siRNA) PC3 (B), MDA-MB-231 (C, D), or LNCaP (E) cells. β-actin Western blotting verified equaling protein loading (5 μg per lane). Data are presented as the mean ± S.D. of triplicate analyses. ** indicates $p < 0.01$. **** indicates $p < 0.001$.

To validate the role LYPLA2 plays in PG-G hydrolysis, multiple experimental approaches were used to investigate LYPLA2-dependent modulation of cellular PG-G levels (66). For example, siRNA knockdown of LYPLA2 expression across a wide range of cancer cell lines caused significant decreases in the levels of PG-G hydrolytic compared to control cells (Figure 1.7). Furthermore, cDNA overexpression of LYPLA2 in HEK293 cells, which do not express the protein normally, caused elevated PG-G hydrolytic activity compared to fractions from untransfected cells (Figure 1.8). These experiments confirm the serine hydrolase, LYPLA2, as a major PG-G hydrolytic enzyme in human cells.

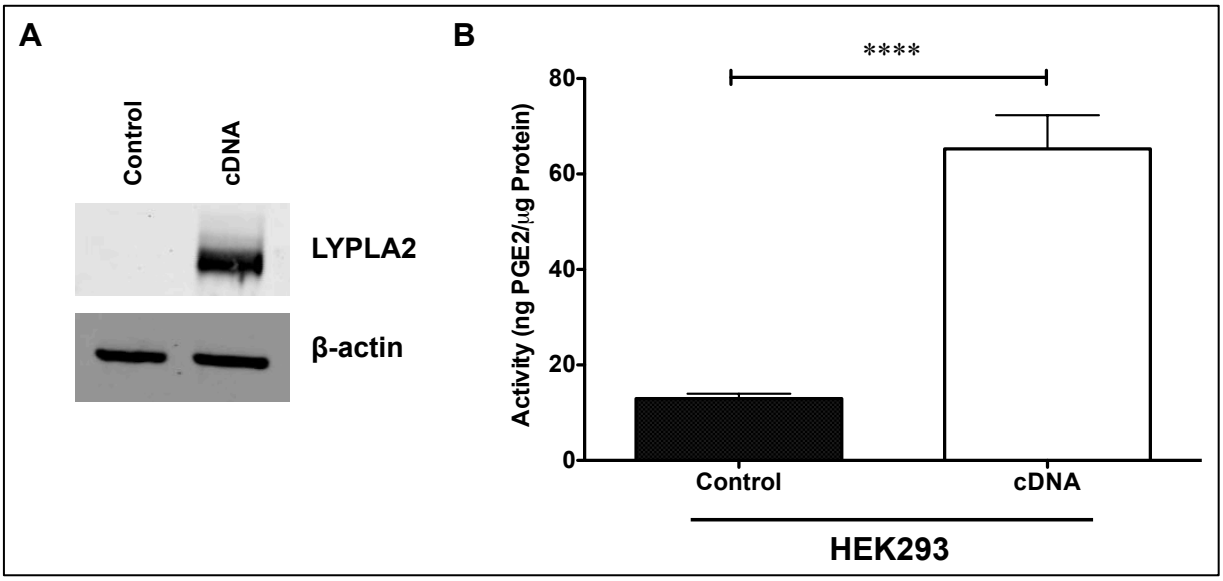

Figure 1.8: LYPLA2 overexpression in HEK293. (A) Western blot analysis of LYPLA2 in control HEK293 cells (control) and LYPLA2-overexpressing HEK293 cells (cDNA). β-actin Western blotting verified equaling protein loading (5 μg per lane). (B) PGE_2-G hydrolytic activity of cytosol obtained from HEK293 (control) or LYPLA2-overexpressing (cDNA) cells. Data are presented as the mean ± S.D. of n = 6 analyses. **** indicates $p < 0.001$ by t-test.

1.3 Serine Hydrolases

Serine Hydrolase Family

Serine hydrolases are one of the most prominent families of enzyme with over 200 identified examples. They are thought to comprise more than 1% of the human proteome (78,79). Serine hydrolases are responsible for the hydrolysis reaction of an enormous range of ester, thioester, amide, phosphate, and sulfonate bonds from peptides, protein, lipids, deoxyribonucleic acid (DNA), ribonucleic acid (RNA), and other small molecule substrates. The active site Ser of these enzymes is activated by a series of amino acids in a charge relay system, generally known as a catalytic triad (Figure 1.9). This system involves the particular orientation of Ser in proximity to a hydrogen bond acceptor, most commonly His, to increase its nucleophilicity.

Additionally, the His is situated near an Asp to further promote a hydrogen bond forming between the His and Ser, though this is not always necessary and multiple serine hydrolases with catalytic diads exist (80).

Serine hydrolases are organized into multiple superfamilies depending on their substrates, but can more simply be categorized into two groups: proteases, which degrade proteins by hydrolyzing peptide bonds; and metabolic serine hydrolases, which hydrolyze all of the smaller molecules. The majority of the metabolic serine hydrolases are folded similarly, with a highly conserved α/β fold involving 8 central β-strands connected by 6 surrounding α helices. This specific fold positions the catalytic triad in an active conformation, which is conserved within the superfamily (81,82).

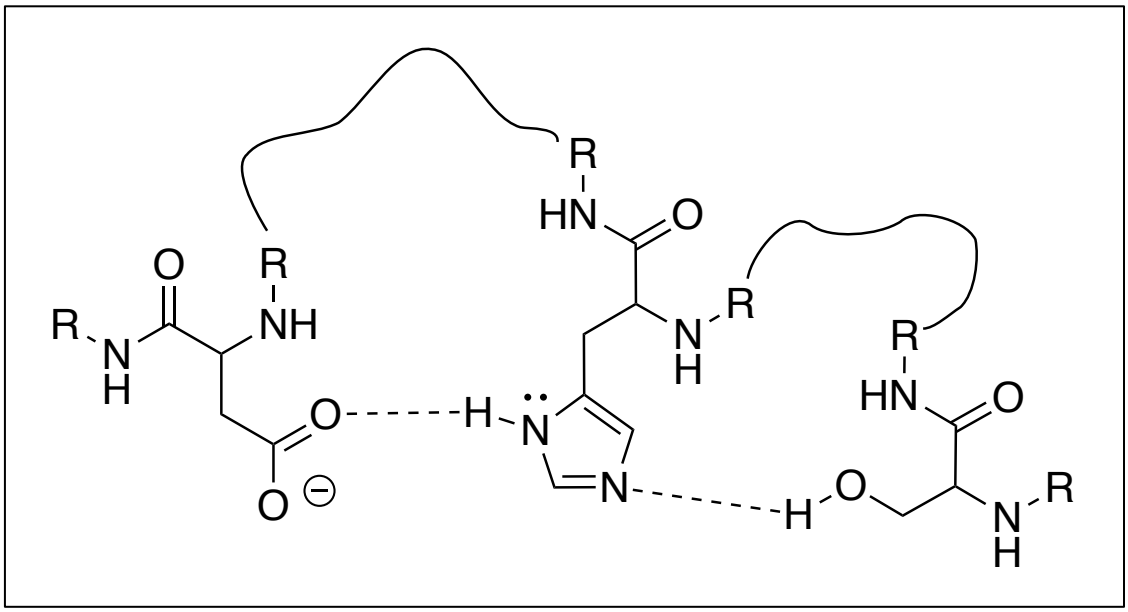

Figure 1.9: Catalytic triad (Asp-His-Ser) in the active site of serine hydrolase enzymes.

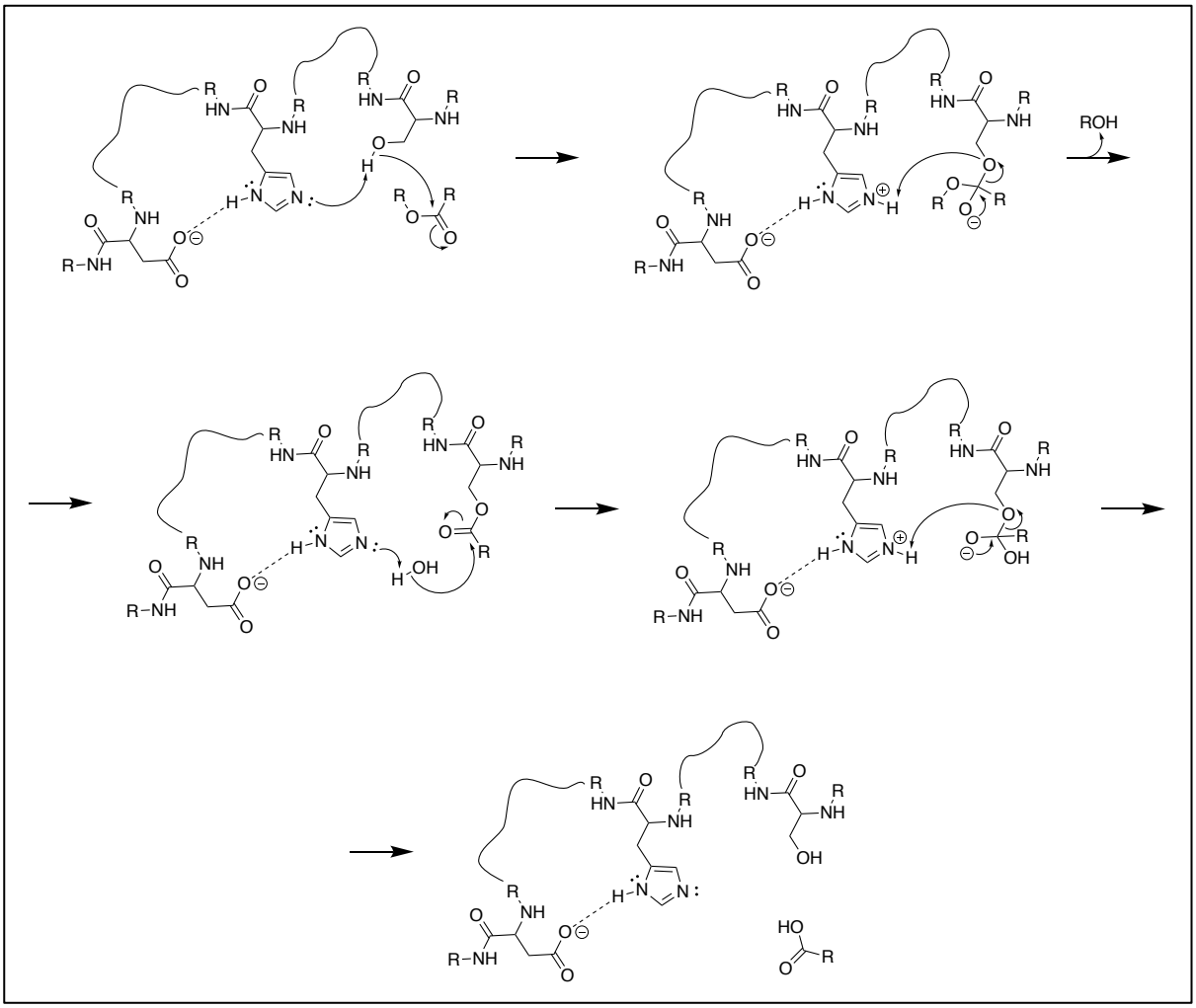

Figure 1.10: Mechanism of serine hydrolases demonstrating the role of the charge relay system in promoting nucleophilic attack by the active Ser. Asp-His-Ser imparts a partial negative charge on the active Ser, allowing for the formation of a tetrahedral intermediate with an ester (shown above), thioester, amide, etc. Following release of a leaving group, in this case an alcohol, water can displace the serine to generate a carboxylic acid product.

Mechanism of the Catalytic Triad

The specific placement of the catalytic triad in the active site of serine hydrolase enzymes, as shown in Figure 1.9, enables the protein to generate a strong nucleophile that is otherwise unavailable from the 20 natural amino acids. The position of each amino acid in the catalytic triad allows for proton transfer from the active serine to the proximal His as the nucleophilic hydroxyl group interacts with an electrophilic substrate (Figure 1.10). Depending on

the serine hydrolase, the substrate can be an ester, thioester, amide, etc., and interaction with the nucleophilic Ser generates a tetrahedral intermediate covalently bound to the enzyme. Generally, the resulting negative charge formed is stabilized by partially positively charged backbone amides in the active site, called the oxyanion hole (83). Following acid catalysis, the alcohol/thiol/amine is released as a leaving group, leaving an acylated active serine and a basic His. The His can then activate a nearby water molecule to react with the electrophilic acyl serine to reform a tetrahedral intermediate. Again, acid catalysis induces the breakdown of the tetrahedral intermediate, releasing a hydrolyzed carboxylic acid and restoring the charges of the active Ser and His (84,85).

1.4 Lipid Metabolism

The Lands Cycle and Lipid Metabolism

The contents of cells are contained by the cell membrane, composed of a lipid bilayer (86-88). This fluid barrier is made up of amphiphilic phospholipids with hydrophilic phosphate headgroups and lipophilic acyl tails. The membrane is arranged in two layers of these phospholipids, resulting in a sheet of liquid hydrocarbons surrounded by two polar borders that prevent the passage of small molecules into or out of the cell. In addition to a barrier, the lipid bilayer acts as a medium for membrane-bound proteins to organize in specific locations and elicit a variety of vital functions for the cell (89-92). Membrane protein functions include intercellular communication, small molecule transport, enzymatic chemical reactions, and maintenance of membrane structure and lipid composition. The structure, fluidity, and permeability of the

membrane are all determined by its lipid composition (93-99).

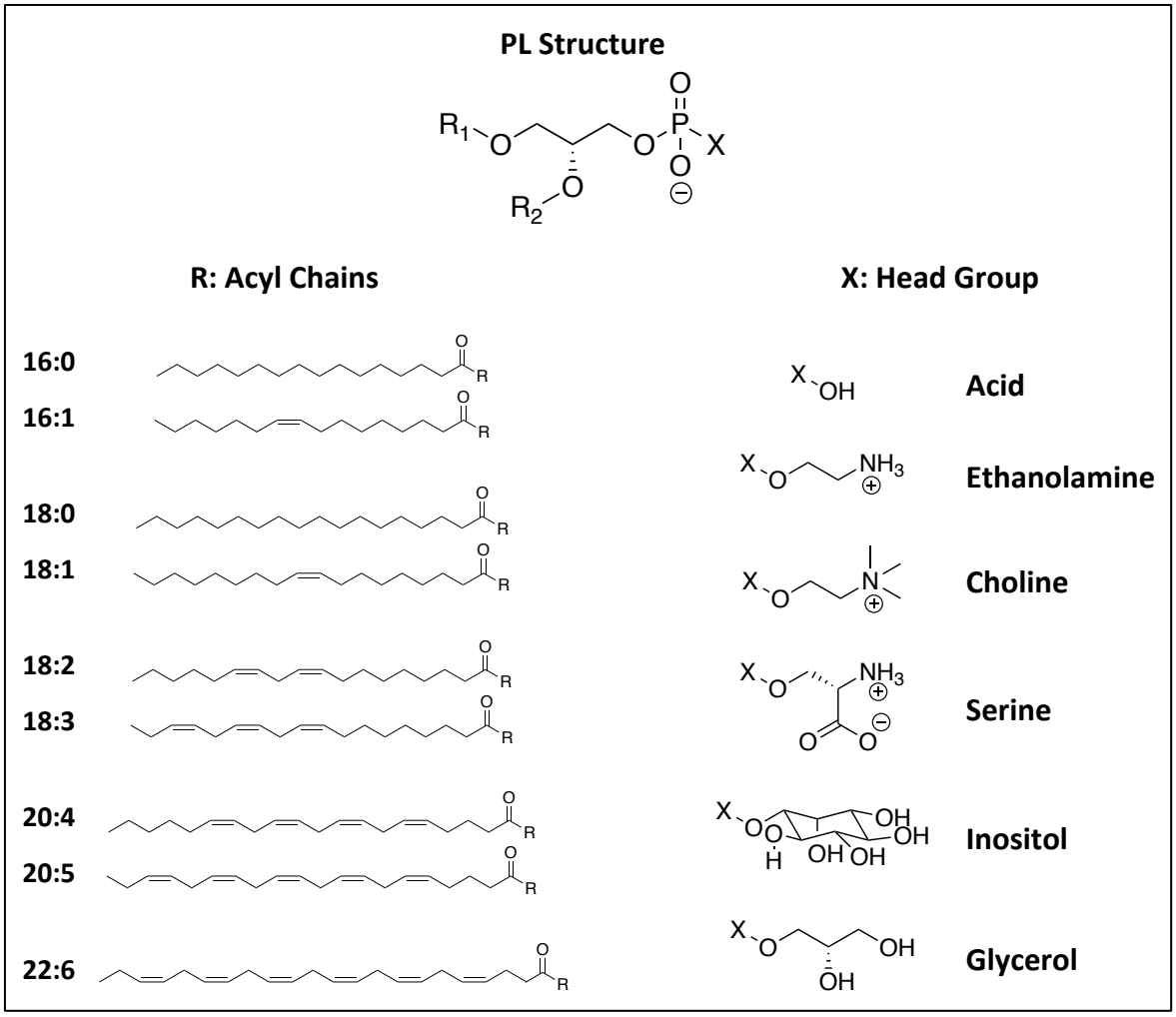

Figure 1.11: Phospholipid structure and nomenclature. Most common acyl chains, from 16-22 carbons and 0-6 degrees of unsaturation, and phosphate headgroups, including, phosphatidic acids, cholines, ethanolamines, glycerols, inositols, and serines, are shown as substituents of a general glycerophosphate backbone.

Phospholipids are comprised of three main components: lipophilic acyl chains of multiple lengths and degrees of unsaturation, a glycerophosphate backbone, and a polar headgroup with a variety of functionalities, most commonly unsubstituted phosphatidic acid, choline, ethanolamine, glycerol, inositol, and serine (Figure 1.11). The sn1 position (R_1 in Figure 1.11) is

generally substituted with a saturated acyl chain, while the sn2 position (R_2 in Figure 1.8) is generally substituted with an unsaturated acyl chain (100,101). Each of these components can be removed and replaced to restructure the composition of phospholipids in the lipid membrane. This is done by a variety of enzymes in a process called the Lands Cycle (Figure 1.12) (102-105).

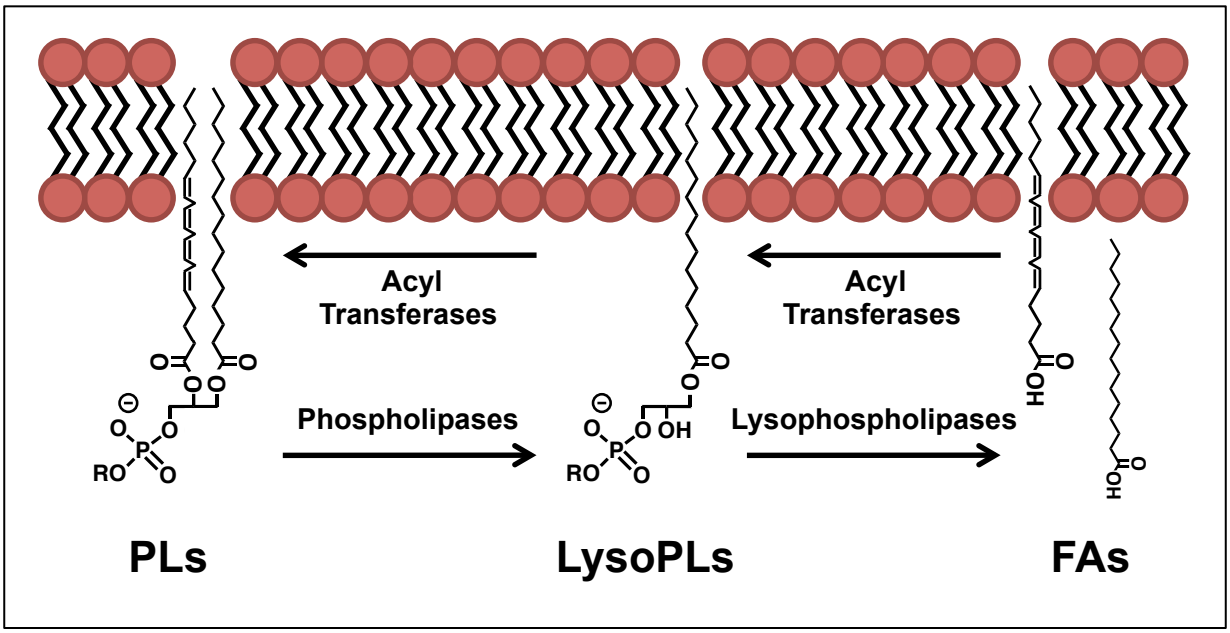

Figure 1.12: Phospholipid metabolism in the Lands Cycle. FAs of phospholipids and LysoPLs are liberated by phospholipases and lysophospholipases, respectively. LysoPLs are also precursors of a different class of lipid mediators including platelet-activating factors, LPAs, and endocannabinoids. Alternatively, phospholipids and LysoPLs are generated by acyltransferases in the presence of acyl-CoA and LysoPLs or glycerophosphates, respectively.

In this process, acyltransferase enzymes append FAs to glycerophosphate substrates to generate lysophospholipids (LysoPL), with "lyso" referring to the lipid lacking one acyl chain. Other acyltransferases can then add a second FA to the LysoPL to generate a diacylglycerol or phospholipid. Additionally, transacylase enzymes can transfer acyl chains directly from one phospholipid to another, or to alternative positions such as the amine of ethanolamines, as in the

case of NAPE synthesis (10,106,107). Alternatively, phospholipids are hydrolyzed by a variety of phospholipases, as described in Figure 1.13, to remove specific acyl chains and phosphate headgroups. Products of these reactions include FAs and LysoPLs, in the case of PLAs, PLA1 and PLA2; diacylglycerol and a substituted phosphate group, in the case of PLC; and a diacylglycerophosphate and an alcohol in the case of PLD. Additionally, diacylglycerols can be further hydrolyzed to FAs and LysoPLs by DAGL, and LysoPLs can be further hydrolyzed to FAs and glycerophosphates by the lysophospholipase enzymes, lysophospholipase A1 (LYPLA1) and lysophospholipase A2 (LYPLA2).

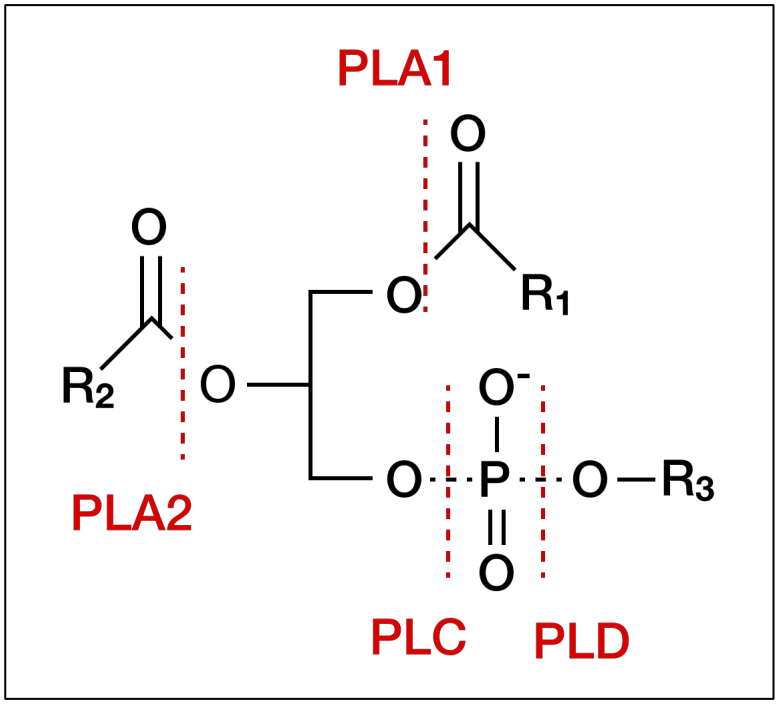

Figure 1.13: Specific activities of PLA, PLC, and PLD enzymes, with sites of hydrolysis for each designated by a red, dotted line.

LysoPLs in Membrane Structure

LysoPLs are formed from the hydrolysis of phospholipids, as described above. LysoPLs play an especially critical role in modulating the structure, shape, and fluidity of cell membranes (108-110). Their smaller size results in curvature stress in the membrane and destabilization of the bilayer, as depicted in Figure 1.14 (111-116). In contrast to a fully substituted phospholipid, whose lipophilic region is roughly the same size as its hydrophilic region to create a planar monolayer, FA and LysoPL shapes are irregular (Figure 1.14A). In the case of LysoPLs, the phosphate headgroup is larger than the size of the acyl chain, so high concentrations of LysoPLs cause positive curvature in the membrane. In the case of FAs, the opposite effect is seen where the size of the acyl chain overtakes the size of the polar carboxylic acid to cause negative curvature (Figure 1.14B). Normally, these properties are utilized to enable vesicular fusion to the membrane, as depicted in Figure 1.14C. As a result of elevated LysoPL species in cells, ion permeability through the membrane increases, bilayer hydration increases, membrane channel function is altered, and susceptibility to cell lysis is increased (117-120). While this is generally due to purposeful increases in PLA2 activity, uncontrolled increases in LysoPLs can be detrimental to cell health. In fact, certain parasites, such as *Schistosoma mansoni*, and bacteria, such as *Helicobacter pylori*, take advantage of this effect by releasing high concentrations of LysoPLs to disrupt host membranes and neutralize attacking neutrophils (121,122).

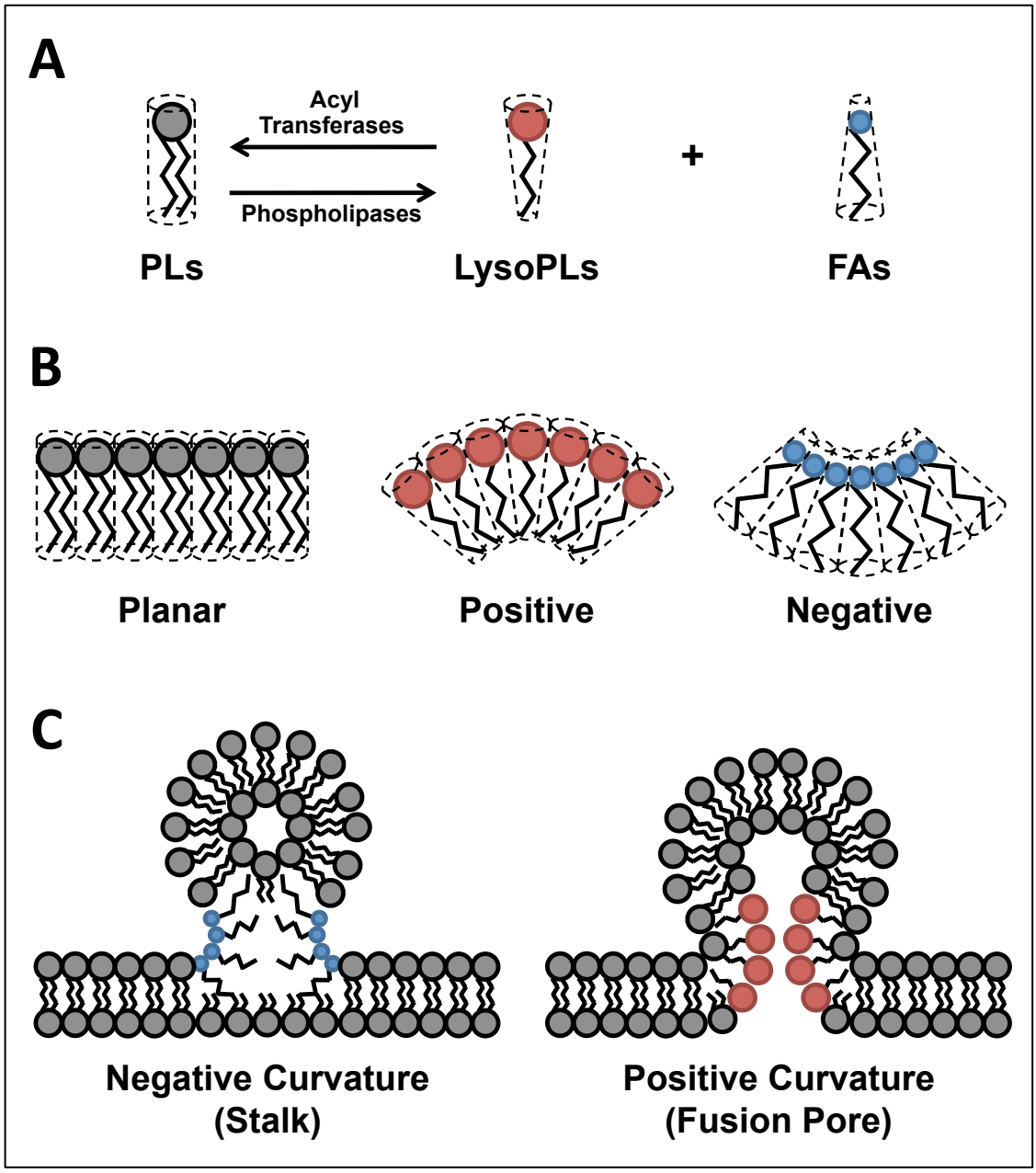

Figure 1.14: (A) Phospholipids in which the polar headgroup and the FA chains have similar sizes are thought to adopt a cylindrical shape in membranes (filled circles symbolize the polar headgroups, wavy lines represent the FA chains). Phospholipases convert phospholipids into conical FAs and inverted conical LysoPL products. (B) In an aqueous environment, cylindrical lipids produce stable planar monolayers, whereas inverted-conical (LysoPLs) and conical (FAs) lipids produce monolayers with positive or negative curvature, respectively. (C) The two steps of membrane fusion: left, during stalk formation, two adjoining membranes merge their outer leaflets producing a negatively curved monolayer region (blue) that is facilitated by cone-shaped lipids such as FAs; right, widening of the stalk generates a fusion pore that is lined by a positively curved monolayer region (red), which is favored by inverted cone-shaped lipids, such LysoPLs. Adapted from Piomelli et al., 2007 (116).

LysoPLs	Target Cells	Pharmacological Responses	Receptor
LPS	Peritoneal mast cell (rodent)	Enhancement of degranulation	?
	PC12	Enhancement of NGF-induced differentiation	?
	T lymphocyte	Growth inhibition	?
	L2071 (fibroblast)	Migration	?
	U87 (glioma)	Migration	?
	Macrophage	Engulfment	G2A
	Myotube 3T3-L1 (adipocyte)	Glucose uptake	?
	?	Depression, hypothermia (in vivo)	?
LPG	OVCAR-3 (ovarian cancer)	Intracellular calcium increase	?
	HUVEC	ERK phospholilation, migration, tube formation	?
	Natural killer cell	ERK phospholilation, migration	?
	Neutrophil, monocyte	Inhibition of chemokine-induced migration and IL-1β production	?
		intracellular calcium increase	?
LPE	PC12	Activation of MAPK, neuronal differentiation	?
	SK-OV3 (ovarian cancer)	Intracellular calcium increase, migration, invasion	?
	MDA-MB-231 (breast cancer)	Intracellular calcium increase	LPA_1CD97
LPI	Pancreatic islet	Insulin release	?
	Hippocampal neuron	Prevention of ischemia-induced cell death (in vivo)	?
	Ras-transformed thyroid epithelial cell	Proliferation	GPR55
	neuroblastoma cell	Activation of MAPK, neuronal differentiation	GPR55
	PC12	Intracellular calcium increase, exocytosis	?
	Endothelial cell	Wound healing	?

Table 1.1: Receptor-mediated action of LPSs, LPGs, LPEs, and LPIs. Modified from Makide, et al. (123)

LysoPLs in Cell Signaling

LysoPLs were originally thought to be a relatively minor lipid species in cells – just a byproduct of phospholipid hydrolysis (124). Even after realizing levels of LysoPLs were higher than previously thought in the mid-60's, the idea that LysoPLs could act as signaling molecules was not seriously considered (125). It was not until the late 80's – early 90's that the biological activity of LysoPLs, specifically lysophosphatidic acids (LPA), as signaling molecules had been established (126-130). Even still, biological effects of LPAs remain the most extensively

characterized. Numerous GPCRs across multiple cell lines have been attributed to LPA action through ligand-receptor interactions (131-133). Depending on the receptor and cell type, LPAs have been shown to induce a wide range of physiological responses, such as platelet aggregation, calcium mobilization, phagocyte activation, and vascular smooth muscle cell proliferation (134-136).

However, multiple other classes of LysoPLs (Figure 1.8), including lysophosphatidylcholines (LPC), lysophosphatidylethanolamines (LPE), lysophosphatidylglycerols (LPG), lysophosphatidylinositols (LPI), and lysophosphatidylserines (LPS), have also been shown to induce a variety of effects in cells and animals (119,135,137-148). While these effects are usually stimulated through ligand interactions with mostly uncharacterized GPCRs (Table 1.1) (123), certain LysoPLs can induce changes in protein function and conformation by binding directly to the protein or altering the membrane structure surrounding membrane-bound proteins (149-152). For example, LPCs' high physiological concentrations (~200 μM in human plasma) call into question a receptor agonist role in some circumstances, and accruing evidence supports the hypothesis they can elicit effects by altering membrane properties or interacting directly with proteins in ways other than saturable binding to a specific site (153-156). Specifically, LPCs have been shown to directly promote Ras-mediated activation of the mitogen-activated protein kinase (MAPK) signaling pathway by a mechanism that does not involve characterized LysoPL receptors (151). In contrast, LPEs, LPGs, and LPIs have also been shown to activate this signaling pathway, but they do so via respective receptor interactions (139,142,146,157,158).

In any case, LysoPLs are well established as important signaling molecules in cells, adding significance to the metabolic pathways that modulate their levels and resulting effects in

cells. LYPLA1- and LYPLA2-mediated hydrolysis of these lipids is likely a major mechanism of regulation of LysoPL signaling; however, little is known about how these enzymes act to maintain lipid homeostasis in cells. As part of this work, we have characterized the cellular roles of LYPLA in lipid metabolism and identified physiological processes regulated by their activity (159).

1.5 Protein Acylation

Effects of Protein Palmitoylation

Acyltransferases covalently attach FAs to a nucleophilic substrate. For example, acyltransferases are used in the Lands Cycle to restructure phospholipids, as described above. However, acyltransferases can also covalently attach FAs to protein substrates (160-163). Protein acylation is an abundant post-translational modification (PTM), especially in eukaryotic cells where it is estimated that 10-15% of proteins undergo palmitoylation (164). Notably, protein palmitoylation is estimated to be the fifth most common PTM in eukaryotic cells (165). This prevalent process involves the appendage of a palmitate functional group to the free side chain of an amino acid, specifically the thiol of Cys (S-palmitoylation), the amine of lysine or the N-terminus (N-palmitoylation), or the alcohol of Ser or Thr (O-Palmitoylation) (166,167). S-palmitoylation is the most common type of these acylation reactions. It is a dynamic process involving the addition of palmitate to Cys to potentially alter protein localization, structure, and activity (160,166,168).

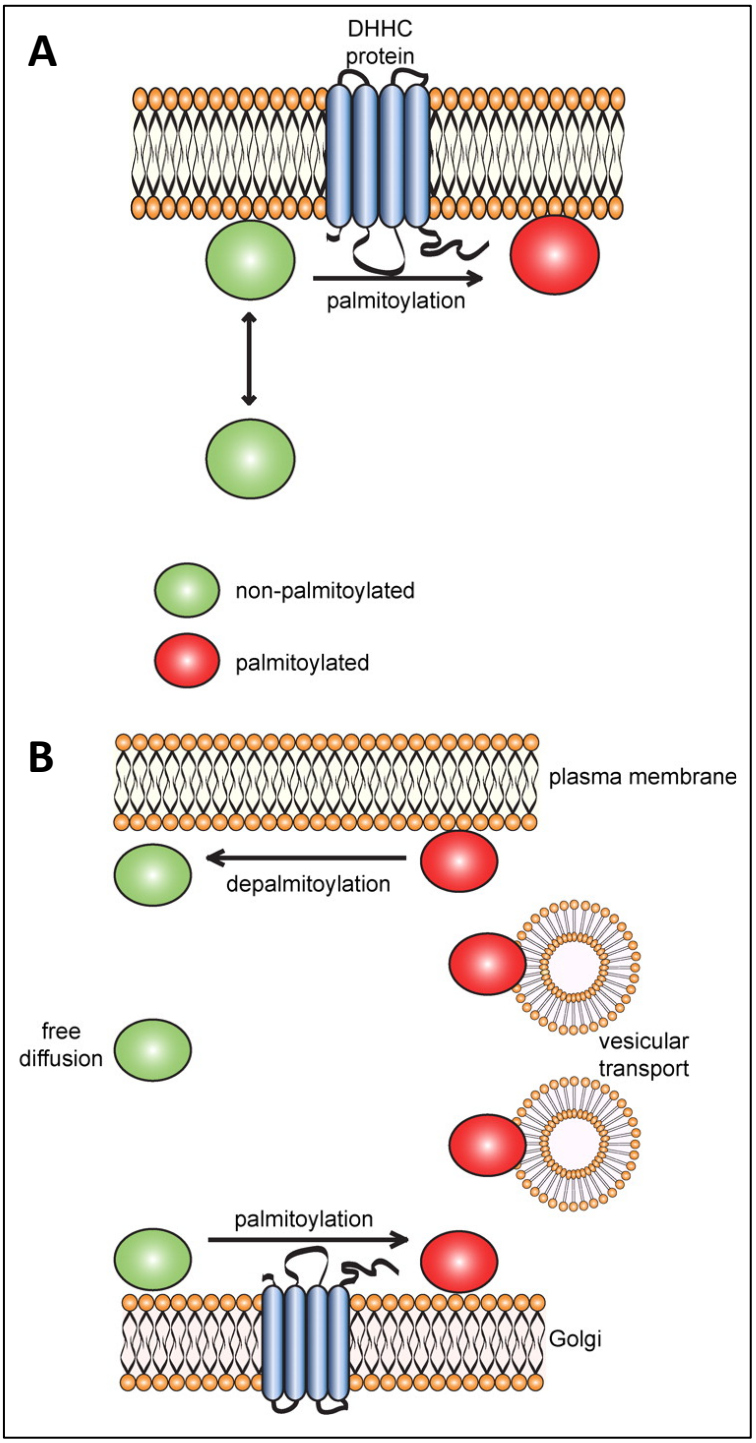

Figure 1.15: Regulation of membrane binding and trafficking of proteins by palmitoylation. (A) Modification with palmitoylation by membrane-bound DHHC proteins promotes stable membrane association. (B) Dynamic palmitoylation of proteins by golgi-localized DHHC proteins leads to membrane trafficking via transport vesicles (red circles). Depalmitoylation of the protein releases it from the membrane allowing for free diffusion (green circles) ©2010 Salaun, C., et al. J. Cell Biol. https://doi.org/10.1083 (167)

Proteins are palmitoylated by the highly conserved DHHC domain present in many membrane-bound palmitoyltransferase enzymes, as depicted in Figure 1.15A (169-171). This modification serves as a hydrophobic tether, allowing the protein to embed itself into a lipid bilayer. By associating with transport vesicles, the palmitoylated protein can be trafficked to specific subcellular locations. This transport mechanism allows for membrane localization of proteins without large membrane-binding domains and the ability to release the protein from the membrane by removing the acyl modification (172).

In addition to regulating subcellular localization, protein acylation is able to induce structural changes to proteins (173-175). These changes in conformation can alter the stability of the protein, enabling it to avoid proteolysis, as well as cause the protein to become activated or inactivated. This mechanism of controlling protein activity is particularly common with GPCRs (176-178). Drugs targeting these transmembrane receptors account for more than half of all drugs on the market and in development, and are used in the treatment of a variety of pathologies, including cardiovascular, metabolic, neurodegenerative, psychiatric, and oncologic diseases (179,180). However, the effect of palmitoylation on the activity of these receptors has not been fully characterized, necessitating further study into this mechanism of GPCR control.

Acyl-Protein Thioesterase Activity

Dynamic protein palmitoylation, specifically, involves both the attachment *and* removal of palmitoyl modifications. Following the trafficking of proteins to specific subcellular locations, proteins are able to elicit their respective activity at the appropriate area of the cell. Cells are able to regulate the inherent activity of these proteins by changing their acylation state to attach it to or detach it from the membrane (Figure 1.15B). This process is especially important in neuronal

cells, where proteins have especially long lifespans, and regulating activity and subcellular location of proteins far from the nucleus is easier than new protein synthesis (181,182).

Acyl-protein thioesterase enzymes are responsible for removing acyl modifications by hydrolyzing the thioester bonds of palmitate-modified Cys (163,172,183,184). In addition to their role in maintaining cellular lipid content, LYPLA1 and LYPLA2 are two of only three recognized cytosolic acyl-protein thioesterases that are responsible for the hydrolysis of S-Cys acyl modifications, in addition to ABHD17 (185). Whereas LYPLA1 has been shown to depalmitoylate multiple proteins, including LYPLA2 (both LYPLAs are palmitoylated themselves (186)), growth-associated protein 43 (GAP-43) is the only known palmitoylated protein substrate of LYPLA2 (186-190). GAP-43 is an important protein in neurons, responsible for the folding of neurites to induce dendritic outgrowth, and mutations or deletions of the GAP-43 gene have been shown to impede neuronal development. As the site of palmitoylation of GAP-43 is highly conserved in GPCRs, it is possible that LYPLA2 is also able to depalmitoylate these proteins to regulate activity. However, little is known regarding the role of any of these thioesterases in dynamic palmitoylation. As part of this dissertation project, we have developed methodologies to identify lipoprotein substrates of acyl-protein thioesterase enzymes, and have begun identifying such substrates of LYPLA1 and LYPLA2.

1.6 Dissertation Aims

The aims proposed in this dissertation project will test the hypothesis **that unique structural features of LYPLAs dictate and modulate their distinct substrate selectivity in**

vitro and in intact cells. Specifically, this project is designed to define the physiological role of LYPLA1 and LYPLA2 in the regulation of endocannabinoid metabolites, LysoPLs, and lipoproteins through completion of the following specific aims:

Specific Aim 1: Validate the role of LYPLAs in PG-G hydrolysis in cells.

LYPLA2 has been identified as a tentative PG-G hydrolase *in vitro*. Small molecule inhibition, siRNA knockdown, and cDNA overexpression will be utilized to characterize the roles of LYPLA1 and LYPLA2 in PG-G hydrolysis. Multiple cancer cell lines will be tested to validate the significance of LYPLAs in endocannabinoid metabolism in cellular settings.

Specific Aim 2: Characterize the molecular determinants of substrate binding in the active site of LYPLA2.

A crystal structure of LYPLA2 generated recently in our laboratory suggests that the enzyme metabolizes a range of lipid and lipid-modified substrates by accommodating these molecules in multiple binding regions of the protein's active site. The crystal structure data, in comparison of that of LYPLA1, will be used to design and generate targeted site-directed mutants of the enzyme to be screened for hydrolytic activity against LysoPL and PG-G substrates.

Specific Aim 3: Evaluate the role of lysophospholipases in modulating cellular levels of bioactive lipids using a CRISPR-Cas9 knockout cell line.

Stable deletions of LYPLA1 and LYPLA2 in neuro2a neuroblastoma cells will be

developed using the CRISPR-Cas9 genome editing system. Differential lipidomics experiments will be performed using target-based LC-MS/MS techniques to compare substrates and products of LYPLAs in the wild-type (WT) and knockout neuro2a cells. These experiments will identify LysoPL substrates of LYPLA2 and compare them to those of LYPLA1. Physiological effects of preventing LYPLA expression will then be evaluated in the neuro2a cells.

<u>Specific Aim 4</u>: Identify protein substrates of LYPLA1 and LYPLA2 depalmitoylation.

WT, *Lypla1*$^{-/-}$, *Lypla2*$^{-/-}$ and *Lypla1*$^{-/-}$/*Lypla2*$^{-/-}$ neuro2a cells will be enriched with ω-alkynylpalmitic acid (*a*PA). *a*PA-modified proteins will be isolated and quantified. Click chemistry will then be performed with IR-active or fluorescent tags to measure differential protein palmitoylation via western blot. To identify protein targets of LYPLA1 and LYPLA2 activity, stable-isotope labeling of amino acids in cell culture (SILAC) and streptavidin affinity will be employed. Quantitative changes in palmitoylation of enriched proteins will be used to identify protein substrates of LYPLA1 and LYPLA2.

2

Identification of the Major Prostaglandin Glycerol Ester Hydrolase in Human Cancer Cells

2.1 Introduction

Endocannabinoids are a class of AA-containing bioactive lipids that have myriad physiological functions (191-197). Key endocannabinoids include 2-AG and AEA, which are produced from membrane phospholipids and initiate cellular responses through interactions with the cannabinoid receptors, CB1 and CB2 (195-197). Their effects are mitigated via metabolism by the serine hydrolases, MAGL, ABHD6, ABHD12, and FAAH (198-202). In addition to these lipases, endocannabinoids have been shown to be selective substrates for cyclooxygenase enzymes, particularly COX-2. Oxidation of 2-AG by COX-2, followed by metabolism via PG synthases, results in the production of PG-Gs (Figure 2.1). These lipids are of growing interest because they elicit an array of cellular responses, including activation of calcium mobilization, modulation of synaptic transmission, induction of hyperalgesia, exacerbation of neurotoxicity and neuroinflammation, and elicitation of anti-inflammatory effects upon lipopolysaccharide stimulation (56-58,203-206).

We chose to investigate the hydrolase responsible for PG-G metabolism in human cancer cell lines because of the high PGE_2-G hydrolytic activity detected in preliminary experiments, the ease of cell maintenance, and the potential for straightforward biochemical and genetic manipulation. The various enzymes described above are serine hydrolases, so we explored the possibility that the PGE_2-G hydrolase(s) in human cancer cells is (are) a member of this

superfamily.

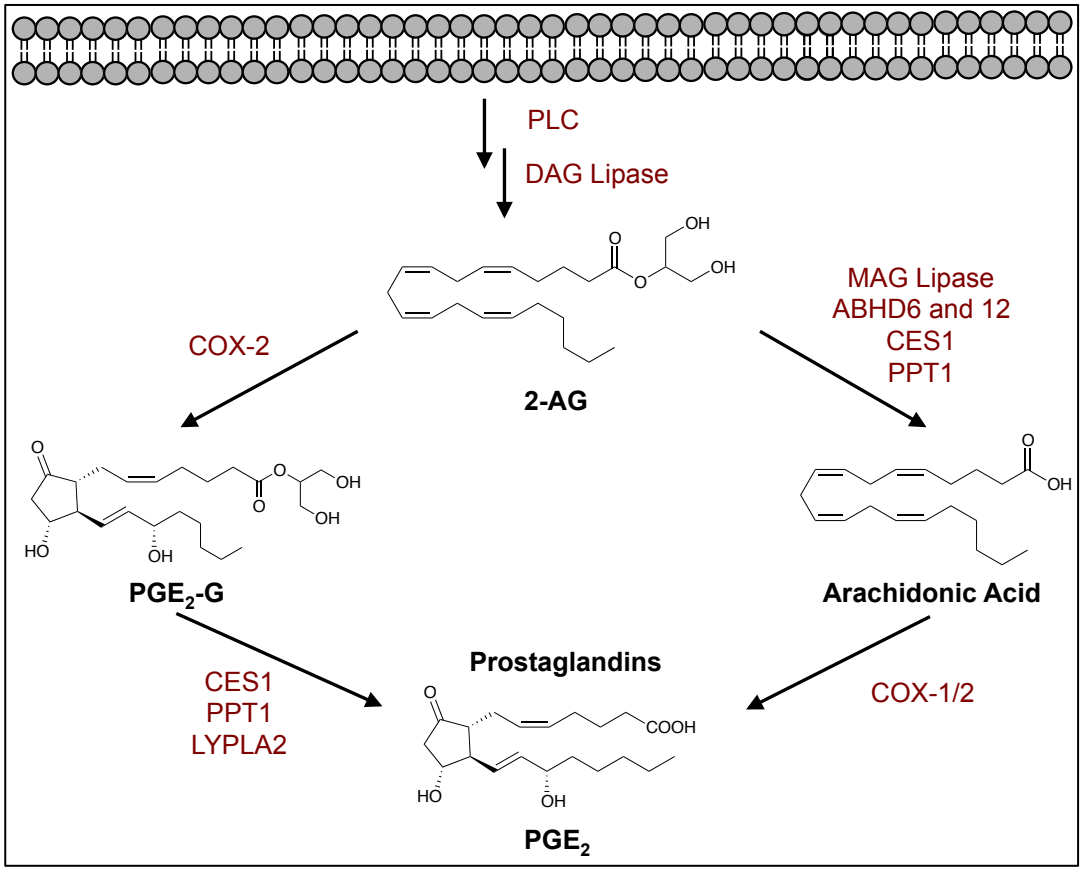

Figure 2.1: Biosynthesis and metabolism of 2-AG. Following production of 2-AG, lipases (MAG lipase, ABHD6 and 12, CES1 and PPT1) can hydrolyze 2-AG to AA, which can be oxidized to form PGs. Additionally, 2-AG is oxidized by COX-2 to form PG-Gs. These PG-Gs can be hydrolyzed by CES1, PPT1 or an unidentified enzyme to form the free acid PGs.

Serine hydrolases are a diverse class of enzymes that include lipases, proteases, and esterases (207,208), and many class members are involved in lipid biosynthesis and metabolism (199-202). A unifying feature of the serine hydrolase family is a catalytic mechanism that involves the activation of a serine nucleophile for attack on substrates containing esters, amides, or thioester bonds (208). This conserved mechanism has enabled the development of irreversible fluorophosphonate probes that can covalently modify the active site serine and render the

enzyme catalytically inactive (207). Nomura et al. (76,77) coupled fluorophosphonate probe binding with mass spectrometric proteomics techniques, known as activity-based protein profiling with multi-dimension protein identification technology (ABPP-MudPIT) to determine the relative activity levels of serine hydrolases across different cancer cell lines. Utilizing these inventories and comparing the relative activities of individual serine hydrolases to PGE_2-G hydrolase activities has allowed us to identify LYPLA2 as a principal hydrolase responsible for PG-G metabolism in human cells.

Lysophospholipases are an important class of serine hydrolases that metabolize LysoPLs to form free FA and the glycerophosphate-containing headgroup (209). Thus, we have identified a novel function and substrate for LYPLA2. Specifically, we identify LYPLA2 as the serine hydrolase responsible for hydrolysis of PG-Gs across a number of different cancer cell lines. siRNA knockdown and cDNA overexpression validated the involvement of LYPLA2 in PG-G hydrolysis. Active enzyme was expressed and purified in *E.coli,* which allowed for kinetic evaluation of an array of different substrates. In contrast to other PG-G hydrolyzing enzymes, we found that LYPLA2 exerted no action on 2-AG, or AEA. Thus, this is the first report of a hydrolase that preferentially hydrolyzes PG-Gs with no effects on the endocannabinoids.

2.2 Materials and Methods

Chemicals, Cells and Reagents

2-AG, AEA, PG-Gs (PGE_2-1 glycerol ester, PGD_2-1 glycerol ester, $PGF_{2\alpha}$-1 glycerol ester), prostaglandin serinol amide (PGE_2-SA), deuterated PGs and PG-Gs (PGE_2-d_4 and PGE_2-

G-d_5) and deuterated AA (AA-d_8) were purchased from Cayman Chemicals (Ann Arbor, MI). All LysoPLs and plasmalogens were purchased from Avanti Polar Lipids (Alabaster, Al). LC-MS solvents were from Fisher Scientific (Chicago, Il). DharmaFECT 1 and methoxy fluorophosphonate coupled to tetramethylrhodamine (FP-TAMRA) was acquired from Thermo Scientific (Pittsburgh, PA). All siRNA, Lipofactamine 2000 and Lipofectamine RNAiMAX were from Life Technologies (Carlsbad, CA). Human breast cancer adenocarcinoma cell lines; MDA-MB-231 and MCF7, prostate cancer cell lines; PC3 and LNCaP, human embryonic kidney cells, HEK293, and mouse macrophage like RAW264.7 were obtained from the American Type Culture Collection (ATCC, Manassas, VA). All cell culture media was from Gibco (Carlsbad, CA). Recombinant LYPLA1 cDNA, recombinant LYPLA2 cDNA and Turbofect were purchased from OriGene Technologies (Rockville, MD). Fetal bovine serum (FBS) was from Atlas Biologicals (Fort Collins, CO). HIS-Select Nickel Affinity beads are from Sigma (St. Louis, MO). 120 mL HiPREP 16/60 Sephacryl S-200 HR was from GE Healthcare (Piscataway, NJ). Luna liquid chromatography reverse phase C18 column was from Phenomenex (Torrance, CA). Thermo liquid chromatography reverse phase C4 column was from Thermo Scientific. Synthetic reactions were monitored by thin-layer chromatography (TLC). Column chromatography was performed using commercial silica gel and eluted with solvent systems as indicated. The spin multiplicities are indicated by the symbols s (singlet), d (doublet), dd (doublet of doublets), dt (doublet of triplets), t (triplet), m (multiplet).

Culture Conditions

MDA-MB-231, MCF7, LNCaP, and HEK293 cells were maintained as an adherent culture in RPMI medium supplemented with 10% (v/v) FBS at 37°C and 5% CO_2. PC3 cells

were grown in DMEM/F12 supplemented with 10% (v/v) FBS. RAW 264.7 mouse macrophage cells were maintained in high glucose DMEM supplemented with 10% FBS. All cells were grown to no more than 75% confluence.

Preparation of Cell Lysates

Cells were harvested by scraping, pelleted by centrifugation, and washed once with phosphate-buffered saline. The cells were resuspended in 500 μL ice-cold 25 mM Tris buffer (pH 7.5) containing 0.1 mM of both ethylenediaminetetraacetic acid (EDTA) and dithiothreitol (DTT). Cells were lysed by sonication (Virsonic Cell Disrupter model 16-850, 10 x 10 sec pulses at relative output of 0.5, on ice), and the cytosolic fractions were separated by centrifugation (100,000 x *g* for 1 h). Protein concentrations were determined using the BCA reagent kit according to the manufacturer's instruction (Pierce, Rockford Il).

PG-G Hydrolase Assay

Hydrolytic activity was determined by adding 10 nmol of PGE_2-G to 100 μL cell lysates (250 μg/mL total protein) at 37°C. Reactions were quenched after 2 h by addition of 1 mL of ethyl acetate containing deuterated internal standard (PGE_2-d_4). The organic layer was removed, evaporated to near dryness under nitrogen, and reconstituted with 50% methanol. Samples were analyzed by LC-MS/MS for the hydrolytic product, PGE_2, which was quantified against the internal standard using stable isotope dilution.

Serine Hydrolase Inhibition

The general serine hydrolase probe, FP-TAMRA was used to determine the involvement

of serine hydrolases in the metabolism of PG-Gs. FP-TAMRA (100 nM) or dimethyl sulfoxide (DMSO) was added to 100 uL of MDA-MB-231 cytosol and allowed to incubate for 30 min at 37°C. PG-G hydrolase activity was determined as described above, except samples were incubated from 0 to 60 min to obtain a full hydrolysis time course.

Western Blot Analysis

Protein expression was determined by western blot analysis. Samples were separated by sodium dodecyl sulfate (SDS) polyacrylamide gel electrophoresis (PAGE). Then, proteins were transferred to a nitrocellulose membrane and probed with either rabbit anti-LYPLA2 (1:500 v/v, Thermo Scientific), rabbit anti-LYPLA1 (1:500 v/v, Thermo Scientific) or anti-COX-2 (1:1000 v/v, Cell Signaling) and goat anti-β-actin (1:5000 v/v, Santa Cruz) overnight at 4°C. Membranes were washed and incubated with IR-visible anti-rabbit or anti-goat secondary antibodies (1:5000 v/v, LI-COR). Blots were visualized using an Odyssey IR Imager.

Recombinant Human LYPLA1, LYPLA2 and His-tagged LYPLA2 E.coli Expression

Full-length LYPLA2 was cloned into an untagged (pC6H) or a hexahistidine-tagged (p6Hb) vector using overlap PCR and isothermal assembly (210). These LYPLA2 constructs were subsequently transformed into BL21 Rosetta *E. coli* cells (Catalog # 71402, EMD Millipore) for protein expression. Large-scale expression was carried out in 10 L of autoinduction medium (211) at 37°C overnight.

His-tagged LYPLA2 E.coli Purification

All purification was performed at 4°C. *E.coli* cell pellets were resuspended in 20 mM

sodium phosphate buffer (pH 7.4) containing 500 mM NaCl, 20 mM imidazole, and 0.1 mM DTT. Cells were lysed by sonication (10 x 10 sec pulses at relative output of 0.5, on ice) and the cytosolic fraction was separated by centrifugation (100,000 x *g* for 1 h). HIS-Select Nickel Affinity beads pre-equilibrated with Buffer A (20 mM sodium phosphate buffer (pH 7.4), 500 mM NaCl, 20mM imidazole, and 0.1 mM DTT) were added to the cytosolic fraction, and protein was bound overnight. Beads were packed into a column and washed with 4 column volumes of Buffer A. His tagged protein was eluted by linear gradient from 0 to 100% Buffer B (20 mM sodium phosphate buffer (pH 7.4), 500 mM NaCl, and 500 mM imidazole). Eluted protein was collected and concentrated using a Millipore 3000 MWCO centrifugal filter. Protein was loaded onto a 120 mL HiPREP 16/60 Sephacryl S-200 HR size exclusion column pre-equilibrated with 2 column volumes of running buffer (Tris buffer (pH 7.5)), 0.1 mM EDTA, 0.1 mM DTT). The column was eluted with 1 column volume of running buffer at a flow rate of 0.5 mL/min, protein was collected, and purity was validated by SDS-PAGE.

LYPLA2 Kinetic Analysis

Hydrolysis reactions with recombinant LYPLA2 (100 nM protein) were performed in 25 mM Tris buffer (pH 7.5) with 0.1 mM EDTA and 0.1 mM DTT, with or without 0.5% (w/v) bovine serum albumin (BSA). Substrates dissolved in either 50% ethanol (PG-Gs), methanol (LysoPLs) or 2-propanol (plasmalogens) were added at varying concentrations, ranging from 0-200 μM. After preincubation of LYPLA2 for 5 min at 37°C, reactions were initiated with the addition of substrate. Reactions were quenched after 5 min with either 1 mL of ethyl acetate containing 20 ng/mL of either PGE_2-d4 (for PGE_2-G and PGD_2-G), $PGF_{2\alpha}$-d4 (for $PGF_{2\alpha}$-G), AA-d_8 (for 2-AG, 1-AG and AEA), or with 150 μL of ethanol containing 20 ng/mL of l7:0

lysoPC (for stearoyl, palmitoyl, and oleoyl lysoPC). 17:0 lysoPA (for palmitoyl lysoPA), 17:1 lysoPS (for palmitoyl lysoPS and oleoyl lysoPE) or 18:0(plasm)/18:1 PC plasmalogen (for 18:0(plasma)/20:4 plasmolagen). The optimal time for determining kinetic parameters was 5 min. The organic layer was collected and dried to completion under nitrogen. Samples were reconstituted in 50% methanol and analyzed by LC-MS/MS. Kinetic parameters were determined by performing non-linear regression analysis using a Michaelis-Menton equation with Prism Graphpad.

Synthesis of ML349

Vilsmeier-Haack Formylation: N,N-dimethylformamide (DMF) (5 mL) and phosphorous oxychloride (3.02 mmol, 1 eq.) were added to a dried flask containing dichloromethane (DCM) (10 mL) and stirred at 0°C for 0.5 hours. Thiochroman-4-one, **1**, (3.02 mmol) was then added and stirred for another 0.5 hours at 0°C. The reaction was brought to room temperature and stirred for 22 hours. The reaction mixture was a light yellow color that turned darker as the reaction progressed. It was then quenched with 1N sodium acetate (15 mL) and extract with DCM. This was washed with brine twice to remove as much DMF as possible, and the organic layer was dried with sodium sulfate and concentrated under reduced pressure. The Vilsmeier-Haack product, **2**, was then column purified with a 15:1 hexanes:ethyl acetate solvent system to give a bright yellow oil. 420 mg of product were collected (>98% pure by NMR) to give a 66% yield. ^{1}H NMR (400 MHz, $CDCl_3$): δ (ppm) 3.73 (s, 2H), 7.29 (m, 1H), 7.35 (m, 1H), 7.40 (mm, 1H), 7.94 (m, 1H), 10.35 (s, 1H).

Thiophene Cyclization: Vinyl chloride product, **2**, (1.99 mmol) and ethyl thioglycolate (2.193 mmol, 1.1 eq.) were dissolved in DCM (20 mL) and cooled to 10-15°C. Triethylamine

(556 µL, 2 eq.) was added and the reaction was warmed to room temperature while stirring overnight. The reaction mixture was a bright yellow color, and fluoresced under 365 nm light as product was formed. The reaction was quenched with 48% potassium hydroxide (2 eq.) and stirred for another 15 minutes before diluting with water and extracting with DCM. The organic layer was dried with sodium sulfate and concentrated under reduced pressure to give a crude yellow oil product, **3**, that was carried over to the next step without further purification.

Saponification: The crude thiophene ester, **3**, was dissolved in tetrahydrofuran (THF) (10 mL) and stirred at room temperature. Sodium hydroxide (9.97 mmol, 5 eq.) was dissolved in water (4 mL) and added dropwise while stirring. The reaction was then heated to 60°C and stirred overnight. The reaction solution was biphasic, with a clear brown organic layer and a lighter tan aqueous layer. The reaction was quenched with water and washed with DCM. The deprotonated product remained in the aqueous layer, which was a clear yellow color. The aqueous solution was then acidified with 2 M HCl to pH=2. The protonated product, **4**, then precipitated out of solution to give a powdery yellow solid. This was washed three times with water and finally 3:1 methanol:water then dried on a lyophilizer for 24 hours. 472 mg of beige powder product were collected (>98% pure by NMR) to give a 95% yield for the last two steps. ^{1}H NMR (400 MHz, Acetone-d_6): δ (ppm) 4.12 (s, 2H), 7.30 (m, 2H), 7.43 (m, 1H), 7.62 (m, 1H), 7.72 (s, 1H). *m/z* = 247.0.

Sulfur Oxidation: Thiophene acid, **4**, (1.81 mmol) was dissolved in THF (15 mL) and stirred at room temperature. Oxone (3.90 mmol, 2.1 eq.) was dissolved in water (11.3 mL) and added dropwise while stirring. This was stirred for 3.5 hours at room temperature. The reaction mixture was biphasic, with a clear brown organic layer and a cloudy tan aqueous layer. The reaction was then diluted with water and washed with ethyl acetate. The organic layer was dried

with sodium sulfate and concentrated under reduced pressure to give a tan powder product, **5**. 513 mg of product were collected (>85% pure by HPLC) to give a 99% yield. ^{1}H NMR (400 MHz, DMSO-d_6): δ (ppm) 4.94 (s, 2H), 7.68 (dt, 1H, J = 1.9 / 11.46 Hz), 7.77 (s, 1H), 7.81 (m, 1H), 7.80 (m, 1H), 7.83 (m, 1H). *m/z* = 279.1.

Amide Coupling: The oxidized benzothiopyran acid, **5**, (1.83 mmol), 1-(4-methoxyphenyl)piperazine, **6**, (1.83 mmol, 1 eq.) and HATU (2.75 mmol, 1.5 eq.) were dissolved in DMF (27.5 mL) and stirred at room temperature under argon. Diisopropylethylamine (1.26 mL, 4 eq.) was added dropwise and stirred overnight at room temperature forming a clear brown color. The reaction was quenched with ethyl acetate and washed with water. The product, **7**, precipitated out of solution and was filtered then washed three times with hexane and once with 3:1 hexanes:ethyl acetate. The product was a tan powder. 343 mg of product were collected to give a 41% yield, and an overall yield of 25%.^{1}H NMR (600 MHz, DMSO-d_6): δ (ppm) 3.11 (t, 4H, J = 5.1 Hz), 3.71 (s, 3H), 3.84 (s, 4H), 4.91 (s, 2H), 6.90 (m, 4H), 7.56 (s, 1H), 7.67 (m, 1H), 7.80 (m, 2H), 7.99 (d, 1H, J = 7.6Hz). ^{13}C NMR (600 MHz, DMSO-d_6): δ (ppm) 161.64, 153.88, 145.45, 137.63, 135.18, 134.67, 134.18, 131.27, 130.21, 130.00, 129.97, 126.50, 123.86, 118.55, 114.80, 55.66, 50.87, 50.52. *m/z* = 455.4.

Hydrolytic Activity of LYPLA2 Following Small Molecule Inhibition

Inhibition reactions were conducted in 25 mM Tris buffer (pH 7.5) with 0.1 mM EDTA and 0.1 mM DTT containing 100 nM of recombinant LYPLA2. 100 µL of protein was preincubated with 0-100 µM of either ML348 or ML349 (212), or the PGE_2-G structural analog (PGE_2-SA) for 5 min. Reactions were initiated by addition of 5 µM of PGE_2-G and then quenched after 5 min with 1 mL of ethyl acetate containing 20 ng/mL of PGE_2-d_4. The organic

layer was evaporated to dryness under nitrogen, reconstituted in 50% methanol, and analyzed by LC-MS/MS for PGE_2.

LYPLA2 Inhibition in RAW 264.7 Murine Macrophage-like Cells

The effects of LYPLA2 inhibition on PG-G production were tested by exposure of cells to ML349. RAW 264.7 cells were plated at 3 x 10^6 cells per 100 mm^2 plate and incubated for 24 h in DMEM supplemented with 10% FBS. Medium was replaced with serum-free DMEM containing either 1 μg/mL of lipopolysaccharide (LPS) (Sigma), 10 μM ML349, or a combination of both, and allowed to incubate for 6 h. Cells treated with LPS were then spiked with 5 μM of ionomycin (Calbiochem) for 45 min. Ionomycin stimulates the production of 2-AG and AA from endogenous sources (213). Lipids were extracted from the cell medium by addition of 2x volume of ethyl acetate containing PGE_2-d_4, PGE_2-G-d_5 and AA-d_8 internal standards. The organic layer was dried under nitrogen, and the residue was reconstituted in 50% methanol for analysis of PGs, PG-Gs, and AA by LC-MS/MS.

LC-MS Analytical Procedures

Analysis of prostanoids was accomplished by reverse phase chromatography followed by mass spectrometric detection by selected reaction monitoring (SRM) using a Shimadzu LC-20 HPLC system coupled to an Applied Biosystems 3200 QTrap mass spectrometer. Separation of PGs and LysoPCs was achieved by gradient elution of a Phenomenex Luna C18 column (50 mm x 2.0 mm, 3 μm particle size). Solvent A was HPLC grade water with 0.1% formic acid, and solvent B was acetonitrile (ACN) with 0.1% formic acid. Samples were injected onto the column with a starting condition of 80% solvent A and 20% solvent B at a flow rate of 0.5 mL/min. A

linear gradient of increasing solvent B to 98% was run over 2 min and then held for 1.5 min. SRM transitions were as follows; PGE_2 transition m/z 351.3→271.2, PGE_2-d4 m/z 355.3→275.2.

Separation of PGs and PG-Gs was accomplished with a gradient formed between solvent A, HPLC grade water with 5mM ammonium acetate (pH 3.6), and solvent B, ACN supplemented with 6% (v/v) of solvent A. Samples were injected onto the column with a starting condition of 70% solvent A and 30% solvent B at a flow rate of 0.6 mL/min. A linear gradient of increasing solvent B to 100% was run over 3.1 min and then held for 1.8 min. SRM transitions were as follows; PGE_2-G transition m/z 444.3→391.3, PGE_2-G-d_5 m/z 449.3→396.3, PGE_2 m/z 370.3→317.2, PGE_2-d_4 m/z 374.3→321.2.

Separation of AA was achieved by gradient elution. Solvent A was HPLC grade water with 80 μM silver acetate, and solvent B was methanol with 118 μM silver acetate. Samples were injected onto the column with a starting condition of 80% solvent A and 20% solvent B at a flow rate of 0.4 mL/min. A linear gradient of increasing solvent B to 100% was run over 1 min and then held for 2 min. SRM transition was as follows; AA m/z 518.9→411.1, AA-d8 m/z 526.9→419.1.

Separation of choline-containing LysoPLs was achieved by gradient elution using a Thermo C4 reverse phase column. Solvent A was HPLC grade water with 0.1% formic acid, and solvent B was ACN with 0.1% formic acid. Samples were injected onto the column with a starting condition of 30% solvent A and 70% solvent B at a flow rate of 0.5 mL/min. A linear gradient of increasing solvent B to 99% was run over 2 min and then held for 1 min. SRM transitions were as follows; 18:0 LPC m/z 524.3→184.3, 18:1 LPC 524.3→184.3, 17:0 LPC m/z 510.3→184.3, 16:0 LPC m/z 496.3→184.3.

Separation of all other LysoPLs was achieved by gradient elution using a Thermo C4 reverse phase column. Solvent A was HPLC grade water with 0.1% formic acid, and solvent B was ACN with 0.1% formic acid. Samples were injected onto the column with a starting condition of 50% solvent A and 50% solvent B at a flow rate of 0.5 mL/min. A linear gradient of increasing solvent B to 99% was run over 4 min and then held for 2.5 min. SRM transitions were as follows; 16:0 LPA m/z 409.2→152.8, 17:0 LPA m/z 423.4→152.8, 16:0 LPS m/z 496.4→153.0, 17:1 LPS m/z 508.4→153.0, 18:1 LPE m/z 478.3→281.2.

Resolution of plasmalogens was achieved by gradient elution using a Thermo C4 reverse phase column. Solvent A was HPLC grade water with 0.1% formic acid, and solvent B was 2:1 ratio of 2-propanol to ACN with 0.1% formic acid. Samples were injected onto the column with a starting condition of 50% solvent A and 50% solvent B at a flow rate of 0.5 mL/min. A linear gradient of increasing solvent B to 100% was run over 2 min and then held for 5 min. SRM transitions were as follows; 18:0(plasm)/18:1 PC plasmalogen m/z 773.5→184.3, 18:0(plasm)/20:4 PC plasmalogen m/z 795.3→184.3.

2.3 Results

Expression, Isolation, and Activity of Recombinant Human His-tagged LYPLA2

Having demonstrated that LYPLA2 is involved in PGE_2-G hydrolysis (66), we next aimed to elucidate the biochemical activities of this serine hydrolase utilizing expressed and purified his-tagged recombinant human enzyme. Expression of LYPLA2 or his-tagged LYPLA2 in *E.coli*, significantly increased PGE_2-G hydrolytic activity as compared to the activity of

control *E.coli* cells (Figure 2.2A). The his-tagged LYPLA2 was purified as a single 25 kDa band as determined by protein staining and western blotting (Figure 2.2B), matching the predicted molecular weight of LYPLA2, and had no change in activity to untagged protein. On the basis of Coomassie blue staining, the expressed his-tagged LYPLA2 was >95% pure.

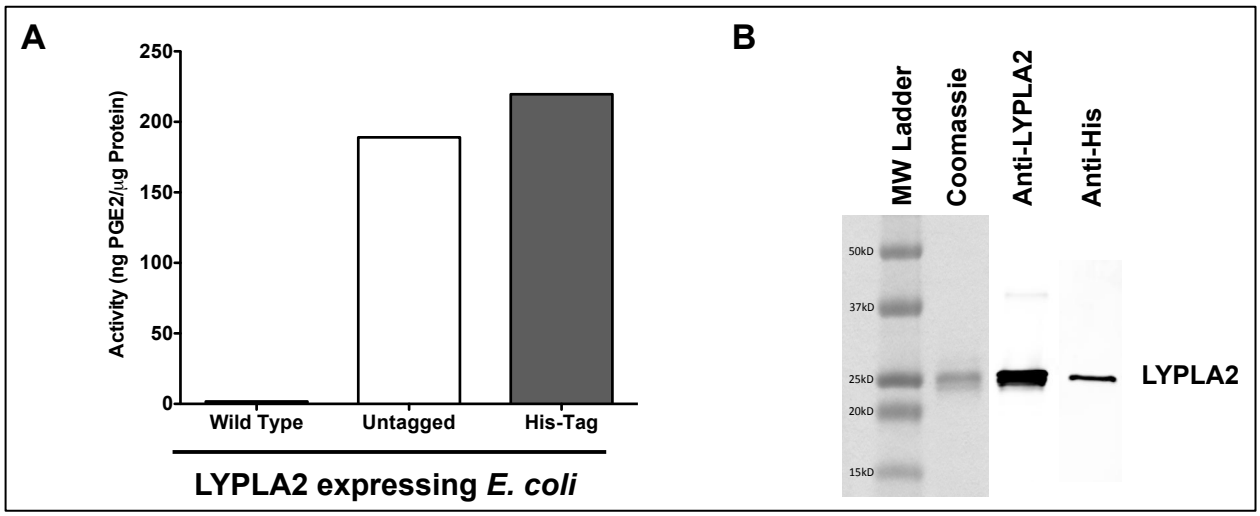

Figure 2.2: Production and hydrolytic activity of recombinant human LYPLA2 by overexpression in *E.coli*. (A) PGE_2-G hydrolytic activity of cytosol obtained from WT *E. coli* and *E. coli* overexpressing recombinant human LYPLA2 or recombinant His_6-tagged human LYPLA2. (B) Coomassie blue staining (left), Western blot analysis of LYPLA2 (center) and His_6 tag (right) of purified, recombinant his-tagged LYPLA2 produced by *E. coli*.

LYPLA1 Involvement in PGE_2-G Hydrolysis

LYPLA2 is a member of the serine hydrolase family responsible for LysoPL metabolism. There is a second isoform present in all tested cancer cell lines, named LYPLA1. Similarly to LYPLA2, LYPLA1 is responsible for hydrolysis of LysoPLs and shares over 60% sequence homology with LYPLA2. To investigate the role LYPLA1 plays in PGE_2-G hydrolysis, siRNA knockdown of LYPLA1 was conducted in MDA-MB-231 cells. The levels of LYPLA1 were markedly reduced (70%) in MDA-MB-231 cells upon transfection with siRNA as determined by

western blot analysis (Figure 2.3A). Cytosolic fractions obtained from MDA-MB-231 cells following LYPLA1 knockdown displayed a minor reduction in hydrolysis of PGE_2-G compared to control cells (Figure 2.3B).

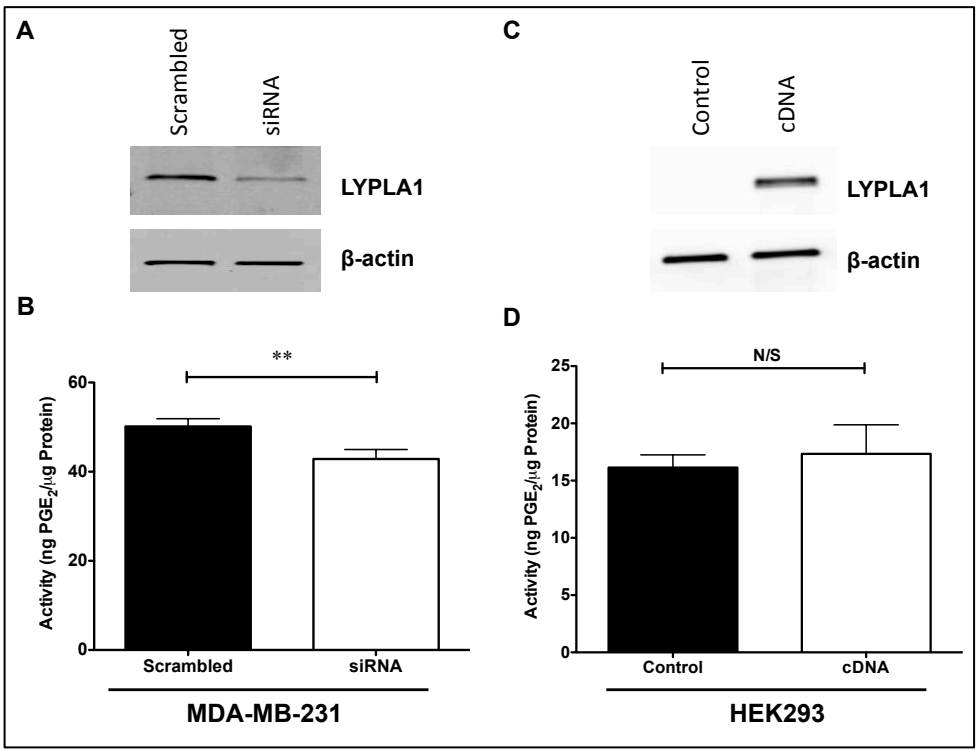

Figure 2.3: LYPLA1 siRNA knockdown in MDA-MB-231 cells and LYPLA1 overexpression in HEK293. (A) Western blot analysis of LYPLA1 in control MDA-MB-231 cells (scrambled) and LYPLA1-depleted cells (siRNA). β-actin Western blotting verified uniform protein loading (5 μg per lane). (B) PGE_2-G hydrolytic activity of cytosol obtained from MDA-MB-231 control cells (scrambled) or LYPLA1-deficient MDA-MB-231 cells (siRNA). (C) Western blot analysis of LYPLA1 in control HEK293 cells (control) and LYPLA2-overexpressing HEK293 cells (cDNA). β-actin Western blotting verified equaling protein loading (5 μg per lane). (D) PGE_2-G hydrolytic activity of cytosol obtained from HEK293 (control) or LYPLA1-overexpressing (cDNA) cells. Data are presented as the mean ± S.D. of triplicate analyses. ** indicates $p < 0.01$ by t-test. N/S indicates no significance.

To further test LYPLA1 involvement in PGE_2-G hydrolysis, cDNA for human LYPLA1 was transfected into HEK293 cells. *LYPLA1* was successfully transfected into HEK293 cells, and the cytosolic fraction from the transfected cells demonstrated high expression of LYPLA1 by

western blot (Figure 2.3C) compared to control cells. Importantly, upon overexpression of LYPLA1, HEK293 cytosolic fractions showed no significant increase in PGE_2-G hydrolytic activity compared to untransfected cells (Figure 2.3D). Unlike the siRNA knockdown data, the overexpression data do not confirm LYPLA1 as a serine hydrolase responsible for PGE_2-G hydrolysis in highly hydrolytically active cancer cell lines.

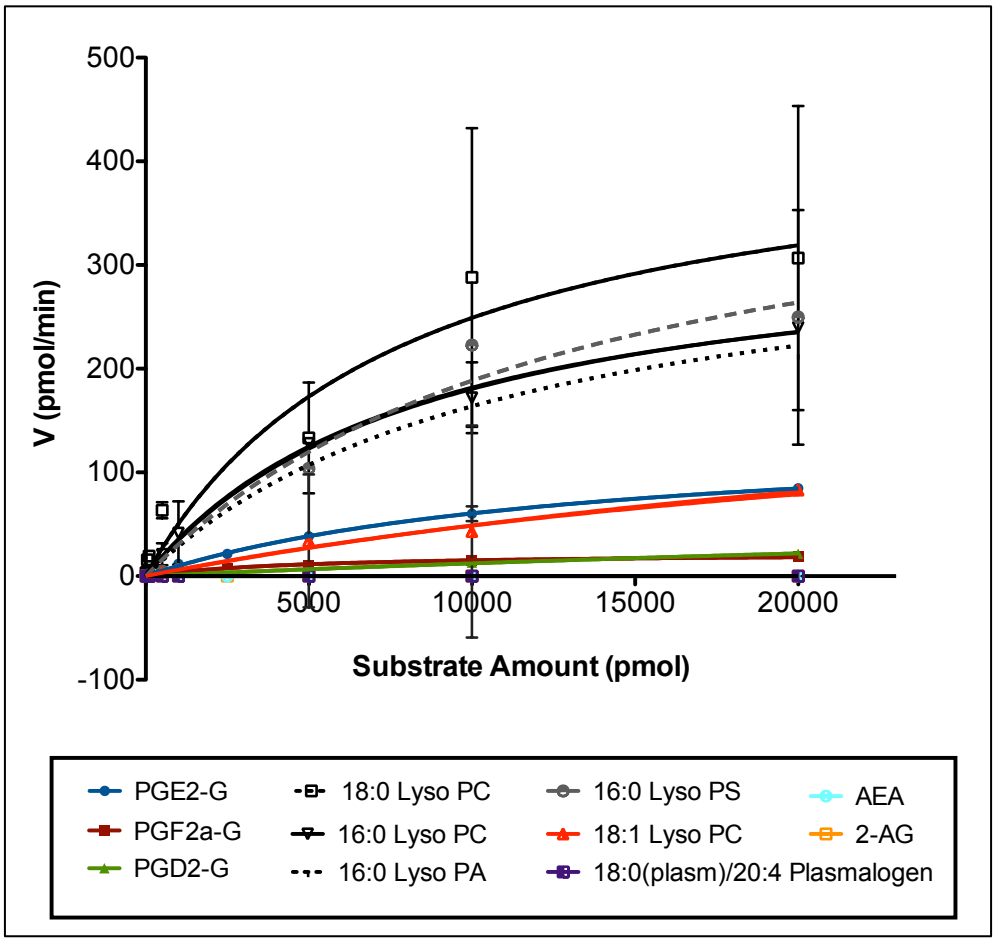

Figure 2.4: LYPLA2 hydrolytic activity against multiple lipid substrates. Substrate concentration (pmol) vs. reaction velocity (pmol/min) plots for recombinant his-tagged LYPLA2. Data are presented as the mean ± S.D. of triplicate analyses.

Substrate Specificity of Recombinant LYPLA2

We evaluated the kinetics of LYPLA2 hydrolysis against an array of substrates, including

multiple PG-Gs (PGE_2-G, PGD_2-G, $PGF_{2\alpha}$-G), endocannabinoids (2-AG, 1-AG and AEA), and LysoPLs (palmitoyl (16:0), stearoyl (18:0) or oleoyl (18:1) LPC, palmitoyl LPS, and palmitoyl (16:0) LPA). Analysis of substrate concentration-velocity plots (Figure 2.4) yielded steady-state Michaelis-Menton kinetic parameters (Table 2.1) for LYPLA2 hydrolytic activity against all substrates tested. Initially, we determined activity towards LysoPL substrates and found that the catalytic efficiencies of LYPLA2 for palmitoyl and stearoyl LPC, palmitoyl LPA and palmitoyl LPS (k_{cat}/K_m = 4.0, 5.6, 3.1 and 3.3 $min^{-1}\mu M^{-1}$, respectively) were comparable to published values (209). Interestingly, addition of a single site of unsaturation in the lipid (18:1 LPC) significantly reduced the catalytic efficiency of the enzyme (K_{cat}/K_m = 0.6 $min^{-1}\mu M^{-1}$), suggesting the unsaturated lipids hinder hydrolysis. LYPLA2 did not display any catalytic activity against plasmalogens.

Substrate	k_{cat} (min^{-1})	K_m (μM)	k_{cat}/K_m ($min^{-1}\ \mu M^{-1}$)
PGE_2-G	14.1 ± 0.4	13 ± 1.1	1.08 ± 0.10
$PGF_{2\alpha}$-G	2.2 ± 0.3	5.0 ± 1.1	0.44 ± 0.11
PGD_2-G	9.5 ± 1.6	67 ± 14	0.14 ± 0.04
LysoPC (16:0)	33.3 ± 1.7	8.3 ± 1.0	4.0 ± 0.52
LysoPC (18:0)	44.3 ± 10.2	7.8 ± 4.4	5.6 ± 3.41
LysoPC (18:1)	24.8 ± 9.1	40.7 ± 20.6	0.6 ± 0.38
LysoPA (16:0)	34.6 ± 4.7	11.1 ± 3.2	3.1 ± 0.99
LysoPS (16:0)	44.1 ± 10.4	13.3 ± 6.2	3.3 ± 1.72
1-AG	1.7 ± 0.07	7.6 ± 1.2	0.23 ± 0.04
2-AG	N/A	N/A	N/A
AEA	N/A	N/A	N/A
Plasmalogen (38:4)	N/A	N/A	N/A

Table 2.1: Kinetic parameters for hydrolysis of multiple lipid substrates by recombinant human LYPLA2.

LYPLA2 had lower hydrolytic efficiency towards PG-Gs relative to its activity with LysoPLs. LYPLA2 showed a greater catalytic efficiency for PGE_2-G (K_{cat}/K_m = 1.1 $min^{-1}\mu M^{-1}$) than for $PGF_{2\alpha}$-G and PGD_2-G (k_{cat}/K_m = 0.44 and 0.14 $min^{-1}\mu M^{-1}$, respectively).

Commercially available PG-Gs are an equilibrium mixture of the 2-glyceryl ester (~15%) and the 1(3)-glyceryl ester (~85%). To evaluate the regiochemistry of hydrolysis, we modified the LC conditions to enable separation of the isomers. LC-MS/MS analysis of PGE_2-G following LYPLA2 incubation demonstrated that the 1(3)-glyceryl ester was selectively hydrolyzed; no hydrolysis of the 2-glyceryl ester was observed (Figure 2.5A). Neither of the endocannabinoids, 2-AG or AEA, was hydrolyzed by LYPLA2. Since commercial 2-AG is nearly pure 2-glyceryl ester, we incubated 2-AG in 25 mM Tris buffer (pH 7.5) overnight to allow it to equilibrate with the 1(3)-AG isomer. Addition of LYPLA2 to this equilibrium mixture demonstrated hydrolysis of the 1(3)-AG but no hydrolysis of 2-AG (Figure 2.5B). The k_{cat}/K_m for hydrolysis of 1-AG was lower than that of PGE_2-G (Table 2.1). Consideration of the substrate-specificity data summarized in Table 2.1 suggests that LYPLA2 only hydrolyzes 1(3)-glyceryl esters.

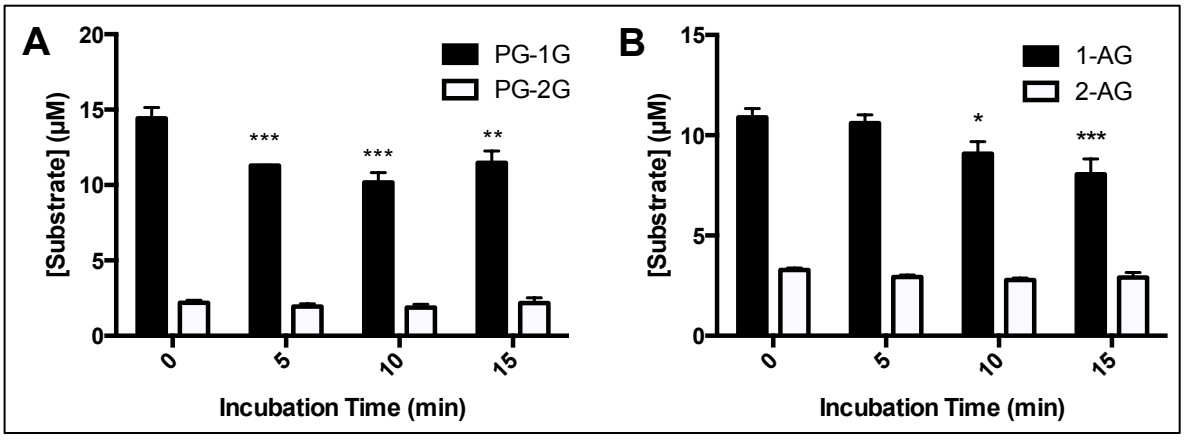

Figure 2.5: Hydrolytic activity of LYPLA2 against sn1- (black) and sn2-isomers (white) of PGE_2-G (A) and AG (B). Data are presented as the mean ± S.D. of n=6 analyses. *$P< 0.05$, **$P< 0.01$, ***$P< 0.001$.

It was recently reported that addition of BSA to incubations of PGD_2-G with human MAGL increases the rate of hydrolysis of PGD_2-G. Therefore, we determined the relative activity of LYPLA2 to a series of substrates in the presence of 0.5% BSA (w/v). The activity of LYPLA2 toward PGE_2-G increased whereas the activity to 1-AG, 16:0-LPC and 18:0-LPC decreased (Figure 2.6). In fact, PGE_2-G is the preferred substrate of LYPLA2 in the presence of BSA.

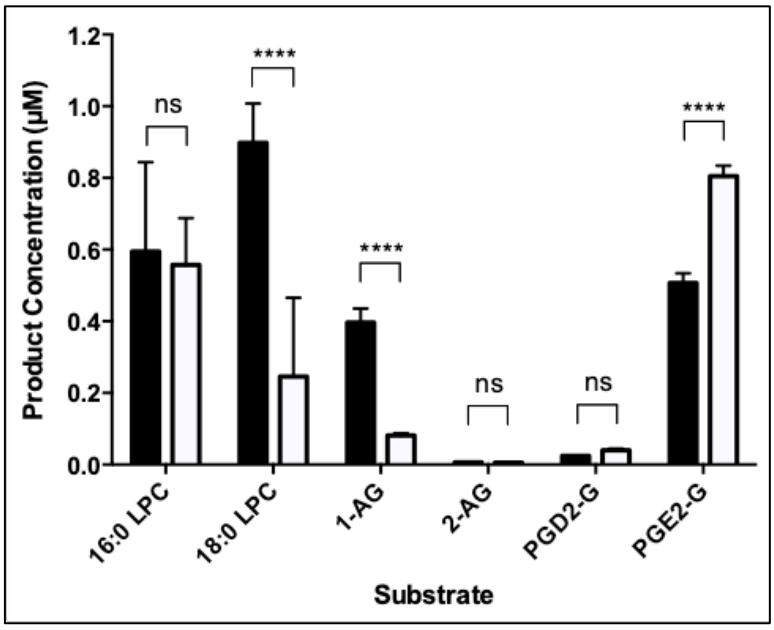

Figure 2.6: Hydrolytic activity of LYPLA2 against a variety of lipid substrates in the absence (black) or presence (white) of BSA. Data are presented as the mean ± S.D. of n=6 analyses. **** indicates $p < 0.0001$; ns, no significance.

Synthesis and Characterization of LYPLA2 Inhibitors

Synthesis of the specific LYPLA2 inhibitor, ML349, began with thiochroman-4-one, **1**, and was carried out within 5 steps (Scheme 2.1). The synthesis was successfully completed with an overall yield of 25%, producing 343 mg of purified material. **1** is commercially available and was readily converted to **2** via a Vilsmeier-Haack formylation, involving the addition of an aldehyde moiety at the three position, and substitution of the ketone with a chloride leaving group. The initial synthetic scheme involved the oxidation of **1** to a sulfone prior to formylation

in order to avoid oxidation of the thiophene ring; however, this resulted in a complex reaction mixture with a minimal amount of the desired product. This may be due to the introduced sulfone stabilizing the ketone and reducing the acidity of the alpha carbon. The sulfone may also have further destabilized the formylated product, as **2** was found to begin decomposing within four hours of isolating the purified material. With **2** produced at a 66% yield, it was immediately column purified and carried over into the next reaction to produce the cyclized thiophene, **3**. This was then saponified without any further purification to form the deprotonated carboxylate, **4**, which crashed out of aqueous solution when acidified to give a >98% pure product at a 95% yield from the last two steps. **4** was then oxidized to the sulfone species, **6**, with oxone in a biphasic solution of THF and water, with a yield of 99%. Peracetic acid was also considered as an alternative oxidizing agent but did not form the desired product. A HATU-promoted coupling of **5** with **6** was then performed to produce the final product, **7**, with a 44% yield, resulting in an overall yield of 25%. ML349 was found to be highly insoluble in most organic solvents, specifically dichloromethane, which was useful in purification. When the reaction solution was diluted with dichloromethane, ML349 precipitated and was then filtered and washed with hexanes to give a purified product without the need for column purification.

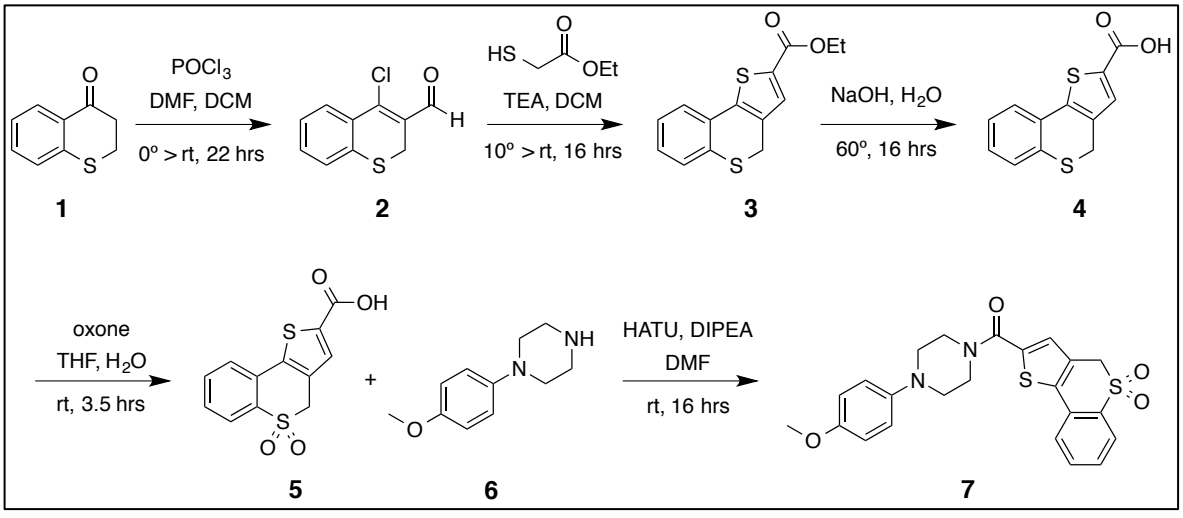

Scheme 2.1: Synthesis of ML349 from thio-4-chromanone (**1**) and N-paramethoxyphenylpiperazine (**6**).

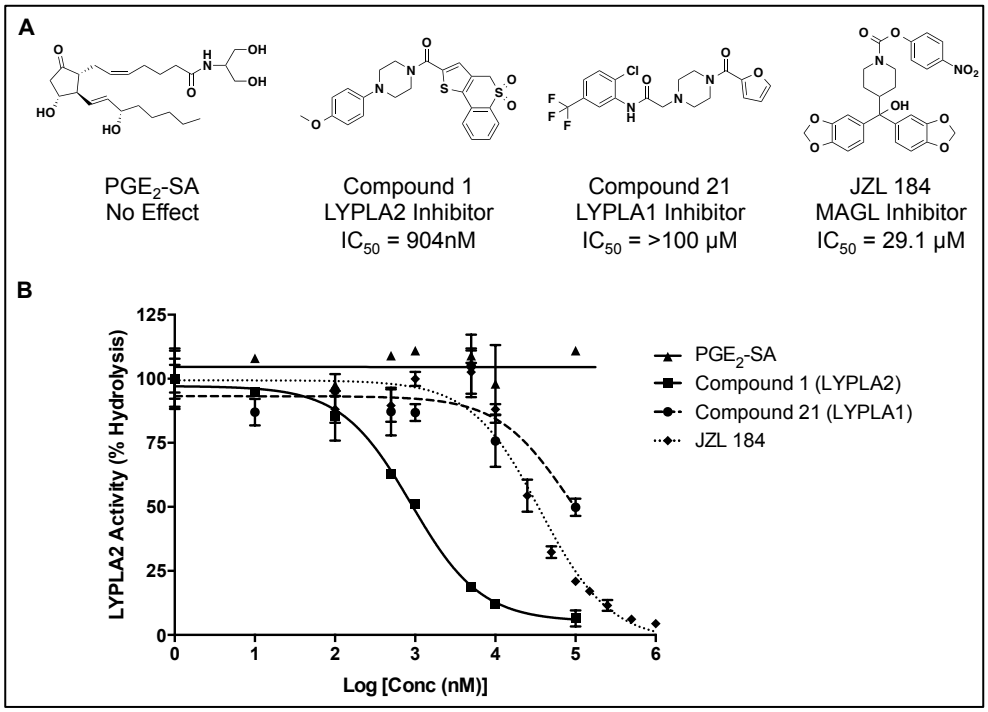

Figure 2.7: Inhibition of LYPLA2 by small molecule inhibitors. (A) Chemical structures and IC_{50} values for ML349 (Compound 1 - LYPLA2 inhibitor), ML348 (Compound 21 - LYPLA1 inhibitor), JZl-184 (MAGL inhibitor), and PGE2-SA (structural analog of PGE_2-G). (B) Inhibition curves of LYPLA2-mediated hydrolysis of PGE_2-G by ML349 (Compound 1), ML348 (Compound 21), PGE_2-SA, and JZL184. Data are presented as the mean ± S.D. of triplicate analyses.

Inhibition of Recombinant LYPLA2 Results in Decreased Hydrolysis of PG-Gs

LYPLA1 is a homologue that shares over 60% sequence homology with LYPLA2 (209) but utilizes a wider array of substrates. Selective inhibitors of LYPLA2 and the related enzyme LYPLA1 have recently been discovered (214). We assessed the effects of these inhibitors – named ML349 (LYPLA2-specific inhibitor) and ML348 (LYPLA1-specific inhibitor) (Figure 2.7A) – on the hydrolytic activity of LYPLA2. ML349 inhibited the PGE_2-G hydrolysis activity of purified LYPLA2 with an inhibitory concentration at 50% maximum response (IC_{50}) of 904 nM (Figure 2.7B), comparable to previously reported values (510 nM) for the inhibition of hydrolysis of a fluorescent substrate, resorufin acetate (214); ML348, however, did not affect

LYPLA2 activity. An amidated PGE_2-G structural analog, PGE_2-SA, was also assessed for LYPLA2 inhibition. PGE_2-SA had no effect on the hydrolysis of PGE_2-G, indicating the enzyme may have very tight requirement for substrate binding.

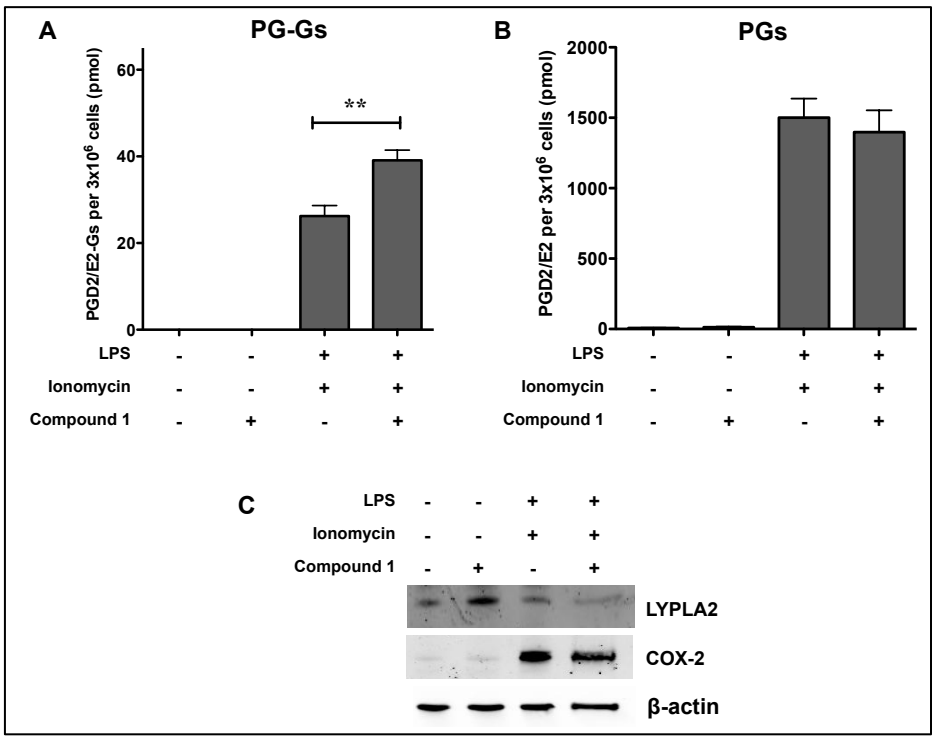

Figure 2.8: LYPLA2 inhibition significantly increases endogenous levels of PGE_2-G/PGD_2-G formed in RAW264.7 murine macrophage-like cells. Cells were treated with LPS (1 μg/mL) in the presence or absence of 10 μM ML349 (Compound 1) for 6 h in serum-free medium followed by treatment with ionomycin (5 μM) for 45 min. The culture medium was removed and lipids extracted for LCMS/MS analysis for PGE_2-G/PGD_2-G (A), and PGE_2/PGD_2 (B). (C) Western blot analysis of untreated and treated RAW264.7 macrophages confirmed the expression of COX-2 and LYPLA2 in cells. β-actin Western blot verified equal protein loading (10 μg per lane). Data are presented as the mean ± S.D. of triplicate analyses. ** indicates $p < 0.01$

LYPLA2 Inhibition Increases PG-G Levels in RAW 264.7 Cells

To assess the physiological relevance of PG-G hydrolysis by LYPLA2, murine RAW264.7 macrophage-like cells were stimulated to produce PGE_2-G and PGD_2-G by priming cells with LPS (1 μg/mL) to induce expression of COX-2 (Figure 2.8) followed by treatment

with the calcium ionophore ionomycin (5 μM) to promote release of 2-AG/AA. We determined whether inhibition of LYPLA2 by ML349 could affect the amount of PG-Gs produced in stimulated RAW264.7 cells. Upon simulation, RAW264.7 cells produce high levels of PGD_2 and PGE_2 and lower levels of PGD_2-G and PGE_2-G all of which are secreted into the culture medium, as previously reported (215) (Figure 2.8). Pretreatment of stimulated RAW264.7 cells with 10 μM ML349 prior to addition of ionomycin, increased the levels of PGD_2/PGE_2-G in the medium compared to those in the medium of uninhibited cells (40 vs 26 pmol). A concomitant decrease in PGD_2/PGE_2 was not observable, likely because of the large excess of PGs to PG-Gs in stimulated RAW cells.

2.4 Discussion

Endocannabinoids are lipid mediators that elicit a variety of physiological effects, including analgesia and suppression of inflammation (22,196,197). COX-2 oxygenates 2-AG to form PG-Gs, which display effects that are frequently opposite those of endocannabinoids, e.g., hyperalgesia and neuroinflammation (56-58,203-206). However, complete elucidation of the effects of PG-Gs *in vivo* has been challenging due to their hydrolytic instability (55). The present studies have identified a serine hydrolase, LYPLA2, as a major enzyme responsible for PGE_2-G hydrolysis in human cancer cells.

LYPLA2 was expressed in *E. coli* and purified to apparent homogeneity in order to determine its specific activity against a range of substrates. LYPLA2 exhibited higher catalytic efficiency against LysoPLs than against PG-Gs when assays were conducted in the absence of

albumin. However, the inclusion of albumin in the assay buffer led to a reversal of substrate specificity such that PGE_2-G was hydrolyzed more rapidly than other substrates, including LysoPLs. Among the PG-Gs tested, PGE_2-G was the preferred substrate, followed by $PGF_{2\alpha}$-G and PGD_2-G. The PG-Gs assayed as substrates were an equilibrium mixture of the 1(3)- and 2-glycerol esters; the 1(3)-glycerol ester comprises 85% of the mixture. Monitoring the isomeric composition in the presence of LYPLA2 under conditions in which hydrolysis was faster than isomerization revealed that LYPLA2 selectively hydrolyzed the 1(3)- but not the 2-isomer. LYPLA2 also displayed no activity against 2-AG or AEA but did hydrolyze 1(3)-AG at rates lower than PGE_2-G. In fact, in the presence of albumin, PGE_2-G was hydrolyzed nearly 10-fold faster than 1(3)-AG. Figure 2.8 summarizes the lipid substrates for LYPLA2.

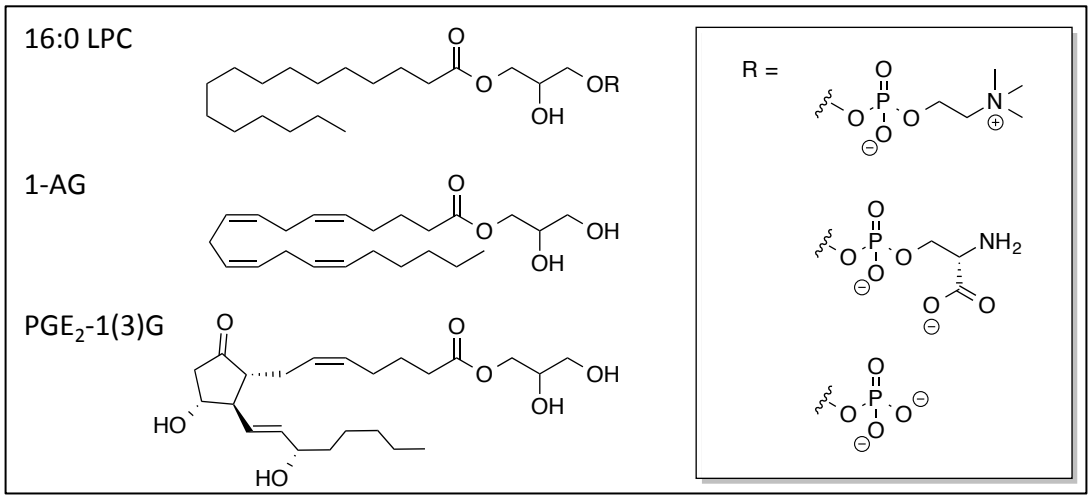

Figure 2.9: Lipid substrates for hydrolysis by LYPLA2 demonstrate preference for sn1-isomers.

The preference of LYPLA2 for 1(3)-glycerol esters over 2-glycerol esters is reminiscent of ABHD6 and ABHD12, which hydrolyze 1(3)-AG faster than 2-AG, but is different than MAGL, which hydrolyzes 2-AG faster than 1(3)-AG (68,216). The relative activity of ABHD6, ABHD12 and MAGL for the 2- or 1(3)- isomers of PG-Gs is not known, but MAGL appears to

hydrolyze the 2-glycerol isomer of the PGD_2-G dehydration product, 15-deoxy-PGJ_2, quite efficiently. In fact, MAGL exhibited higher activity against the 2-glycerol ester of 15-deoxy-PGJ_2 than the 1(3)-isomers of PGE_2-G or PGD_2-G (68). Whether this is due to the more polar nature of PGE_2-G and PGD_2-G compared to 15-deoxy-PGJ_2 or to the isomeric differences in the glycerol ester moiety is unknown.

LYPLA2 is more active against PG-Gs than the three enzymes previously reported to exhibit PGE_2-G hydrolase activity. LYPLA2's catalytic activity for PGE_2-G is 2-fold, 17-fold and 52-fold greater than those reported for CES1, MAGL, and PPT1, respectively (63,65). However, inclusion of albumin in the buffer solutions increases the rates of PGE_2-G hydrolysis by LYPLA2 and MAGL. Furthermore, unlike LYPLA2, which does not hydrolyze 2-AG, CES1, MAGL, and PPT1 are all more active against 2-AG than against PGE_2-G (65,69,75).

Since multiple enzymes hydrolyze PG-Gs with different rates and under different conditions, selective inhibitors or genetic manipulations will be important in dissecting the contributions of individual hydrolases to PG-G hydrolysis in intact cells or tissues. ML349, which had been previously reported to inhibit LYPLA2 (212), exhibited 32-fold selectivity for inhibition of PGE_2-G hydrolysis compared to the MAGL inhibitor JZL-184, and greater than 100-fold selectivity compared to the LYPLA1 inhibitor ML348. JZL-184 is a potent MAGL inhibitor but is frequently used *in vitro* and *in vivo* at concentrations much higher than its stated IC_{50} for MAGL of 50 nM (217). ML349 significantly reduced PGE_2-G hydrolysis by LYPLA2 *in vitro* and increased endogenous levels of PGD_2-G/PGE_2-G in LPS-activated RAW macrophages. This is the first demonstration of the elevation of a lipid substrate by inhibition of LYPLA2 in intact cells.

While ML349 is able to selectively inhibit LYPLA2 over other serine hydrolases with

high sequence homologies, its IC_{50} is barely submicromolar, leaving room for improvement. Alterations of the starting materials **1** and **6** could easily be incorporated into the structure of ML349 to prepare a library of molecules in order to identify a more potent inhibitor against recombinant LYPLA2 using the assays described above to directly quantify hydrolytic activity of the enzyme towards its substrates.

The specificity of LYPLA2 for 1(3)-glycerol ester substrates suggests that isomerization of the initially formed 2-glycerol esters of PGE_2-G/PGD_2-G occurred following LPS treatment of the RAW cells. The half-life to spontaneous acyl migration of 2-glycerol esters to 1(3)-glycerol esters is ~10 min in serum-free medium but reduces to ~3 min in the presence of serum (13). Since the synthesis of PGE_2-G/PGD_2- G took place over 45 min following addition of ionomycin to trigger 2-AG release, there was ample time for isomerization to occur. The possibility also exists that isomerization of 2-AG to 1(3)-AG occurred during this time course and that addition of ML349 inhibited 1(3)-AG hydrolysis by LYPLA2 leading to elevated levels of PGE_2-G/PGD_2-G following COX-2 oxygenation. This possibility seems less likely than ML349 inhibition of LYPLA2 hydrolysis of PGE_2-G/PGD_2-G because 1(3)-AG is an inferior substrate for LYPLA2 compared to PG-Gs and because 1(3)-AG is a poorer substrate than 2-AG for oxygenation by COX-2.

The biological effects of PG-Gs that have been documented in the literature have all been recorded with commercial material, which are primarily the 1(3)-glycerol esters. It is not known if the 2-glycerol esters of PG-Gs have more potent or different effects in the same assays. Therefore, it seems likely that LYPLA2 plays an important role in controlling the biological effects of endocannabinoid-derived PG-Gs. The present work demonstrates that it is a major and perhaps the major PG-G hydrolase in human cancer cells. However, the multiplicity of enzymes

that hydrolyze these compounds, either the 2- or the 1(3)- isomers, suggests that different enzymes will play significant roles in controlling the activities of PG-Gs depending on the cell type and physiological state. It will be exciting to dissect the contributions of individual enzymes to PG-G hydrolysis using a combination of chemical biological and genetic approaches.

3

Structural Investigation into Substrate Specificity of Lysophospholipases

3.1 Introduction

LYPLA1 and LYPLA2 share 68% sequence identity and are 83% similar. Despite this high degree of conservation, the enzymes are thought to have distinct substrate preferences based on *in vitro* studies using purified recombinant protein assays (209,218-220). LYPLA2 is considered the less promiscuous hydrolase with increased activity toward LPC and LPE classes of LysoPLs, whereas LYPLA1 displays comparable activity toward all LysoPL classes. Additionally, LYPLAs have been shown to hydrolyze a variety of other types of substrates. For example, the endocannabinoid, 2-AG, is oxygenated by COX-2 to generate PG-Gs (47,221). Our previous work has identified LYPLA2 as a PG-G hydrolase, converting PG-Gs to free PGs, though only 1-isomers of these glyceryl esters were tested in these studies (66). This suggests a role for LYPLA2 in endocannabinoid metabolism. Furthermore, LYPLA1 and LYPLA2, also called APT1 and APT2, respectively, are among a small pool of enzymes known to exhibit thioesterase activity on palmitoylated proteins such as the $G_{5\alpha}$ subunit of heterotrimeric G proteins, Ras, and GAP-43 (183,186,190,222,223). LYPLA1 and LYPLA2 act to remove these acyl modifications as part of a dynamic palmitoylation process, regulating the subcellular location and conformation of a variety of specific cellular proteins (183,184,186,222).

In addition to their specificity toward LysoPL substrates, LYPLA1 and LYPLA2 have distinct preferences toward these eicosanoid and lipoprotein substrates. As opposed to LYPLA2,

LYPLA1 does not seem to have a significant role in PG-G hydrolysis in a cellular setting (66). Additionally, whereas multiple lipoprotein substrates of LYPLA1 have been identified, GAP-43 is the only palmitoylated protein shown to be deacylated by LYPLA2 (172,183,186,187,190,222,224-227). Moreover, both enzymes are specific toward their respective lipoprotein substrates with no apparent overlap in acyl-protein thioesterase activity.

The crystal structure of apo-LYPLA1 (PDB ID: 1FJ2) suggests that the enzyme is unusual in that it lacks the traditional cap domain found in other members of the α/β-hydrolase superfamily (228). Instead, the β4-α2 loops are positioned as a flexible lid covering the active site serine, creating a potential hydrophobic channel for lipid binding. With such a high degree of sequence identity, we hypothesized that LYPLA2 would be folded similarly to LYPLA1, but would have distinct structural differences in its active site that could potentially explain the divergent substrate preferences of the two enzymes. To understand the substrate specificity of LYPLAs, we employed x-ray crystallography to determine the structure of LYPLA2 and compare the two enzymes. We then used the resulting structural information to guide site-directed mutagenesis studies to compare recombinant activity of WT and mutant enzymes toward various LyoPL and PG-G substrates in order to elucidate key residues of LYPLA2 important for its distinct substrate specificity.

3.2 Materials and Methods

Chemicals, Cells and Reagents

Eicosanoid substrates were purchased from Cayman Chemicals (Ann Arbor, MI), unless

otherwise noted. LysoPLs and plasmalogens were purchased from Avanti Polar Lipids (Alabaster, Al). LC-MS solvents were from Fisher Scientific (Chicago, Il). HIS-Select Nickel Affinity beads are from Sigma (St. Louis, MO). 120 mL HiPREP 16/60 Sephacryl S-200 HR was from GE Healthcare (Piscataway, NJ). Luna liquid chromatography reverse phase C18 column was from Phenomenex (Torrance, CA). Thermo liquid chromatography reverse phase C4 column was from Thermo Scientific. Synthetic reactions were monitored by thin-layer chromatography (TLC). Column chromatography was performed using commercial silica gel and eluted with solvent systems as indicated. The spin multiplicities are indicated by the symbols s (singlet), d (doublet), dd (doublet of doublets), dt (doublet of triplets), t (triplet), m (multiplet).

X-Ray Crystallography

Recombinant human LYPLA2 (10 mg/mL) was pre-incubated with phenylmethylsulfonyl fluoride (PMSF) (10X molar ratio). Crystals were produced by hanging drop vapor diffusion with drops containing 2 μL of enzyme-inhibitor complex and 2 μL of reservoir solution containing 0.1 M sodium citrate (pH 5.6) and 15-30% PEG 3350. After 1~2 weeks, irregular crystals formed and were supplemented with 25% glycol for cryopreservation. Diffraction data for LYPLA2-PMSF were collected on the Advanced Photon Source LS-CAT beamline 24-ID-E at 100 K. The data were processed with XDS and solved to 2.70 Å resolution by molecular replacement using Phaser with the A chain of LYPLA1 (PDB ID: 1FJ2) as the search model. Two monomers were present in one asymmetric unit. Difference electron density maps contoured at 3σ showed the presence of a phenylmethylsulfonyl moiety associated with active Ser122. Data collection and refinement statistics for each structure are listed in Table 3.1. Figures were generated using PyMol Molecular Graphics system (Schrödinger). Atomic

coordinates for LYPLA2-PMSF have been deposited in the PDB (ID: 6BJE).

LYPLA2•PMSF	
Data Collection	**PDB ID: 6BJE**
Wavelength (Å)	0.9792
Resolution range (Å)	139.81 - 2.66 (2.81 - 2.66)
Space group	$P4_32_12$
Unit cell (a, b, c)	54.8, 54.8, 279.6
Total reflections	155,367 (16,080)
Unique reflections	12,993 (1,618)
Multiplicity	12.0 (9.9)
Completeness (%)	98.4 (88.7)
Mean I/sigma(I/σ)	7.6 (1.5)
Wilson B-factor (Å^2)	43.4
R-merge	0.196 (0.693)
$CC_{1/2}$	0.988 (0.565)
Refinement	
Resolution	69.91- 2.70 (2.91 -2.70)
R-work/R-free	22.1/26.4 (30.2/33.8)
Number of atoms (total/protein/ligands/solvents)	3347/ 3291/181/38/18
R.M.S. (bond/angle)	0.003/0.695
Ramachandran favored/outliers (%)	97.0/0
Average B-factor	45.76/45.02/65.91/55.82

No. of Crystals = 1. The values in parentheses are for the highest resolution shell; $R_{merge} = \frac{\sum_{hkl}\sum_i|I_i(hkl)-\bar{I}_i(hkl)|}{\sum_{hkl}\sum_i I_i(hkl)} \times 100\%$ and $R = \frac{\sum_{hkl}||F_o|-|F_c||}{\sum_{hkl}|F_o|} \times 100\%$, where F_o and F_c are the observed and calculated structure factors, R_{free} test set is 10.0%.

Table 3.1: X-ray data collection and refinement statistics for LYPLA2-PMSF.

Synthesis of 16:0-d$_3$-LysoPC (Scheme 3.1)

Phosphoglyceride Acylation: Dicyclohexylcarbodiimide (DCC) (0.34 g, 1.7 mmol) and 4-dimethylaminopyridine (DMAP) (0.20 g, 1.6 mmol) were added to a milky solution of sn-glycero-3-phosphocholine:$CdCl_2$ (0.24 g, 0.54 mmol) and d_3-palmitic acid (0.43 g, 1.7 mmol) in anhydrous $CHCl_3$ (10 mL). Crushed glass was added to the reaction mixture and it was

sonicated. After 6 h, the reaction mixture was filtered and the glass washed with MeOH. Purification by column chromatography (70:25:5, CH_2Cl_2:MeOH:H_2O) afforded the product d_6-dipalmitoylphosphatidylcholine (d_6-DPPC) as a white powder (0.18 g, 46%).

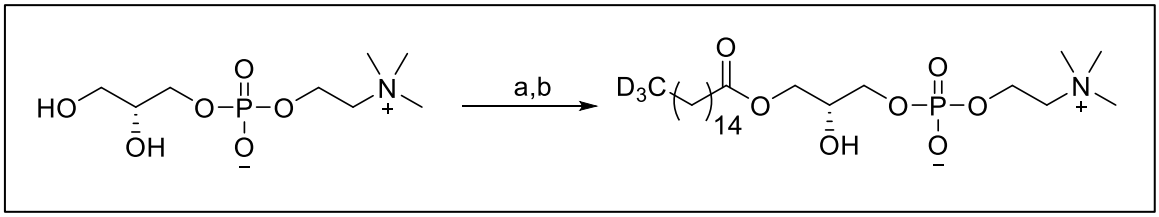

Scheme 3.1: Synthesis of 16:0-d_3-LPC using DCC coupling of palmitic acid-d_3 to glycerol-3-phosphocholine followed by *sn2*-selective hydrolysis via PLA2 isolated from snake venom. Reagents: a: d_3-palmitic acid, DCC, DMAP, $CHCl_3$; b: snake venom PLA2, $CaCl_2$, pH 7 phosphate buffer.

Selective sn2-Hydrolysis: Snake venom PLA2 (~5 mg) was added to a milky solution of the d_6-DPPC (0.18 g, 0.24 mmol) in a mixture of ether (5 mL), MeOH (1 mL), and phosphate buffer (pH 7.4, 5 mL) containing $CaCl_2$ (0.7 mM). After 1 h, H_2O (10 mL) was added, and the reaction mixture was extracted with $CHCl_3$:MeOH (2:1, 20 mL). The 16:0-d_3-LPC product was isolated as a white powder (86 mg, 72%) after purification by column chromatography (70:25:5, CH_2Cl_2:MeOH:H_2O). The NMR data were consistent with literature values for lysoPC, with the terminal deuterated methyl group absent. ^{1}H NMR (MeOH-d_4) δ 4.33-4.21 (m, 2H), 4.18-4.02 (m, 2H), 4.01-3.98 (m, 1H), 3.96-3.82 (m, 2H), 3.69-3.67 (m, 2H), 3.26 (s, 9H), 2.37 (t, 2H, J = 7.5 Hz), 1.65-1.51 (m, 2H), 1.30 (m, 24H).

Generation of Mutant LYPLA2 Constructs

Site-directed mutagenesis was performed on His-tagged LYPLA2 plasmid using primers targeting amino acids of interest. The primers were as follows: S122A sense, 5'-

GGAGGCTTTGCACAGGGC-3', S122A antisense, 5'-GCCCTGTGCAAAGCCTCC-3', A43W sense, 5'-GCTGGGCTGACTGGCTCTCCACC-3', A43W antisense, 5'-GGTGGAGAGCCAGTCAGCCCAGC-3', M217W sense, 5'-CCTCAGGAGTGGGCAGCTGTGAAGG-3', M217W antisense, 5'-CCTTCACAGCTGCCCACTCCTGAGG-3', S82A sense, 5'-CTGGGGCATCTGGAGCCAGCCCCATCAGGT-3', S82A antisense, 5'-ACCTGATGGGGCTGGCTCCAGATGCCCCAG-3', S82D sense, 5'-TCTGGGGCATCTGGATCCAGCCCCATCAGGTC-3', S82D antisense, 5'-GACCTGATGGGGCTGGATCCAGATGCCCCAGA-3'. PfuTurbo DNA polymerase was used to amplify the mutant plasmid according to specifications from Agilent. After amplification, 2.5 µL Cutsmart buffer and 1 µL DpnI were added and incubated at 37ºC for 1.5 hr to digest any remaining methylated DNA. The digested product of mutant plasmids were then transformed into DH5α *E. coli* cells by adding 2 µL plasmid product to 50 µL cells and incubating on ice for 30 min. The cells were then heat shocked at 42ºC for 45 sec, incubated on ice for 2 min, and 200 µL S.O.C. media were added. Cell solutions were incubated at 37ºC and shaken at 250 rpm for 1 hour to recover. Cell solutions were then spread onto LB agar plates with kanamycin and incubated at 37ºC overnight. Colonies from each plate were inoculated into 5 mL of LB with 50 µg/mL kanamycin to create glycerol stocks (40% glycerol) and for plasmid purification to sequence and verify successful mutagenesis. Recombinant protein was expressed and purified as described above.

Recombinant LYPLA Activity Assays

Recombinant WT and mutant enzyme solutions (100 nM) were prepared in PBS with or

without 0.5% (w/v) FA-free BSA, and 100 μL aliquots of each solution were preincubated at 37 ºC for 5 min. PGE_2-G, 16:0-LPC, 18:0-LPC, 16:0-d_3 LPC, or a mix of sn1-1 and sn2-18:0 LPC (1.5 nmol) were added in 1 μL ethanol, and samples were vortexed, and then incubated at 37 ºC for 10 min. For quantitation of product formation (PGE_2-G and 16:0-d_3 LPC), enzymatic activity was quenched by adding 1 mL of ice-cold ethyl acetate with 0.5% (v/v) acetic acid containing either 20 ng PGE_2-d_4 or 1 nmol 16:0-d_{31} as internal standards. Samples were vortexed, and the organic layers were collected and dried under nitrogen. To quantify PG-G hydrolysis, extracts were resuspended in 200 μL ACN and analyzed via LC-ESI-MS/MS, as described below. To quantify 16:0-d_3 LPC hydrolysis, samples were derivatized with pentafluorobenzyl (PFB) bromide based on a previously described method with minor adaptions (229). Specifically, extracts were reconstituted in 150 μL ACN, and then 200 μL of 100 nM tetrabutylammonium hydrogen sulfate in 100 nM dibasic sodium phosphate buffer was added. Following addition of 200 μL 2% (v/v) PFB bromide in chloroform, the samples were vortexed and sonicated for 45 min at 35% output using a Virsonic Cell Disrupter (Model 16-850), and then lipids were extracted via the addition of 1 mL of 9:1 hexanes:ethanol. The organic layer was removed, dried under nitrogen, and resuspended in 200 μL ACN for analysis via LC-atmospheric-pressure chemical ionization (APCI)-MS/MS, as described below. For quantitation of substrate remaining (isomeric differentiation of PG-1G vs -2G and sn1- vs sn2-18:0 LPC studies), enzymatic activity was quenched by adding 100 μL of ice-cold ethanol with 0.5% (v/v) acetic acid containing 2 μM 17:0 LPC as an internal standard. Samples were immediately analyzed via LC-ESI-MS/MS, as described below, to prevent the equilibration of sn1- and sn2- isomers via acyl migration.

A: *LC Conditions for PGE_2 Analysis*	
Mobile Phase A = H_2O; B = Acetonitrile each with 0.1% formic acid	
Column C18, 5.0 x 0.2 cm	
Initial Conditions Flow = 500 uL/min %B = 20%	
Time	*%B*
0.25	20%
4.25	98%
5.40	98%
5.80	20%

B: *MS Parameters for PGE_2 and PGE_2-d_4*					
Analyte	**Mode**	**Q1**	**Q3**	**CE**	**DP**
PGE_2	-	351.3	271.2	-24	-30
PGE_2-d4	-	355.3	275.2	-24	-30

Table 3.2: LC-MS/MS conditions for PGE_2 analysis. **(A)** LC parameters for mobile phases, column, and LC gradient. **(B)** MS parameters for PGE_2 and PGE_2-d_4 analytes, including MS mode, fragmentation patterns, collision energy, and deionization potential.

LC-MS Analytical Procedures

Analysis of prostanoids and derivatized FAs was accomplished by reverse phase chromatography followed by mass spectrometric detection by selected reaction monitoring (SRM) using a Shimadzu LC-20 HPLC system coupled to an Applied Biosystems 3200 QTRAP mass spectrometer. Separation and MS analysis of PGs was performed in negative mode on a system configured as described in Table 3.2. Separation and MS analysis of FAs was performed in negative mode on a system configured as described in Table 3.3.

A: *LC Conditions for 16:0-d_3 Analysis*	
Mobile Phase A = 4:1 acetonitrile:H_2O B = 9:1 IPA: acetonitrile	
Column C18, 15.0 x 0.2 cm @ 43C	
Initial Conditions Flow = 320 uL/min %B = 0%	
Time	*%B*
0.25	0%
4.00	70%
6.20	70%
6.70	0%

B: *MS Parameters for 16:0-d_3 and 16:0-d_{31}*					
Analyte	**Mode**	**Q1**	**Q3**	**CE**	**DP**
16:0-d_3	-	258.2	258.2	-5	-60
16:0-d_{31}	-	286.2	286.2	-5	-60

Table 3.3: LC-MS/MS conditions for 16:0-d_3 analysis. **(A)** LC parameters for mobile phases, column, and LC gradient. **(B)** MS parameters for 16:0-d_3 and 16:0-d_{31} analytes, including MS mode, fragmentation patterns, collision energy, and deionization potential.

Separation of PG-Gs was accomplished with a gradient formed between solvent A, HPLC-grade water with 5 mM ammonium acetate (pH 3.6), and solvent B, ACN supplemented with 6% (v/v) of solvent A. Samples were injected onto the column with a starting condition of 70% solvent A and 30% solvent B at a flow rate of 0.6 ml/min. A linear gradient of increasing solvent B to 100% was run over 3.1 min and then held for 1.8 min. SRM transitions were as follows: PGE_2-G transition *m/z* 444.3 → 391.3; PGE_2-G-d_5 *m/z* 449.3 → 396.3.

Resolution of PG-G isomers was achieved by gradient elution using an Agilent Eclipse XDB-C18 column (150 x 2.1 mm, 3.5 µm particle size). Solvent A was HPLC-grade water with 5 mM ammonium acetate (pH 3.6), and solvent B, ACN supplemented with 6% (v/v) of solvent

A. Samples were injected onto the column with a starting condition of 33% solvent A and 67% solvent B at a flow rate of 0.350 ml/min. A linear gradient of increasing solvent B to 53% was run over 6.5 min, followed by a sharp increase of B to 99% over 0.1 min and then held at 99% for an additional 1.9 min. SRM transitions were as follows: PGE_2-1G and PGE_2-2G transition *m/z* 444.3 → 391.3; PGE_2-G-d_5 *m/z* 449.3 → 396.3; and PGE_2-d_4 *m/z* 374.3 → 321.2.

Resolution of AG isomers was achieved by gradient elution using an Agilent Eclipse XDB-C18 column (150 x 2.1 mm, 3.5 µm particle size). Solvent A was HPLC-grade water with 2 mM ammonium acetate, and solvent B was methanol with 10 mM ammonium acetate. Samples were injected onto the column with a starting condition of 15% solvent A and 85% solvent B at a flow rate of 0.325 ml/min. A linear gradient of increasing solvent B to 95% was run over 9.5 min, followed by a sharp increase of B to 100% over 0.5 min and then held at 100% for an additional 3 min. SRM transitions were as follows: 1-AG and 2-AG transition *m/z* 396.2 → 287.1; and 2-AG-d_8 *m/z* 404.2 → 295.1.

Separation of LPCs was achieved by gradient elution using a Thermo C4 reverse phase column. Solvent A was HPLC-grade water with 0.1% formic acid, and solvent B was ACN with 0.1% formic acid. Samples were injected onto the column with a starting condition of 30% solvent A and 70% solvent B at a flow rate of 0.5 ml/min. A linear gradient of increasing solvent B to 99% was run over 2 min and then held for 1 min. SRM transitions were as follows: 16:0 lyso-PC *m/z* 496.3 → 184.3; 18:0 lyso-PC *m/z* 524.3 → 184.3; 18:1 lyso-PC *m/z* 524.3 → 184.3; and 17:0 lyso-PC *m/z* 510.3 → 184.3.

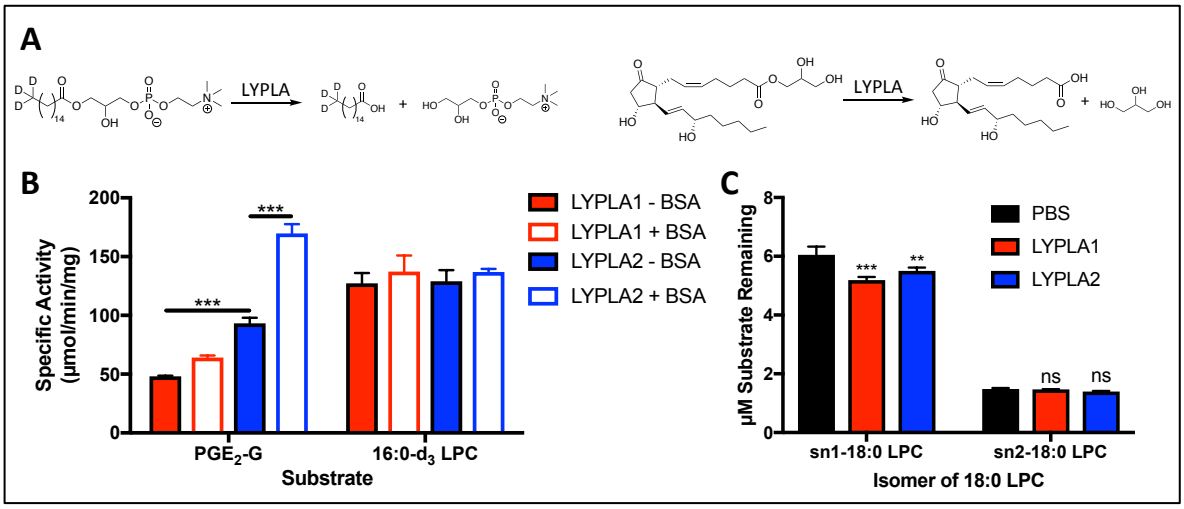

Figure 3.1: Comparison of the activities of recombinant LYPLA1 and LYPLA2. **(A)** Scheme of hydrolysis of 16:0-d_3 LPC (left) and PGE_2-G (right) by LYPLAs. **(B)** Activity of recombinant LYPLA1 and LYPLA2 toward representative substrates, PGE_2-G and 16:0-d_3 LPC with or without 0.5% (w/v) BSA. **(C)** Activity of recombinant LYPLA1 and LYPLA2 toward sn1 and sn2 isomers of 18:0 LPC (1(3)-18:0 LPC and 2-18:0 LPC, respectively). Data is expressed as µM substrate remaining after incubating in no enzyme control (PBS) or with LYPLA1 or LYPLA2. ***P<0.01, ***P<0.001.*

3.3 Results

LYPLA1 is a PG-G Hydrolase *in vitro*

The work described in Chapter 2 identified LYPLA2 as a major PG-G hydrolase in cancer cells. At that time, LYPLA1 was ruled out on the basis of siRNA knockdown in cells, but the enzyme's PG-G hydrolytic activity was not evaluated directly *in vitro* with purified recombinant protein (66). Therefore, we quantified both LYPLA1 and LYPLA2 activity toward a representative PG-G substrate, PGE_2-G. Additionally, as both LYPLA1 and LYPLA2 have been shown to robustly hydrolyze 16:0-LPC, we quantified hydrolytic activity toward the 16:0-LPC species as a representative LysoPL substrate. However, as the products of LysoPL hydrolysis by LYPLAs are a glycerophosphate headgroup (too small and polar for LC

separation) and a FA (notoriously omnipresent in solvents, plastics, and glassware, as well as difficult to ionize and fragment (230-232)) (Figure 3.1A), we utilized an isotopically labeled 16:0-d_3 LPC species and a PFB-Br derivatization for these assays (229). The derivatization yields a PFB-esterified acyl chain, which has electron-capturing properties to enable sensitive ionization and detection in APCI-MS/MS. This method allowed for the LC-MS/MS-based quantification of a FA species by avoiding contamination and ionization issues.

As demonstrated in Figure 3.1B, both enzymes were able to hydrolyze these substrates. LYPLA1 hydrolyzed PGE_2-G at a rate of 48.1 ± 0.5 μmol/min/mg compared to 93.3 ± 4.7 μmol/min/mg for LYPLA2, and LYPLA1 hydrolyzed 16:0-d_3 LPC at a rate of 127 ± 8 μmol/min/mg compared to 129 ± 9 μmol/min/mg for LYPLA2. Thus, contrary to our findings in intact cancer cells, recombinant LYPLA1 displayed substantial PG-G hydrolytic activity. However, whereas the two enzymes hydrolyzed 16:0-d_3 LPC with equivalent specific activity, LYPLA2 was significantly more active than LYPLA1 toward PGE_2-G. It has been reported that BSA is able to improve hydrolysis of lipid substrates in recombinant serine hydrolase activity assays, presumably by acting as a lipid carrier to better mimic the conditions of a cellular setting, and we have recently shown that the presence of BSA has a significant effect on LYPLA2-mediated PG-G hydrolysis (66,68). Therefore, we also added BSA to the enzyme solutions to promote substrate availability and compared enzymatic activity toward both PG-G and LysoPL substrates. In the presence of BSA, LYPLA1 hydrolyzed PGE_2-G at a rate of 64.2 ± 1.7 μmol/min/mg compared to 170 ± 8 μmol/min/mg for LYPLA2, and LYPLA1 hydrolyzed 16:0-d_3 LPC at a rate of 137 ± 14 μmol/min/mg compared to 137 ± 2 μmol/min/mg for LYPLA2. These results suggest that the addition of BSA promotes the hydrolytic activity of LYPLA2 but not LYPLA1 toward PG-Gs, without significantly affecting the activity of either enzyme toward

LysoPLs.

Preliminary studies by our lab have suggested LYPLA2 prefers the sn1-isomer of PG-G and glycerolipids (Figure 2.8) (66). To determine substrate specificity of LYPLAs toward sn1- vs sn2-isomers of LysoPLs, equilibrium mixtures of sn1-18:0 LPC (~80%) and sn2-18:0 LPC (~20%) were added to 100 nM enzyme solutions of LYPLA1, LYPLA2, or a no enzyme control under conditions in which hydrolysis occurred faster than isomeric equilibration. The isomeric composition of the remaining 18:0 LPC substrate was assessed immediately after quenching with acidified ethanol to prevent acyl migration, and PBS controls were included to ensure that changes to isomeric composition were not merely a result of isomeric equilibration. With both LYPLA1 and LYPLA2, only sn1-18:0 LPC isomer levels were significantly decreased after 10 min compared to those in the PBS controls (Figure 3.1C). These data demonstrate the specificity of LYPLAs toward sn1-LysoPLs, which is consistent with our published activity of LYPLA2 toward 1(3)-PG-Gs and 1(3)-AG.

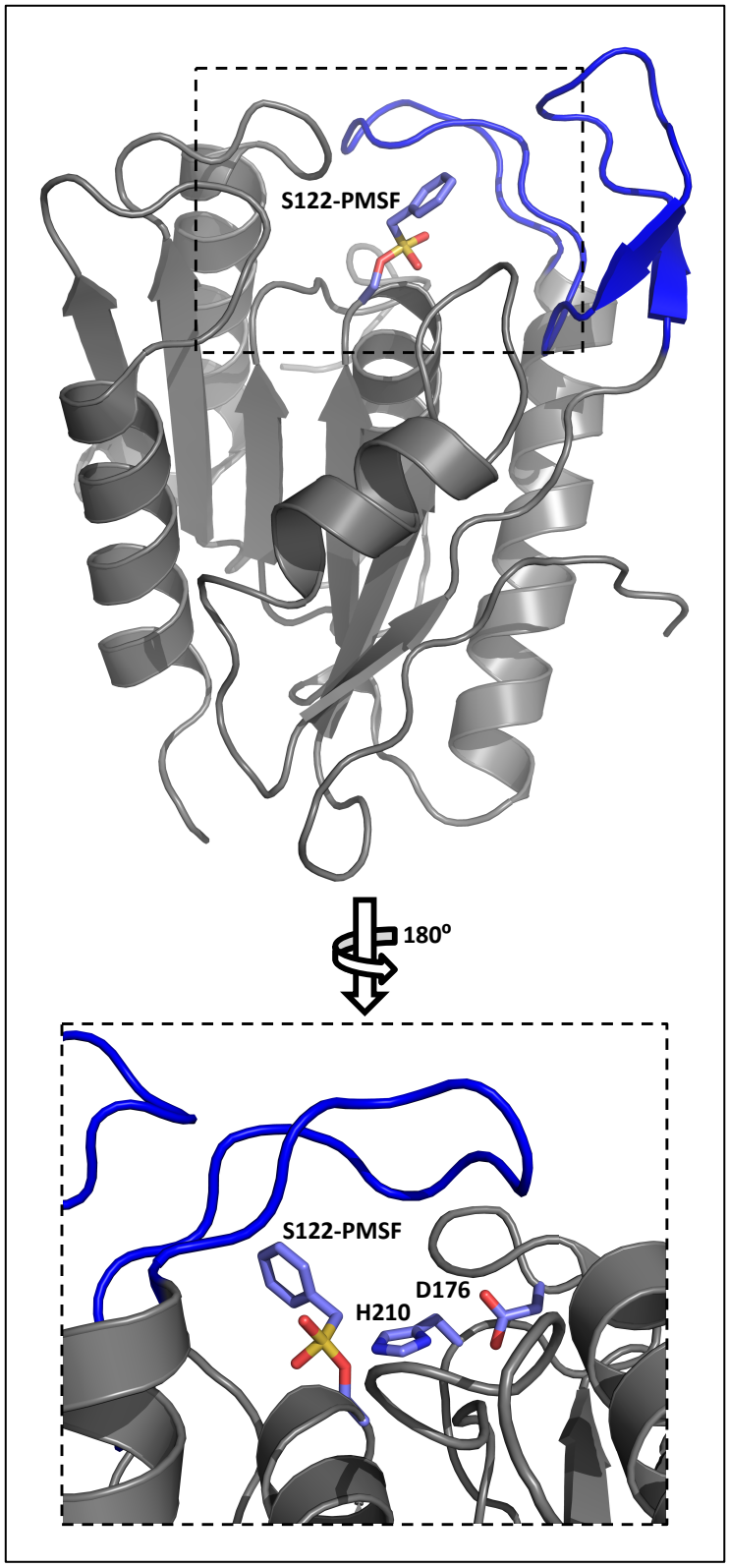

Figure 3.2: Crystal structure of LYPLA2-PMSF (PDB – 6BJE) shown in cartoon representation with orientation exposing active Ser122 with PMSF modification. *B5-α2* loop enveloping the active site is highlighted in blue. Catalytic triad, Asp176, His210, and active Ser122, shown in close-up view, rotated 180º. X-Ray data collection and refinement statistics are described in Table 3.1.

LYPLA1 and LYPLA2 Display High Structural Alignment

Despite a roughly 2-fold higher activity of LYPLA2 toward PG-Gs compared to LYPLA1, the substrates share many similarities in substrate preferences. Though LYPLA1 does not seem to have a clear role in PG-G hydrolysis in cells (Figure 2.5), it is clearly able to hydrolyze the eicosanoids in an *in vitro* setting (Figure 3.1B). Additionally, the enzymes hydrolyze LysoPL and lipoprotein substrate classes, giving three similar substrate pools, all structurally distinct from one another. However, LYPLA1 and LYPLA2 have shown to prefer specific substrates in each class, suggesting a structural basis of substrate binding.

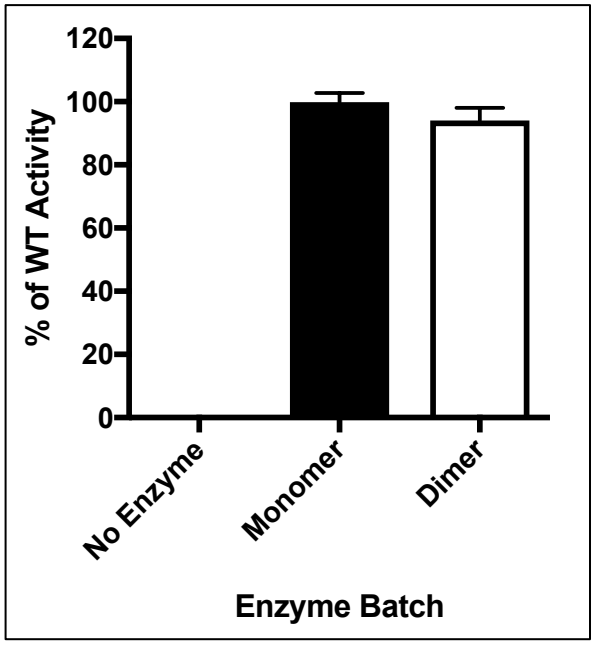

Figure 3.3: LYPLA2 is equally active in monomer and dimer conformations. Hydrolytic activity of WT LYPLA2 from monomer and dimer fractions following size-exclusion purification toward PGE_2-G compared to a no enzyme control; data are normalized to hydrolytic activity of monomer fraction. (N=6)

To understand how the structures of LYPLAs impact their substrate specificity, we employed sparse matrix screening of crystallization to obtain the crystals that were used to solve

the first structure of LYPLA2 covalently modified by the general serine hydrolase inhibitor, PMSF, at 2.7 Å resolution (PDB – 6BJE) (Figure 3.2, Table 3.1). Another crystal structure of LYPLA1 (PDB ID: 5SYM), and the structure of LYPLA2 (PDB ID: 5SYN), have also recently been solved with the specific inhibitors, ML348 and ML349, respectively, bound in their active sites (233). Although the previously reported structures of LYPLA1 and LYPLA2 suggest the proteins form weak dimers, size-exclusion chromatography indicates that LYPLA2 is equally active as a monomer (Figure 3.3).

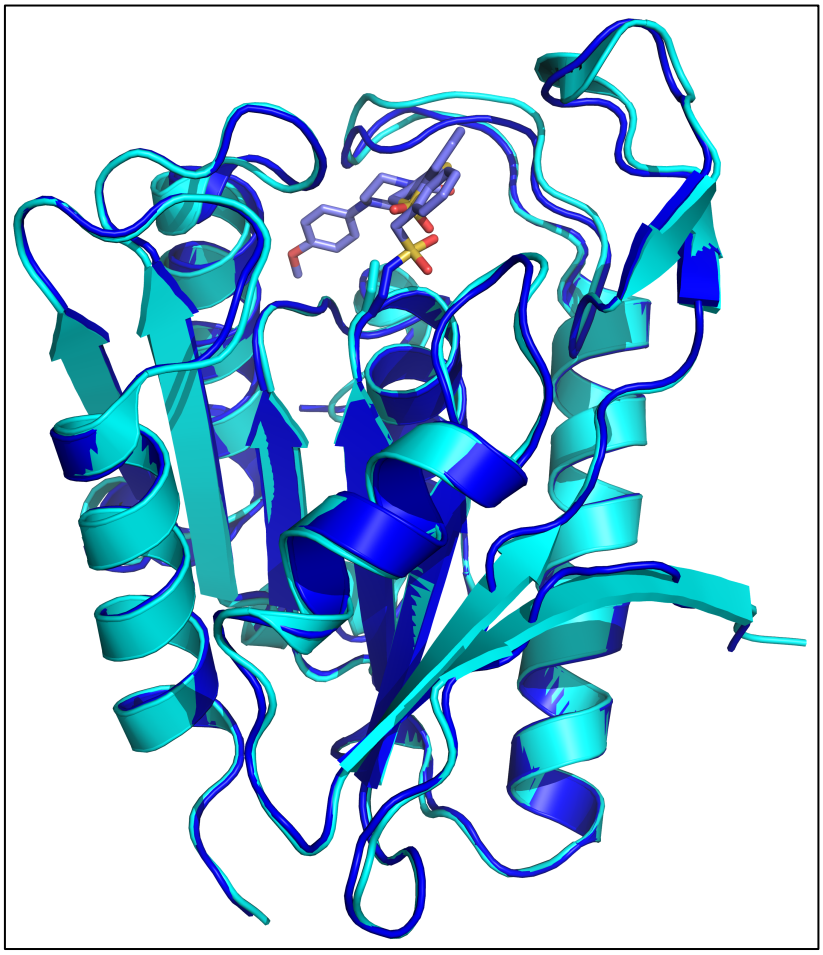

Figure 3.4: Structural alignment of the crystal structures of LYPLA2-PMSF (PDB – 6BJE), shown in blue, and LYPLA2-ML349 (PDB – 5SYN), shown in cyan.

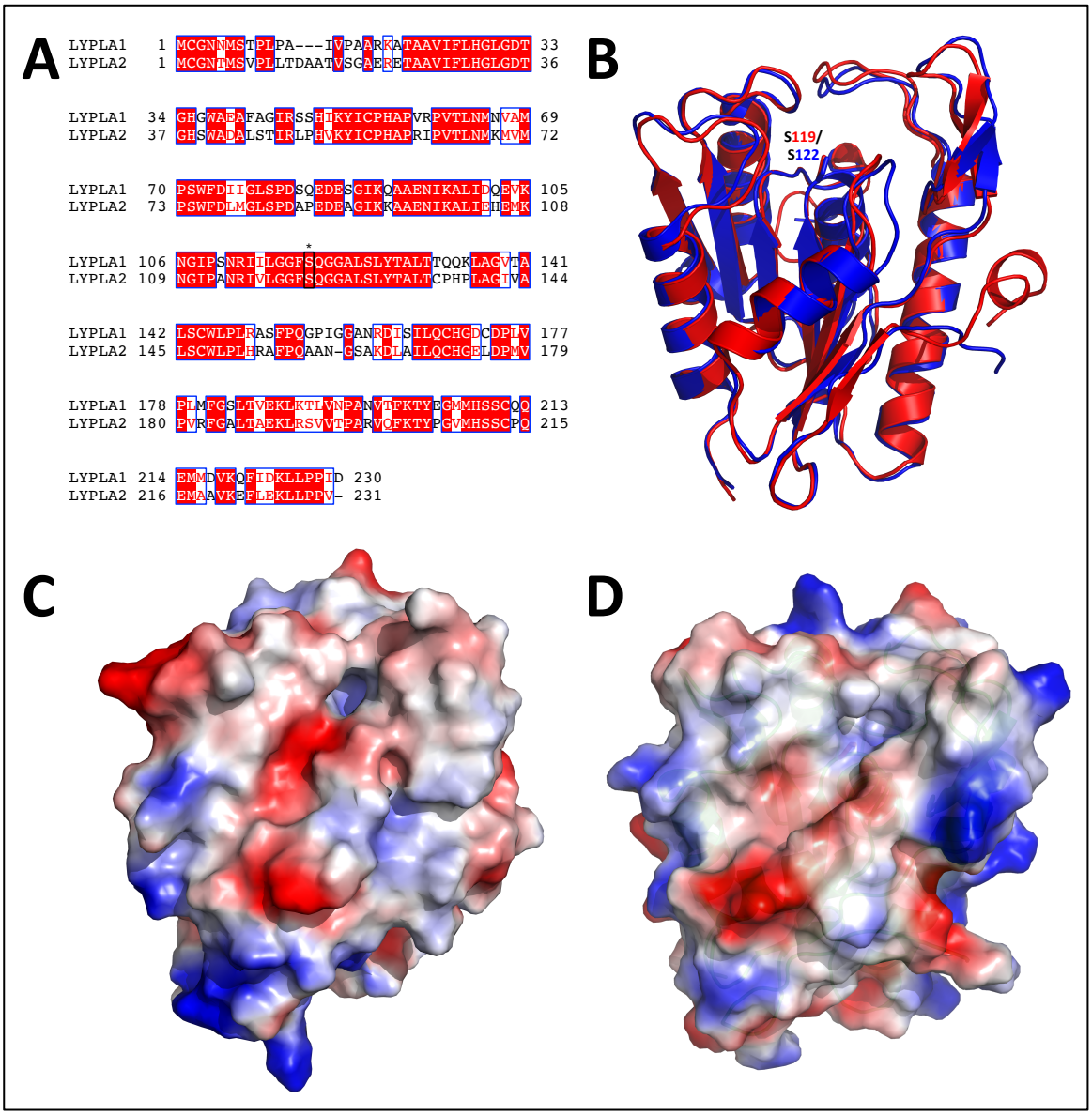

Figure 3.5: Comparison of sequences and structures of LYPLA1 and LYPLA2. (A) Sequence alignment of LYPLA1 and LYPLA2, with identical residues designated by white text highlighted in red, similar residues designated by red text, and similar sequences designated by blue boxes. The catalytic Ser119 and Ser122 of LYPLA1 and LYPLA2, respectively, are marked with a black box and an "*". (B) Structural alignment of LYPLA1 (PDB – 1FJ2), shown in red, and LYPLA2, shown in blue, suggests a high degree of structural similarity between the proteins. Active Ser residues are labeled S119 in red and S122 in blue in LYPLA1 and LYPLA2, respectively. RMSD = 0.878 Å, Q-Score = 0.838. (C) Surface representation of LYPLA1 (PDB – 1FJ2), with red and blue representing negative and positive charges, respectively. (D) Surface representation of LYPLA2-PMSF (PDB – 6BJE), with red and blue representing negative and positive charges, respectively.

Ours is the second structure of LYPLA2 to be published, and the first with a covalent modification of the active site Ser122 (159). Consistent with the previously reported structure, LYPLA2-PMSF crystallized as a dimer, though the enzyme is equally active in monomer and dimer conformations (Figure 3.3). Crystals of apo-LYPLA2 were also obtained but failed to diffract for structure studies due to lattice defects. The data confirm that like LYPLA1, LYPLA2 lacks a cap domain, which is replaced by the β4-α2 loops (highlighted in blue in Figure 3.2) that act as a flexible lid near the active site. The LYPLA2-PMSF structure is very similar to that of LYPLA2-ML349; however, small differences in conformation are noted. For example, the β5-α2 loop in the two structures is present in distinct conformations (Figure 3.4), with the LYPLA2-ML349 loop extended slightly further than that of LYPLA2-PMSF. This suggests the loop is able to move to accommodate substrates or inhibitors binding in the channel adjacent to the active Ser122. Additionally, the modified Ser122-PMSF demonstrates a slight shift in position compared to the unmodified Ser122 of the LYPLA2-ML349 structure, likely due to the steric bulk of the PMSF modification.

Consistent with the relatively high sequence homology of LYPLA1 and LYPLA2 (Figure 3.5A), a least-squares comparison of their coordinates reveals that the two proteins are folded in nearly identical conformations (Figure 3.5B). Superposition across all 215 aligned residues yielded a root-mean-square deviation (RMSD) of 0.878 Å, and a quality of alignment (Q-score) of 0.838, suggesting the protein structures differ by no more than 1 Å (234). This high degree of sequence and structural similarity suggests the two proteins may share significant overlap in substrate specificity and hydrolytic activity. While many of the differences in sequence are found in regions far from the active site of the protein, a group of amino acids with low sequence

homology (Arg149-Ser165 in LYPLA1 and His152-Ala167 in LYPLA2) between the two enzymes are found in an alpha helix near catalytic Ser122 (Figure 3.5A-B). Interestingly, these amino acids form a channel on the surfaces of both LYPLA1 and LYPLA2 as demonstrated in Figure 3.5C-D. The channel on the surface of LYPLA2 appears to be slightly larger than that of LYPLA1, leading to the possibility of a potential binding site for the more rigid and larger PG-G substrates of LYPLA2 that are not hydrolyzed by LYPLA1 in cells (66).

Differences in Sequences Cause Structural Changes Near the LYPLA2 Active Site

The channel at the surface of LYPLA2 is wider and more hydrophobic than that of LYPLA1 as seen in the surface representations of the two enzymes in Figure 3.5C-D. This region of LYPLA2, highlighted in blue in Figure 3.6B, is different in LYPLA2 due to key amino acid changes of α-helix 1. To determine if the size of this channel was the reason for differences in PG-G hydrolytic activity between LYPLAs, Ala43 and Met217 (highlighted in blue in Figure 3.6C) were mutated to Trp to sterically hinder substrates from lying within the channel. We hypothesized that the A43W and M217W mutants would display decreased activity toward PG-G substrates, which would suggest that the wider channel in LYPLA2 is responsible for the increased PG-G hydrolytic activity of LYPLA2 compared to that of LYPLA1.

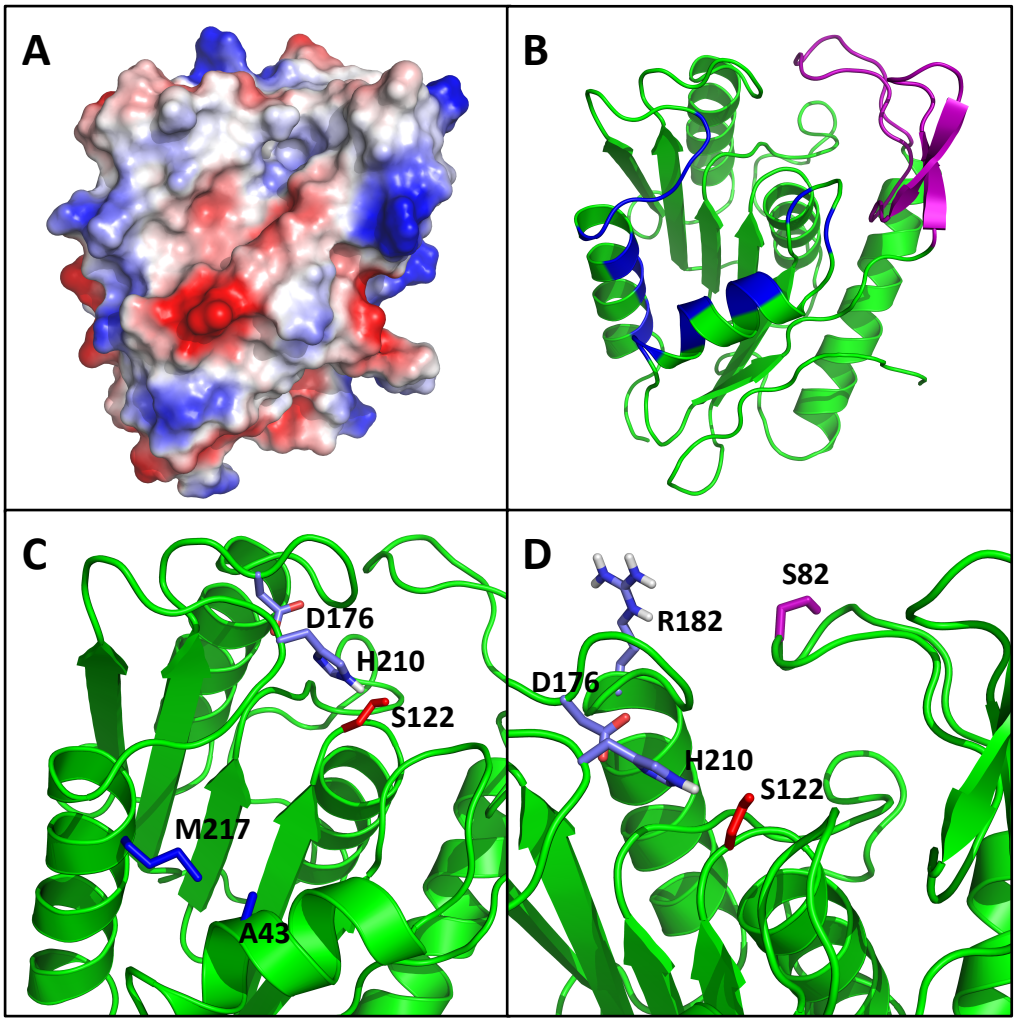

Figure 3.6: Slight differences in the sequence of LYPLA2 cause structural changes to the enzyme that may explain differences in LYPLA activities. Targets of site-directed mutagenesis are highlighted to investigate the role of these regions of LYPLA2 in substrate specificity. **(A)** Surface representation of LYPLA2-PMSF (PDB – 6BJE), with red and blue representing negative and positive charges, respectively. **(B)** Cartoon representation of LYPLA2, with highlighted loop (purple) and channel (blue) regions where variances in LYPLA sequences or PTM state cause structural differences in the conformation of LYPLA2. **(C)** A43 and M217 in the channel region adjacent to the catalytic triad are highlighted in blue. **(D)** Conserved S82, which is only phosphorylated in LYPLA2 and potentially regulates the open/closed state of the flexible loop, is highlighted in purple.

The dynamic loop enveloping the active sites of LYPLA1 and LYPLA2 is another potential mechanism for the different activities toward PG-G substrates. This loop region, highlighted in purple in Figure 3.6B, contains a Ser residue at its tip that is conserved in

LYPLA1 (Ser79 in LYPLA1 and Ser82 in LYPLA2). Ser82 (highlighted in purple in Figure 3.6D) has been identified as a site of phosphorylation, though no such PTM has been observed on Ser79 of LYPLA1 (235). Furthermore, Arg182 of LYPLA2 is present at the top of α-helix 5 in close proximity to Ser82, enabling the potential formation of a phosphoserine-arginine salt bridge. This phosphorylation site would enable regulation of the conformation of the dynamic loop by PTM and offers an explanation to how the active site of LYPLA2 could be altered to accommodate PG-Gs. In contrast to LYPLA2, Arg182 is not conserved in LYPLA1 and is replaced by Met180 removing the possibility of a salt bridge (as depicted in Figure 3.8A), suggesting a LYPLA2-specific mechanism for PTM-based regulation of enzymatic activity. To determine if the phosphorylation state of LYPLA2 is, indeed, a mechanism by which cells mediate PG-G hydrolysis, Ser82 was mutated to Ala or Asp to mimic a permanently unphosphorylated or phosphorylated state, respectively. We hypothesized that the phosphomimetic mutants would display different activities toward PG-G and LysoPL substrates and potentially explain differences in the substrate specificities of LYPLAs.

LYPLA2 Channel Mutants Display Decreased Hydrolytic Activity

LYPLA2 mutants, A43W and M217W, were generated to explore the effects of sterically hindering lipid substrates from binding within the hydrophobic channel depicted in Figure 3.6A-C. The intended effect of these mutants was decreased activity toward one or more of the enzyme's substrate classes depending on their individual binding sites. Indeed, the hydrolytic activity of these mutants compared to WT LYPLA2 was decreased toward both PG-G and LysoPL substrates (Figure 3.7). A43W LYPLA2 hydrolytic activity toward PGE_2-G was only 67.7 ± 3.0% of WT activity, whereas M217W LYPLA2 hydrolytic activity was only 74.3 ± 2.1%

of WT activity. In the case of LysoPLs, A43W LYPLA2 hydrolytic activity toward 16:0 LPC was further decreased at only 21.1 ± 16.1% of WT activity, and M217W LYPLA2 hydrolytic activity was only 36.9 ± 11.8% of WT activity. Additionally, A43W LYPLA2 hydrolytic activity toward 18:0 LPC was 55.2 ± 22.9% of WT activity, and M217W LYPLA2 hydrolytic activity was 43.5 ± 8.5% of WT activity. Together, the overall activity of the channel mutants was generally decreased toward both PG-G and LysoPL substrates compared to that of WT enzyme.

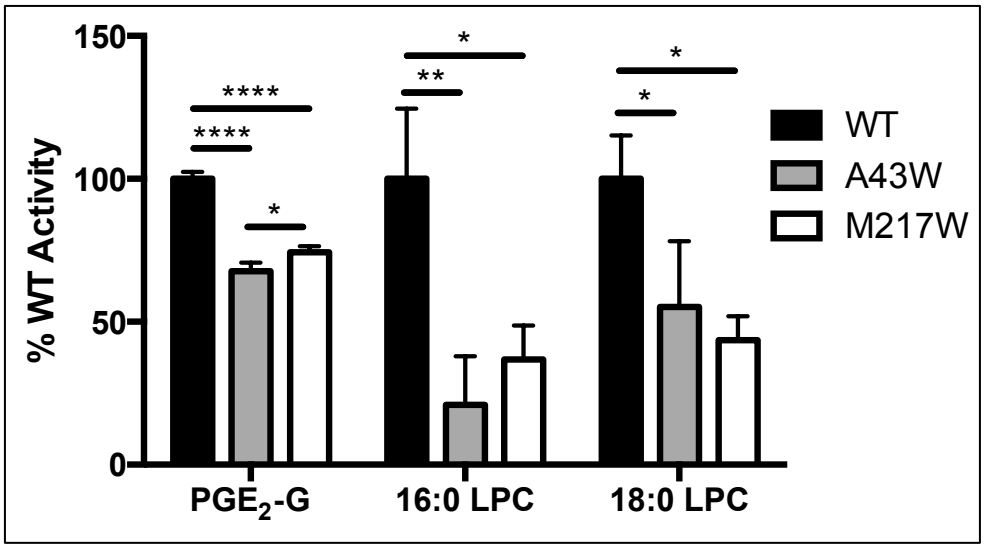

Figure 3.7: LYPLA2 channel mutants display decreased activity toward PG-G and LysoPL substrates. Comparison of activity of recombinant WT, A43W, and M217W LYPLA2 toward PGE_2-G and 16:0 LPC. Data is normalized to WT hydrolytic activity. (N=6) *$P<0.05$, **$P<0.01$, ****$P<0.0001$.

LYPLA2 S82 Mutant Activities Suggest Phosphorylation Regulates Hydrolysis

LYPLA2 mutants, S82A and S82D, were generated to explore the phosphorylation at the dynamic loop by altering the charge of serine by mutating it to an alanine to mimic a permanently unphosphorylated state or to an aspartate to mimic a permanently phosphorylated state (Figure 3.8 B). We hypothesized that phosphorylation of Ser82 would alter the conformation of the dynamic loop by allowing interaction with nearby Arg182 to form a salt

bridge (Figure 3.8A).

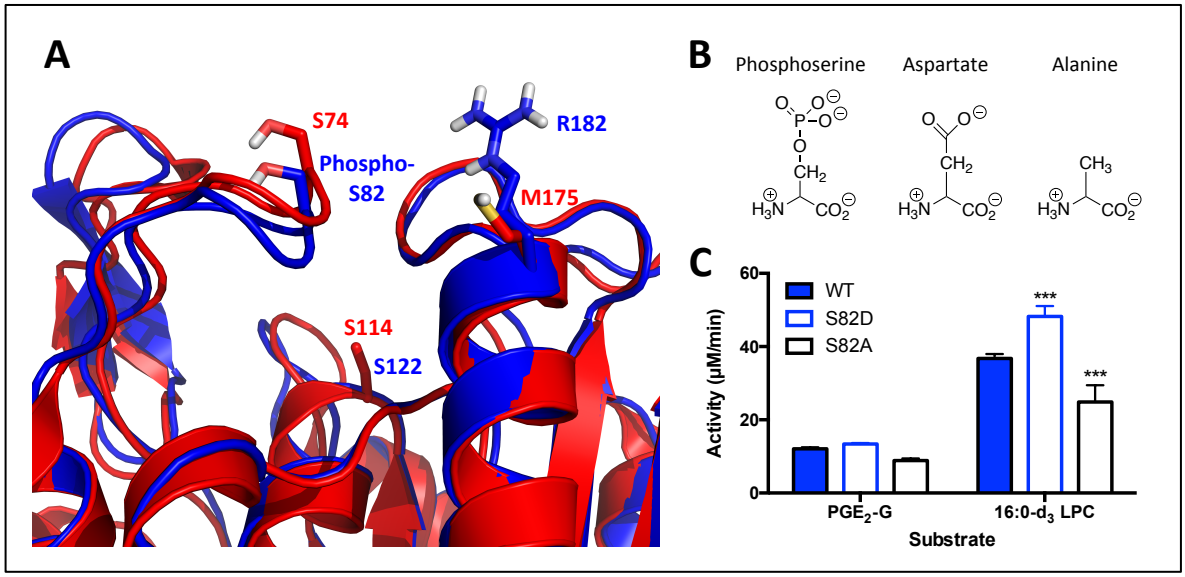

Figure 3.8: LYPLA2 phosphorylation at S82 impacts LysoPL hydrolysis. **(A)** Comparison of LYPLA1 (red) and LYPLA2 (blue) residues near the catalytic serine (S114 and S122 in LYPLA1 and LYPLA2, respectively), with phosphorylated Ser82 and Arg182 highlighted as potential regulators of loop conformation. This binding pair is not present in the structure of LYPLA1. **(B)** Depiction of phosphomimetic mutants, with aspartate acting as a permanently phosphorylated serine mimetic and alanine acting as a permanently unphosphorylated serine mimetic. **(C)** Comparison of activity of recombinant WT, S82A, and S82D LYPLA2 toward PGE_2-G and 16:0-d_3-LPC. Data is expressed as the mean ± SD of product formed (μM) per minute. (N=6) ****P<0.001*.

Whereas altering the charge and shape of Ser82 with the phosphomimetic mutants had no significant effects on PG-G hydrolysis, significant changes in activity were detected in hydrolytic activity toward a representative LysoPL substrate, 16:0-d_3-LPC (Figure 3.8C). In the case of S82D LYPLA2, which represents a permanently phosphorylated enzyme, hydrolytic activity was 48.2 ± 2.9 μM/min compared to that of WT enzyme (36.8 ± 1.2 μM/min). This represents a 31% increase in activity toward LysoPLs. By contrast, in the case of S82A LYPLA2, which represents a permanently unphosphorylated enzyme, hydrolytic activity was 24.9 ± 2.9 μM/min compared to that of WT enzyme. This represents a 67.7% decrease in activity

toward LysoPLs. Together, these data suggest that phosphorylation of S82 promotes hydrolysis of LysoPLs by LYPLA2, whereas unphosphorylated LYPLA2 is less able to hydrolyze LysoPL substrates. Alternatively, phosphorylation has no discernable effect on LYPLA2-mediated hydrolysis of PG-Gs, based on the phosphomimetic mutant studies.

3.4 Discussion

LYPLAs share a high degree of sequence homology and substrate overlap. We hypothesized that the structures of the two enzymes would be accordingly similar, and any slight differences in folding would help explain unique substrate preferences, specifically in regard to PG-G hydrolysis. Indeed, after solving the first reported crystal structure of LYPA2 (Figure 3.2), structural alignment of the enzyme with LYPLA1 revealed nearly identical folding of the proteins (RMSD = 0.878 Å, Q-Score = 0.838) (Figure 3.5). However, two regions of the protein near the catalytic triad displayed unique features between the enzymes that could explain differences in substrate specificity: a hydrophobic channel that is slightly larger in LYPLA2; and a site of phosphorylation at the top of a flexible loop that may regulate its open/closed conformation (Figure 3.6). To assess the role of these regions of LYPLA2 in substrate specificity, we used site-directed mutagenesis to sterically hinder substrates from binding in the channel region with A43W and M217W mutants, and to mimic permanent states of phosphorylated/unphosphorylated with S82D/S82A mutants, respectively.

In the case of the channel region, mutation to Trp decreased the hydrolytic activity of LYPLA2 toward both PG-G and LysoPL substrates (Figure 3.7). While it is possible that the Trp

mutations sterically hindered PG-Gs and LysoPLs from associating with the protein in the proposed binding channel, the more dramatic decreases in activity toward the flexible LysoPL substrates compared to the bulkier, rigid PG-G substrates suggest these effects may not necessarily be due to steric hindrance of substrate binding in the channel. An alternative explanation is that these effects may simply be due to altered folding of the protein in less active conformations due to the drastic changes in pI and folding resulting from the Trp mutations. In the case of the PTM mutants, the phosphoserine mimetic, S82D, displayed increased hydrolytic activity toward LysoPL substrates, whereas the opposite was seen with the unphosphorylated mimetic, S82A (Figure 3.8C). Furthermore, no significant changes to PG-G hydrolysis were detected. These data suggest that LYPLA2 hydrolysis of PG-Gs may simply be regulated in cells by shutting off its LysoPL-hydrolytic activity to allow for increased interaction with PG-G substrates via reduced competition with LysoPLs.

Based on the site-directed mutagenesis studies, substrates bind to LYPLA2 in two potential conformations as demonstrated with computational docking studies in Figure 3.9: lying within the hydrophobic channel, and lying under the dynamic loop in a temporary cavity. Because the sterically hindered channel mutants affected both PG-G and LysoPL substrates, it is possible that both substrate classes bind in the hydrophobic channel. Alternatively, the phosphorylated loop mutant, hypothesized to be in a closed-loop state forming the potential second binding channel, only affected LysoPL substrates, suggesting PG-Gs may not interact with the flexible loop. In either case, it is likely that PG-Gs extrude from the active site toward the exposed hydrophobic channel as depicted in green in Figure 3.9. If phosphorylation of LYPLA2 prevents LysoPL hydrolysis to allow for PG-G hydrolysis via reduced competition, this would explain why PG-G levels are more sensitive to LYPLA2 overexpression/knockdown

(Figure 2.3-4) than LYPLA1 (Figure 2.5).

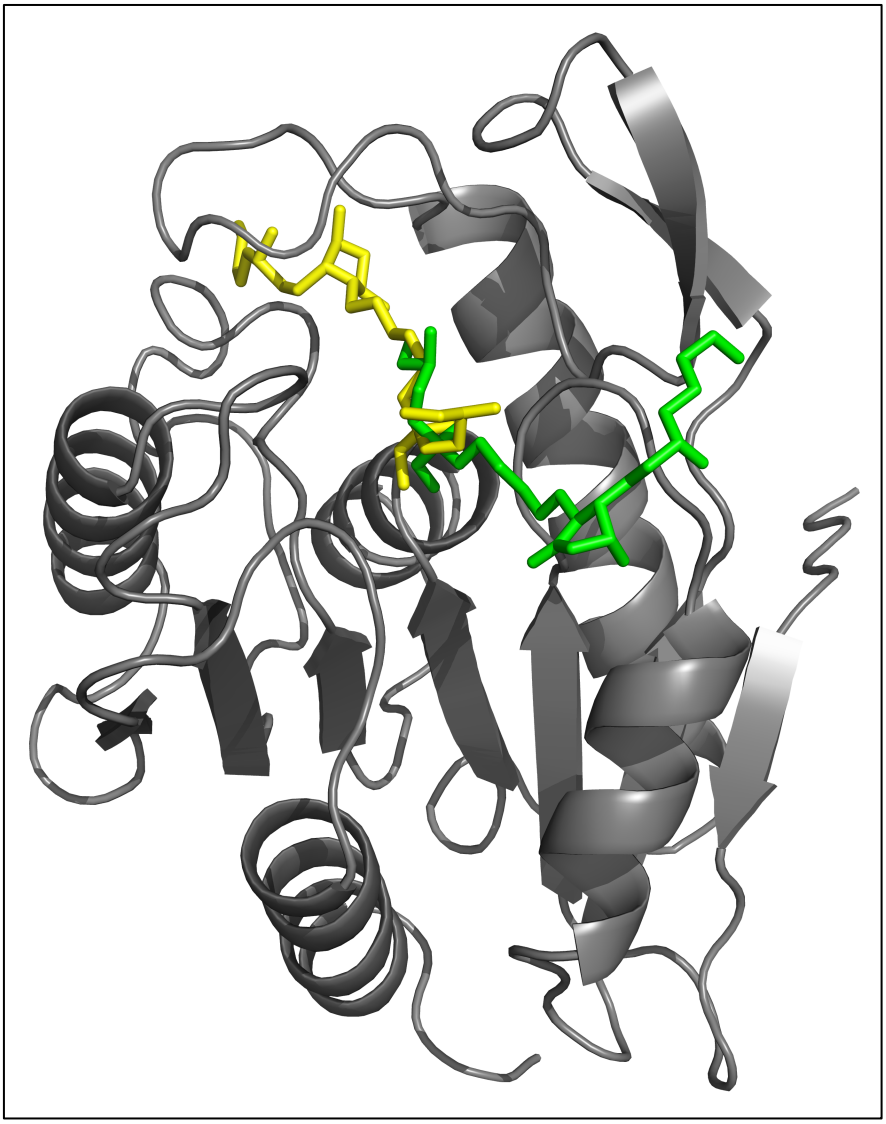

Figure 3.9: Cartoon representation of LYPLA2 with modeled PGE_2-G docked into the active site in two potential conformations. PGE_2-G-Ser lying under the flexible loop is shown in yellow, while PGE_2-G lying within the hydrophobic channel is shown in green.

In contrast to PG-G substrates, the activity of recombinant LYPLA1 and LYPLA2 toward the most prevalent LysoPL substrate, 16:0-LPC, is comparable (Figure 3.1B). This was tested using an isotopically labeled LysoPL species, 16:0-d_3 LPC, in order to avoid

contamination by the FA products of LysoPL hydrolysis. This method allows for LC-MS/MS-based quantitation of LysoPL hydrolysis without relying on expensive radiolabeled lipid substrates or purification steps that reduce sensitivity. These data suggest the proteins have similar activity with respect to LysoPL substrates; however, to determine if the activity of LYPLA1 and LYPLA2 toward other LysoPLs is analogous in a setting where all substrates would be available, cellular models with altered LYPLA expression would be required.

4

Lysophospholipases Cooperate to Mediate Lipid Homeostasis and Lysophospholipid Signaling

4.1 Introduction

LysoPLs are detergent-like lipid species that play a critical role in a wide variety of cellular signaling mechanisms in addition to maintaining the structure, shape, and fluidity of cell membranes (108,110,145). Each LysoPL comprises one nonpolar acyl chain, varying in length and degree of unsaturation, and a polar glycerophosphate headgroup. Based on the structure of the headgroup, LysoPLs belong primarily to one of six classes, including LPAs, LPCs, LPEs, LPGs, LPIs, and LPSs, each with distinct biological functions dependent on physiological location and availability of their respective cellular receptors.

LysoPLs have been shown to elicit a wide range of biological effects, including cell proliferation, intracellular calcium mobilization, metabolic activity, inflammatory and anti-inflammatory processes, and neuritogenesis (136,139,140,144,146,148,151,152,236-244). Regardless of mechanism, accumulated data suggest that LysoPLs play a significant role in modulating the phosphorylation state of the Ras/Raf/MEK/ERK cascade (139,142,146,157,158). This signaling pathway is critical for the regulation of cell cycle progression and differentiation (245-248). Indeed, LysoPL-mediated activation of the MAPK signaling pathway has consistently been shown to induce neuronal differentiation in neuroblastoma cells (139,146,151,243).

As LysoPLs are potent signaling molecules, their cellular levels are carefully regulated

through three primary enzymatic pathways: LYPLA-mediated hydrolysis, acyltransferase-mediated generation of phospholipids, and transacylase-mediated generation of phospholipids. In mammalian cells, the lysophospholipase pathway predominates (209,249-254). The lysophospholipases, LYPLA1 and LYPLA2, are cytosolic serine hydrolases with esterase and thioesterase activity that are partially responsible for the metabolism of LysoPLs. LYPLAs hydrolyze LysoPLs at the sn-1, and to a lesser extent, sn-2 positions to yield a free FA and a derivatized glycerophosphate that can then be recycled by a variety of phospholipases and acyltransferases to restructure the composition of the lipid membrane in a process called the Lands cycle (Figure 4.1) (66,102-104). Inhibition of these regulatory mechanisms and the associated changes in LysoPL homeostasis have been associated with a variety of neurological diseases, including cerebral atherosclerosis, vascular dementia, and Alzheimer's disease (143,156,255-258).

Despite relatively high sequence homology (68% identical, 83% similar), LYPLA1 and LYPLA2 display moderate substrate specificity in regard to LysoPL hydrolysis (209,218-220). For example, whereas LYPLA1 displays general promiscuity in regard to the different LysoPL classes, LYPLA2 is considered more specific, preferring LPCs and LPEs. However, most of this work has been done with recombinant enzymes and exogenous substrate, despite the fact that substrate specificity of serine hydrolases differs between *in vitro* and cellular settings where subcellular location, competitive metabolism, and protein expression levels impact relevant substrate availability (208).

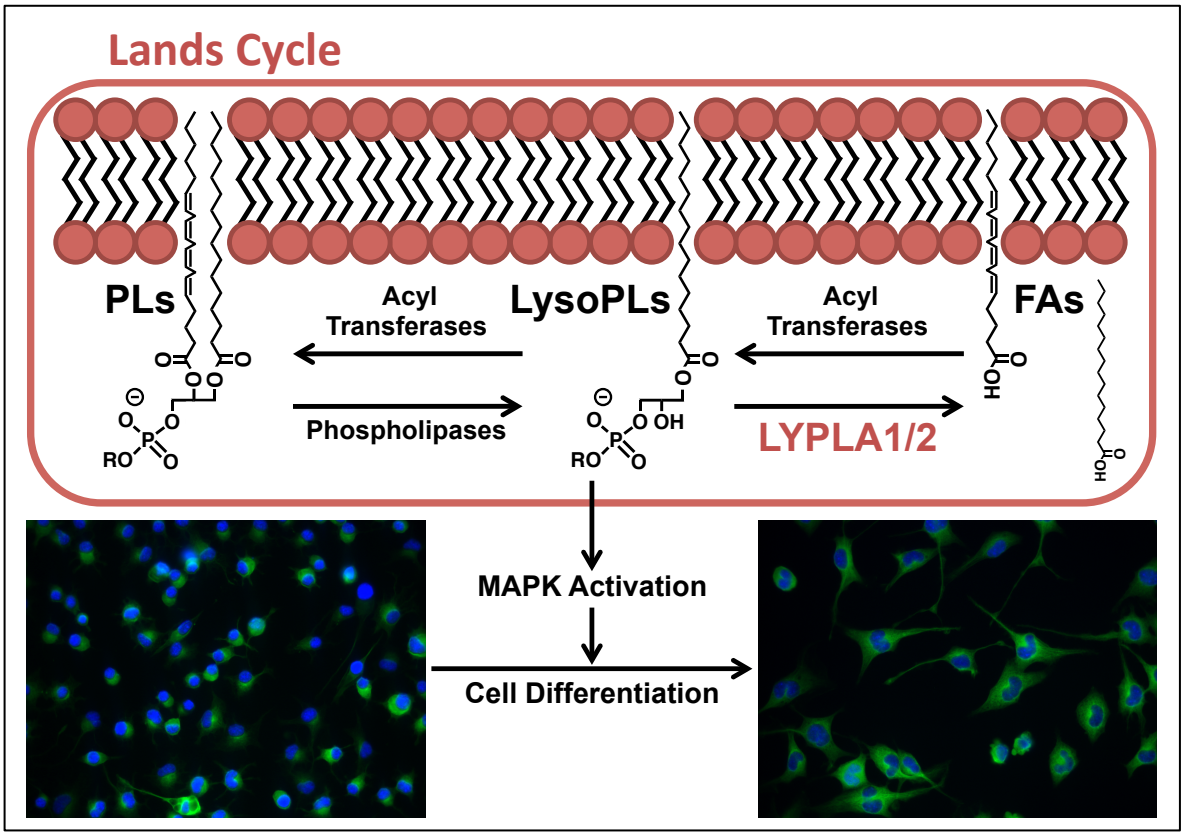

Figure 4.1: The Lands Cycle describes a PL remodeling pathway, demonstrating the interchangeability of acyl moieties and glycerophosphate headgroups by a variety of acyltransferases and phospholipases. Lysophospholipase activity by LYPLA1 and LYPLA2 removes the acyl moieties from various lysoPL species to modulate their potent signaling effects, such as MAPK activation and resultant cell differentiation.

To understand the substrate specificity of LYPLA1 and LYPLA2 in cells, we have utilized a murine neuro2a neuroblastoma model, in which LYPLA activity is relatively high and commonly studied (259,260). Using CRISPR-Cas9 technology, we have generated neuro2a knockout cell lines lacking *Lypla1*, *Lypla2*, or both genes to quantify and compare endogenous LysoPL levels in the absence of respective lysophospholipase activity. This approach offers a physiologically relevant model to determine the roles of LYPLA1 and LYPLA2 in LysoPL hydrolysis, as well as the consequences of the loss of their activity. Our results demonstrate that the roles played by the two enzymes in intact cells are not necessarily reflected by the results

obtained with purified protein preparations.

4.2 Materials and Methods

Chemicals, Reagents, Cells, and Statistics

All reagents were purchased from Sigma Aldrich (St. Louis, MO), unless otherwise stated. PG-Gs and deuterated PGs (PGE_2-d_4) were purchased from Cayman Chemicals (Ann Arbor, MI). All LysoPLs were purchased from Avanti Polar Lipids (Alabaster, AL). LC-MS solvents were from Fisher (Pittsburgh, PA). 16:0-d_3 LPC was synthesized as described above. Recombinant enzyme was expressed and purified as described previously, using cDNA from OriGene Technologies (Rockville, MD) (66). HIS-Select nickel affinity beads were from Sigma Aldrich. HiPrep 16/60 Sephacryl S-200 HR was from GE Healthcare (Little Chalfont, UK). Neuro2a cells were obtained from the American Type Culture Collection (ATCC, Manassas, VA). Cell culture reagents were purchased from Invitrogen (Grand Island, NY). All experiments were performed twice in triplicate, unless otherwise noted, and statistical significance was determined using one-way analysis of variance, unless otherwise noted.

Cell Culture

Neuro2a cells were maintained as adherent cultures in DMEM supplemented with 10% FBS from Atlas Biologicals (Fort Collins, CO). Cells were cultured at 37ºC, 5% CO_2, grown to no more than 75% confluency, and trypsinized to passage.

Generation and Validation of LYPLA Knockout Cells using CRISPR-Cas9

CRISPR technology was utilized to generate genetic knockout cells as described by Ran, et al (261). gRNAs were designed to target early exons of the LYPLA1 and LYPLA2 genes. gRNA oligomers (LYPLA1 gRNA: TCCGATGCCCGCCGTTGTGC; LYPLA2 gRNA: AGCTGAGCGGGAAACGGCCG) were annealed, phosphorylated, and ligated into digested pspCas9(BB)-2A-puro plasmid (plasmid # 62988, Addgene, Cambridge, MA). Neuro2a cells (1.5×10^5) were suspended in 2 mL DMEM supplemented with 10% FBS and plated in 6-well plates. The following day, 5 µg of each plasmid was combined with 10 µL lipofectamine 2000 reagent (Invitrogen) in 1 mL Opti-MEM and incubated at room temperature for 30 min. Neuro2a culture medium was replaced with the appropriate plasmid-lipofectamine solution, and cells were incubated at 37 ºC for 24 h. The medium was then replaced with fresh DMEM plus 10% FBS, and cells were allowed to recover for 24 h at 37 ºC prior to the addition of 0.75 µg/mL puromycin. Cells were incubated at 37 ºC for 48 h before replacing the medium. After recovering for ~1-2 weeks, cells were pelleted, resuspended in sorting buffer (PBS + 4% FBS), and strained to separate clumps of cells. Solutions were sorted by flow cytometry using a 5-laser BD LSRII with a 100 µm nozzle at the Vanderbilt Medical Center Flow Cytometry Core to isolate single cell cultures in 96-well plates for each cell line. Clones were incubated until they reached ~70% confluency and then passaged until enough cells could be harvested for knockout validation via western blotting. Cells lacking both *Lypla1* and *Lypla2* genes, or double knockout (DKO) cells, were generated by repeating this process to target the *Lypla1* gene in the *Lypla2*$^{-/-}$ cells.

Western Blot Analysis

Protein expression was determined by western blot analysis as previously described

(66,262). Samples were separated by SDS-PAGE. Then, proteins were transferred to a nitrocellulose membrane and blocked with Odyssey Blocking Buffer (LI-COR, Lincoln, NE) for 1 h at room temperature, and probed with rabbit anti-LYPLA1 (1:1000 v/v, abcam, Cambridge, UK), rabbit anti-LYPLA2 (1:1000 v/v, Vanderbilt Antibody and Protein Resource Core[2]), rabbit anti-ERK1/2 (1:1000 v/v, Cell Signaling Technologies (CST), Danvers, MA), rabbit anti-phospho-ERK1/2 (1:1000 v/v, CST), rabbit anti-MEK1/2 (1:1000 v/v, CST), rabbit anti-phospho-MEK1/2 (1:1000 v/v, CST), or goat anti-β-actin (1:5000 v/v, Santa Cruz Biotechnologies, Santa Cruz, CA) overnight at 4 °C. Membranes were washed and incubated with IR-visible anti-rabbit or anti-goat secondary antibodies (1:5000 v/v, LI-COR). Blots were visualized using an Odyssey IR Imager.

Assay for LYPLA Activity in Cell Lysates

WT, *Lypla1*$^{-/-}$, *Lypla2*$^{-/-}$, or DKO cells (1 x 10^6) were plated in 8 mL DMEM with 10% FBS in 100 mm plates and incubated at 37 ºC for 24 h prior to harvesting. Cell pellets were suspended in a buffer containing 25 mM Tris (pH 7.5), 0.1 mM EDTA, and 0.1 mM DTT. Cells were sonicated into solution via 10 x 1 s pulses at 35% output. Debris was pelleted via centrifugation at 15,000 *x g* for 10 min, and soluble protein concentration in the supernatant was determined via Pierce™ BCA protein assay (Thermo Scientific, Rockford, IL). Solutions (250 µg/mL) of each enzyme were prepared, and 100 µL aliquots were preincubated at 37 ºC for 5 min. PGE_2-G or 16:0-d_3 LPC (1.5 nmol) was added in 1 µL ethanol, and samples were vortexed and incubated at 37 ºC for 1 h. Enzymatic activity was quenched by adding 1 mL of ice-cold ethyl acetate with 0.5% (v/v) acetic acid containing either 20 ng PGE_2-d_4 or 1 nmol 16:0-d_{31} as internal standards. Samples were vortexed, and organic layers were collected and dried under

nitrogen. FAs were derivatized as described above, and LC-MS/MS analysis was then performed as described below.

LysoPL Extraction

WT, *Lypla1*$^{-/-}$, *Lypla2*$^{-/-}$, or DKO cells (1 x 10^6) were plated in 8 mL DMEM with 10% FBS in 100 mm plates and incubated at 37 ºC for 24 h. Cells were then scraped into 3 mL ice-cold PBS and pelleted. LysoPLs were extracted from cell pellets using a method adapted from Zhao, et al., by resuspending in 200 μL of ice-cold methanol containing 50 nM 17:0 LPA, 250 nM 17:0 LPC, 50 nM 17:1 LPE, 50 nM 17:1 LPG, 50 nM 17:1 LPI, and 150 nM 17:1 LPS (263). Cells were sonicated with 10 x 10 s pulses at 35% output and protein was pelleted. Methanol extracts were collected for lipid analyses via LC-ESI-MS/MS as described below. Protein pellets were resuspended in 1 mL PBS containing 0.2% SDS, sonicated with 10 x 10 s pulses at 35% output, and subjected to BCA assay to quantify input protein.

LC-MS/MS Analysis

For activity assays, samples were run on an LC-MS system consisting of a Shimadzu liquid chromatograph in line with a SCIEX 3200 QTrap mass spectrometer. Analyst software (ver. 1.6.2) was used for instrument control, data acquisition, and data processing. Quantitation was achieved via stable isotope dilution against the indicated internal standard of PGE_2-d_4 or 16:0-d_{31}. For PGE_2 and 16:0-d_3 analyses, reconstituted samples were run in negative mode on a system configured as described in Tables 3.2 and 3.3, respectively. The Luna liquid chromatography reverse phase C18 columns were from Phenomenex (Torrance, CA).

For lipidomics experiments, samples were run on an LC-MS system consisting of a

Shimadzu liquid chromatograph in line with a SCIEX 3200 QTrap or a SCIEX 6500 QTrap mass spectrometer based on methods described by Aaltonen, et al. and Okudaira, et al. (264,265). This method isolates LysoPLs from other glycerolipid and glycerophospholipid species. Analyst software (ver. 1.6.2) was used for instrument control, data acquisition, and data processing. Quantitation was achieved via internal standard dilution against the respective unnatural 17:0 or 17:1 LysoPL depending on the class being investigated. In all cases, the mass spectrometer was configured in electrospray mode and operated in multiple reaction monitoring mode. LPC species were analyzed in positive ion mode with LC parameters described in Table 4.1A. LPE, LPS, LPG, LPA, and LPI species were analyzed in negative ion mode with LC parameters described in Table 4.1B. Fragmentation patterns of all LysoPL species are described in Table 4.2.

A: ***LC Conditions for LysoPL Analysis – Positive Ion Mode***	
Mobile Phase A = 10 mM ammonium acetate, pH 3.3 and methanol; 1:1 B = 2:1 IPA:ACN +1% 1M ammonium formate + 1% formic acid	
Column C18, 5.0 x 0.2 cm	
Initial Conditions Flow = 270 µL/min, %B = 0%	
Time	*%B*
0.30	0%
5.30	100%
7.50	100%
8.00	0%

B: ***LC Conditions for LysoPL Analysis – Negative Ion Mode***	
Mobile Phase A = 10 mM ammonium acetate, unadjusted and methanol; 1:1 B = 2:1 IPA:ACN +4 mM ammonium acetate	
Column C18, 5.0 x 0.2 cm	
Initial Conditions Flow = 280 µL/min, %B = 15%	
Time	*%B*
0.30	15%
5.30	99%
6.00	99%
6.50	15%

Table 4.1: LC conditions for LysoPL analysis. **(A)** LC parameters for mobile phases, column, and LC gradient in positive ion mode. **(B)** LC parameters for mobile phases, column, and LC gradient in negative ion mode.

MS Parameters for LysoPL Species					
Lipid Class	**Mode**	**Acyl Chain**	**Q1**	**Q3**	**CE**
LPC	+	16:0	496.4	184.2	35
LPC	+	18:0	524.4	184.2	35
LPC	+	18:1	522.4	184.2	35
LPC	+	18:2	520.4	184.2	35
LPC	+	18:3	518.4	184.2	35
LPC	+	20:4	544.4	184.2	35
LPC	+	20:5	542.4	184.2	35
LPC	+	22:6	568.4	184.2	35
LPC	+	*17:0 (Int Std)*	*510.4*	*184.2*	*35*
LPI	-	16:0	571.3	255.2	-50
LPI	-	18:0	599.3	283.2	-50
LPI	-	18:1	597.3	281.2	-50
LPI	-	18:2	595.3	279.2	-50
LPI	-	20:4	619.3	303.2	-50
LPI	-	*17:0 (Int Std)*	*583.3*	*267.2*	*-50*
LPE	-	16:0	452.3	255.2	-33
LPE	-	18:0	480.3	283.2	-33
LPE	-	18:1	478.3	281.2	-33
LPE	-	18:2	476.3	279.2	-33
LPE	-	20:4	500.3	303.2	-33
LPE	-	20:5	498.3	301.2	-33
LPE	-	*17:1 (Int Std)*	*464.3*	*267.2*	*-33*
LPA	-	16:0	409.2	152.9	-32
LPA	-	16:1	407.2	152.9	-32
LPA	-	18:0	437.2	152.9	-32
LPA	-	18:1	435.2	152.9	-32
LPA	-	18:2	433.2	152.9	-32
LPA	-	20:4	457.2	152.9	-32
LPA	-	20:5	455.2	152.9	-32
LPA	-	*17:0 (Int Std)*	423.2	152.9	-32
LPS	-	16:0	496.3	152.9	-42
LPS	-	18:0	524.3	152.9	-42
LPS	-	18:1	522.3	152.9	-42
LPS	-	18:2	520.3	152.9	-42
LPS	-	20:4	544.3	152.9	-42
LPS	-	*17:1 (Int Std)*	*508.3*	*152.9*	*-42*
LPG	-	16:0	483.3	255.2	-40
LPG	-	18:0	511.3	283.2	-40
LPG	-	18:1	509.3	281.2	-40
LPG	-	18:2	507.3	279.2	-40
LPG	-	20:4	531.3	303.2	-40
LPG	-	*17:1 (Int Std)*	495.3	267.2	-40

Table 4.2: MS parameters for LysoPLs and odd-numbered LysoPL internal standards, including MS mode, fragmentation patterns, and collision energy.

Immunocytochemistry

WT, *Lypla1*$^{-/-}$, *Lypla2*$^{-/-}$, or DKO Neuro2a cells (4 x 10^3) were plated in 100 µL DMEM with 10% FBS in a 96-well plate. After 48 h, the medium was replaced with 100 µL DMEM containing 2% FBS (established conditions for inducing neuronal differentiation (151,266-268)) and either 2.5 µM retinoic acid, 10 µM PD98059 (an inhibitor of MEK activation used to study neuronal differentiation (269)), 10 µM 16:0 LPA, 10 µM 16:0 LPC, or DMSO control. Cells were cultured for 48 h to promote differentiation, based on a method adapted from Riboni, et al. (270). Cells were then washed 2 x with 100 µL PBS and fixed with the addition of 3.7% formaldehyde in PBS, followed by shaking at room temperature for 20 min. Cells were then washed 2 x with PBS and permeabilized with 0.15% Triton X-100 in PBS for 10 min at room temperature. Cells were again washed 2 x with PBS and blocked with Odyssey Blocking Buffer by shaking for 1 h at room temperature. Cells were then stained with mouse anti-βIII-tubulin (1:2000 v/v, abcam) for 24 h at 4 ºC while shaking. The following day, cells were washed 3 x with TBS containing 0.1% (v/v) Tween (TBS-T) for 10 min while shaking at room temperature, prior to the addition of AlexaFluor 488-conjugated donkey anti-mouse antibody (1:1000 v/v, Life Technologies, Carlsbad, CA) and 4',6-diamidino-2-phenylindole (DAPI) (1:1000 v/v, Invitrogen) for 1 h while shaking at room temperature. Cells were then washed again 3 x with TBS-T and rinsed 3 x with PBS. Stained cells were imaged at 10x power in a 5 x 5 array, and the data were processed using a MetaXpress Micro XL automated microscope imager, which generated a single composite image per well. Neurite outgrowth quantification was performed using the following parameters: minimum neuron area = 120 µm^2, maximum neuron width = 27 µm, minimum neuron intensity above background = 500 gray levels, minimum nuclear width = 5 µm, maximum nuclear width = 14 µm, minimum nucleus intensity above background = 3000

gray levels, maximum neurite outgrowth width = 4 μm, minimum neurite outgrowth length = 10 μm, minimum neurite outgrowth intensity above background = 200 gray levels.

4.3 Results

Knockout of *Lypla* Genes Results in Decreased Hydrolytic Activity

As our results suggested that *in vitro* enzymatic activity does not necessarily reflect the metabolic contribution of that enzyme *in vivo*, we sought to better understand the role of LYPLA1 and LYPLA2 in LysoPL turnover in intact cells. CRISPR-Cas9 technology was utilized to generate stable genetic knockouts of *Lypla1*, *Lypla2*, or both genes in murine neuro2a neuroblastoma cells. Sanger sequencing was used to verify genetic editing at sites in the *Lypla* genes targeted by respective gRNAs and overexpressed Cas9 protein. Genetic knockouts were validated at the protein level using western blotting with antibodies directed toward LYPLA1 and LYPLA2 (Figure 4.2A). Notably, the level of each LYPLA was unaffected by knockout of the other isoform.

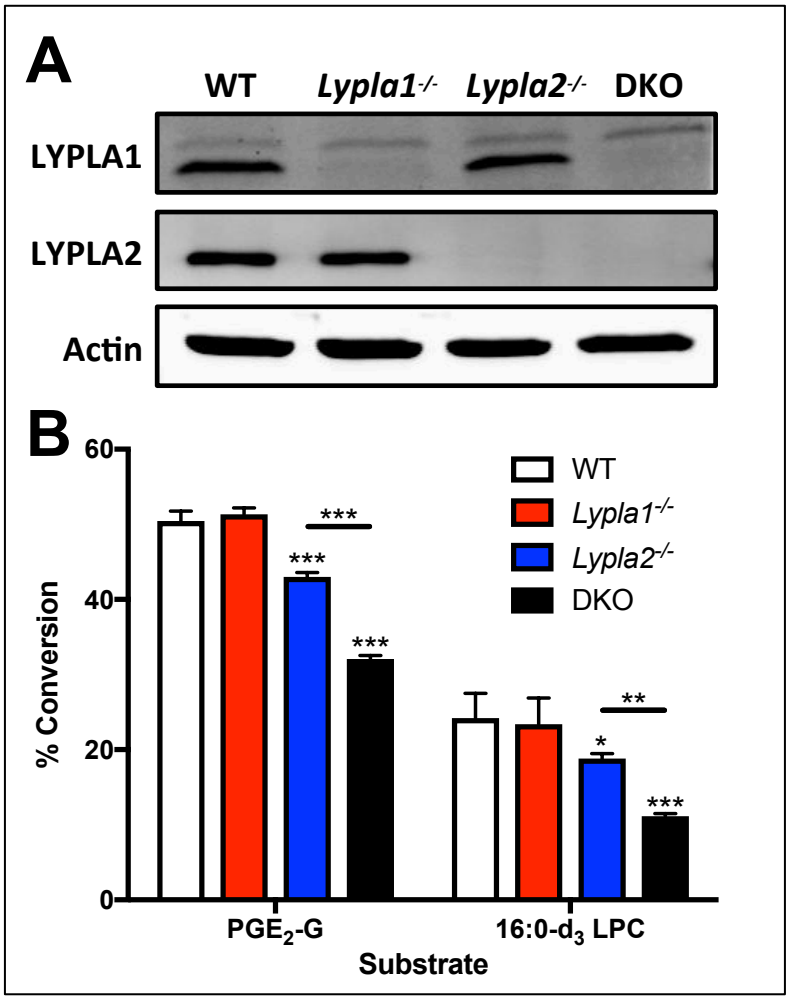

Figure 4.2: Validation of *Lypla1*$^{-/-}$, *Lypla2*$^{-/-}$, and DKO neuro2a cells. **(A)** Western blot analysis of LYPLA1 and LYPLA2 in WT, *Lypla1*$^{-/-}$, *Lypla2*$^{-/-}$, or double knockout (DKO) cells. **(B)** Hydrolytic activity of WT, *Lypla1*$^{-/-}$, *Lypla2*$^{-/-}$, or DKO cell lysates toward representative PG-G and lysoPL substrates; data are shown as percent conversion of exogenous substrate to respective hydrolysis products. *$P<0.05$, **P<0.01, ***$P<0.001$.

The ability of the cell lines to hydrolyze the canonical PG-G and LysoPL substrates of LYPLAs was tested using cellular lysates and the previously described hydrolytic activity assays. In addition to avoiding palmitic acid contamination from plastics and solvents, the use of isotopically labeled 16:0-d_3 LPC in this assay was instrumental to avoid mistaking the endogenous palmitic acid present in cells for hydrolyzed product of the exogenous substrate. This same problem did not arise in the case of PG-G hydrolysis, as neuro2a cells lack the

cyclooxygenase activity required to generate endogenous PG-Gs or PGs. Enzymatic activity of neuro2a lysates that had been normalized for protein concentration was quantified as the percent of each substrate hydrolyzed as described in Figure 3.1A. The percentages of PGE_2-G hydrolyzed in WT, *Lypla1*$^{-/-}$, *Lypla2*$^{-/-}$, and DKO cell lysates were 50.4 ± 1.3%, 51.3 ± 0.9%, 43.0 ± 0.6%, and 32.1 ± 0.4%, respectively, while the percentages of 16:0-d_3 LPC hydrolyzed in WT, *Lypla1*$^{-/-}$, *Lypla2*$^{-/-}$, and DKO cell lysates were 24.2 ± 3.3%, 23.4 ± 3.5%, 18.8 ± 0.7%, and 11.2 ± 0.3%, respectively (Figure 4.2B). Similar to what we observed in our previous work using human cancer cell lines, *Lypla1*$^{-/-}$ cells exhibited the same PG-G hydrolytic activity as WT cells, whereas the activity in *Lypla2*$^{-/-}$ cells was significantly lower than that of WT cells. In DKO cells, PG-G hydrolysis was further decreased, suggesting that both enzymes contribute to PG-G hydrolysis and that LYPLA2 can better compensate for loss of LYPLA1 than vice versa. This same trend is observed with LysoPL hydrolysis. Notably, however, DKO cells retained 64% and 46% of the PGE_2-G and 16:0-d_3 LPC hydrolytic activity of WT cells, respectively, indicating that other enzymes are available to catalyze both reactions. It is not possible to know if expression of these enzymes increases to compensate for the loss of LYPLA1 and/or LYPLA2 in the knockout cells. If so, these results would underestimate the contribution of the LYPLAs to PGE_2-G and 16:0-d_3 LPC hydrolysis in the WT cells.

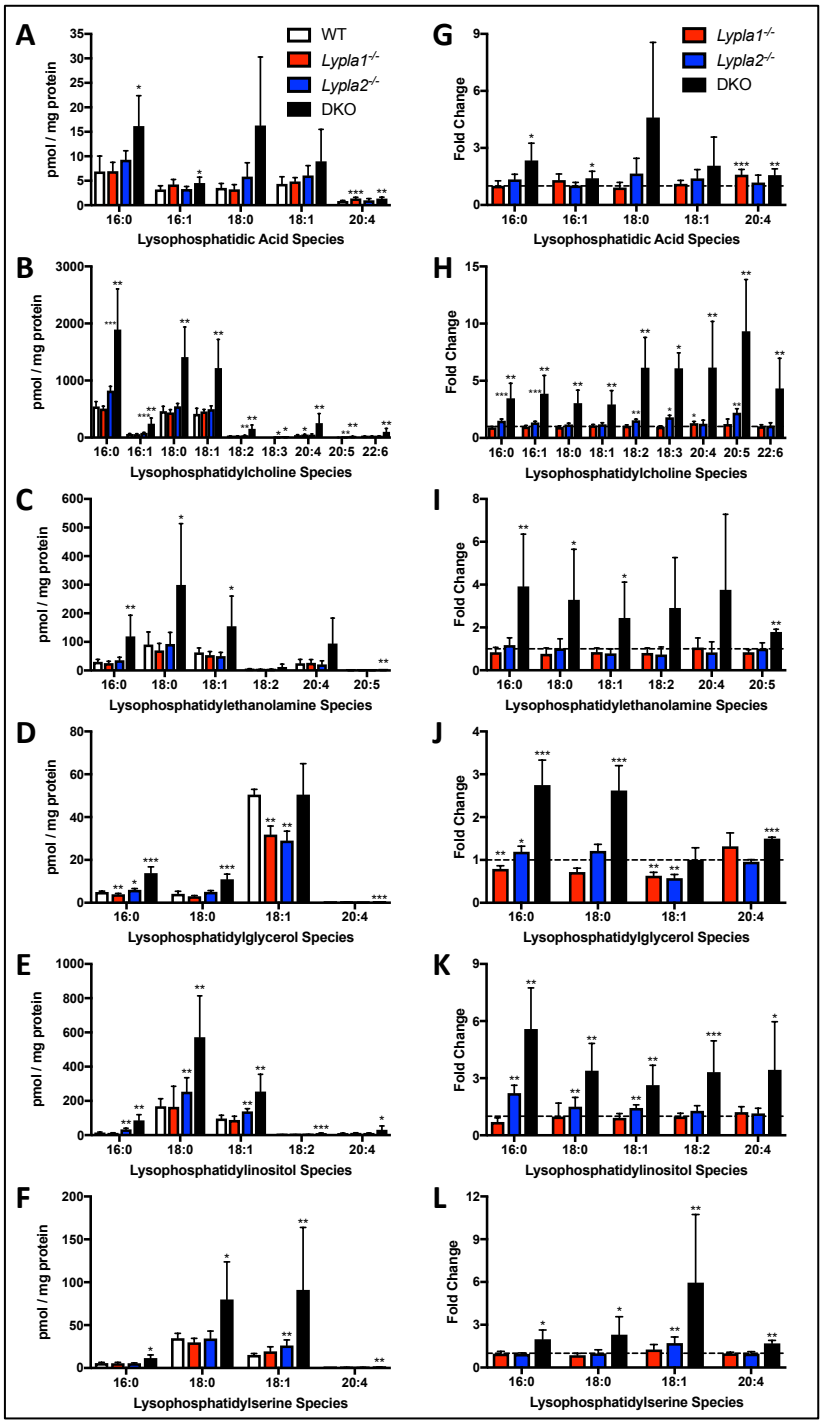

Figure 4.3: LysoPL quantification via LC-MS/MS in methanol extracts of WT, *Lypla1*$^{-/-}$, *Lypla2*$^{-/-}$, and DKO neuro2a cells. Each lipid class was quantified using exogenous 17-carbon length LPL internal standards and normalized to total protein content. **(A-F)** Data represented as pmol LysoPL/mg protein. **(G-L)** Data represented as fold changes normalized to WT values. **P<0.05, **P<0.01, ***P<0.001*, determined by Welch's t-test or the Wilcoxon rank-sum test for samples with normal or abnormal distributions, respectively.

Lipid Species		Cell Line							
		WT		*Lypla1*$^{-/-}$		*Lypla2*$^{-/-}$		DKO	
LPA	**16:0**	6.90	(3.15)	6.95	(1.82)	9.28	(1.84)	**16.2**	**(6.23)**
	16:1	3.23	(0.74)	4.23	(1.05)	3.31	(0.53)	**4.55**	**(1.18)**
	18:0	3.54	(0.92)	3.24	(0.96)	5.85	(2.84)	16.3	(14.0)
	18:1	4.35	(1.49)	4.85	(0.78)	6.08	(2.02)	8.97	(6.54)
	20:4	0.86	(0.11)	**1.38**	**(0.24)**	1.02	(0.34)	**1.36**	**(0.29)**
LPC	**16:0**	545	(86.6)	509	(41.8)	**823**	**(77.1)**	**1890**	**(713)**
	16:1	62.9	(8.52)	62.5	(6.70)	**85.0**	**(6.32)**	**243**	**(101)**
	18:0	464	(83.9)	442	(48.6)	549	(48.9)	**1410**	**(527)**
	18:1	416	(98.5)	460	(34.4)	498	(58.0)	**1220**	**(503)**
	18:2	25.1	(4.48)	26.8	(1.86)	**38.6**	**(2.63)**	**154**	**(66.4)**
	18:3	1.61	(0.30)	1.59	(0.12)	**2.91**	**(0.27)**	**9.81**	**(2.16)**
	20:4	41.4	(10.1)	**53.5**	**(6.34)**	51.4	(13.3)	**255**	**(167)**
	20:5	1.76	(0.46)	2.14	(0.76)	**3.88**	**(0.61)**	**16.4**	**(7.96)**
	22:6	23.3	(3.65)	23.7	(3.19)	24.8	(6.19)	**101**	**(61.5)**
LPE	**16:0**	30.4	(8.19)	25.7	(6.79)	35.8	(10.5)	**119**	**(74.3)**
	18:0	91.0	(44.0)	70.2	(24.6)	93.0	(40.4)	**299**	**(215)**
	18:1	63.3	(15.3)	53.9	(12.3)	50.0	(13.2)	**155**	**(106)**
	18:2	4.23	(1.78)	3.42	(0.99)	3.10	(1.51)	12.3	(9.95)
	20:4	25.2	(13.4)	26.8	(11.2)	21.1	(12.5)	94.5	(88.9)
	20:5	1.29	(0.06)	1.09	(0.16)	1.31	(0.36)	**2.31**	**(0.17)**
LPG	**16:0**	5.04	(0.38)	**3.99**	**(0.36)**	**6.00**	**(0.66)**	**13.8**	**(2.93)**
	18:0	4.18	(1.21)	3.01	(0.37)	5.08	(0.63)	**11.0**	**(2.42)**
	18:1	50.5	(2.44)	**31.9**	**(4.00)**	**29.0**	**(4.40)**	50.5	(14.4)
	20:4	0.24	(0.01)	0.32	(0.08)	0.23	(0.01)	**0.37**	**(0.01)**
LPI	**16:0**	15.4	(2.63)	10.8	(3.26)	**34.2**	**(6.33)**	**86.1**	**(33.3)**
	18:0	169	(44.2)	166	(119)	**254**	**(82.1)**	**572**	**(242)**
	18:1	96.7	(19.3)	88.6	(21.9)	**139**	**(15.6)**	**255**	**(101)**
	18:2	2.60	(0.43)	2.57	(0.44)	3.34	(0.71)	**8.63**	**(4.27)**
	20:4	9.07	(3.27)	11.1	(2.57)	10.5	(2.43)	**31.2**	**(22.9)**
LPS	**16:0**	5.80	(0.76)	5.65	(0.93)	5.52	(0.44)	**11.5**	**(3.73)**
	18:0	34.7	(5.69)	29.9	(4.60)	34.4	(8.78)	**80.0**	**(43.7)**
	18:1	15.3	(1.65)	19.4	(5.31)	**26.3**	**(6.55)**	**91.0**	**(72.9)**
	20:4	0.62	(0.03)	0.61	(0.06)	0.60	(0.08)	**1.05**	**(0.13)**

Table 4.3: Basal LysoPL levels (pmol/mg protein) in WT, *Lypla1*$^{-/-}$, *Lypla2*$^{-/-}$, and DKO cells, presented as mean (standard deviation). Boldface values indicate $P<0.05$, determined by Welch's t-test or the Wilcoxon rank-sum test for samples with normal or abnormal distributions, respectively.

LysoPL Species are Increased in DKO Cells

With the decreased hydrolytic activity observed in the *Lypla* knockout cells, we hypothesized that basal levels of LYPLA substrates would be consequentially increased. To test this hypothesis, we utilized an LC-MS/MS-based targeted lipidomics approach to quantify LPA, LPC, LPE, LPG, LPI, and LPS substrates containing the following acyl moieties at both the sn-1 and sn-2 positions of the glyceryl backbone: 16:0, 16:1, 18:0, 18:1, 18:2, 18:3, 20:4, 20:5, and 22:6. Absolute quantification of each lipid species was normalized to the amount of protein in each sample. As the variance of the LysoPL species were unequal between samples, and values in each sample were not normally distributed, one-way ANOVA could not be used to determine statistical significance. Instead, samples with normal distributions (skewness between -1 and 1) were analyzed by Welch's t-test, and samples with abnormal distributions (skewness less than -1 or greater than 1) were

analyzed by the Wilcoxon rank-sum test. Statistically significant differences in LysoPL levels in *Lypla1*$^{-/-}$, *Lypla2*$^{-/-}$, or DKO cells were compared individually to those of WT cells. Results for every identified LysoPL species are listed in Table 4.3, with values that are significantly different from those of WT cells marked by boldface text. Additionally, these values are displayed in Figure 4.3A-F as absolute quantities, and in Figure 4.3G-L as -fold changes normalized to the LysoPL levels in WT cells (with WT values set to 1, represented by dotted lines).

As expected, LPCs were the most abundant of the LysoPL classes, with more prevalent species found in quantities near 500 pmol/mg protein. LysoPLs containing saturated acyl chains of 16 and 18 carbons were generally found at levels much higher than those containing longer or more unsaturated acyl chains. Whereas the LysoPL concentrations of *Lypla1*$^{-/-}$ cells were mostly

comparable to those of WT cells [with the exception of 20:4 LPA (1.6-fold increase) and 20:4 LPC (1.3-fold increase)], *Lypla2*$^{-/-}$ cells displayed some significant differences from WT cells in certain LysoPL species, such as 16:0 LPC (1.5-fold increase), 18:2 LPC (1.5-fold increase), 18:3 LPC (1.8-fold increase), 16:0 LPI (2.2-fold increase), and 18:0 LPI (1.5-fold increase). However, any differences in the single knockout cells were overshadowed by the much greater increases in the levels of many LysoPLs in the DKO cells. This is especially notable with the LPCs, LPEs, LPIs, and LPSs, of which most lipid species increased by 3- to 9-fold in the DKO relative to the WT cells. These results are consistent with the lysophospholipase activity measured in cell lysates (Figure 4.2B).

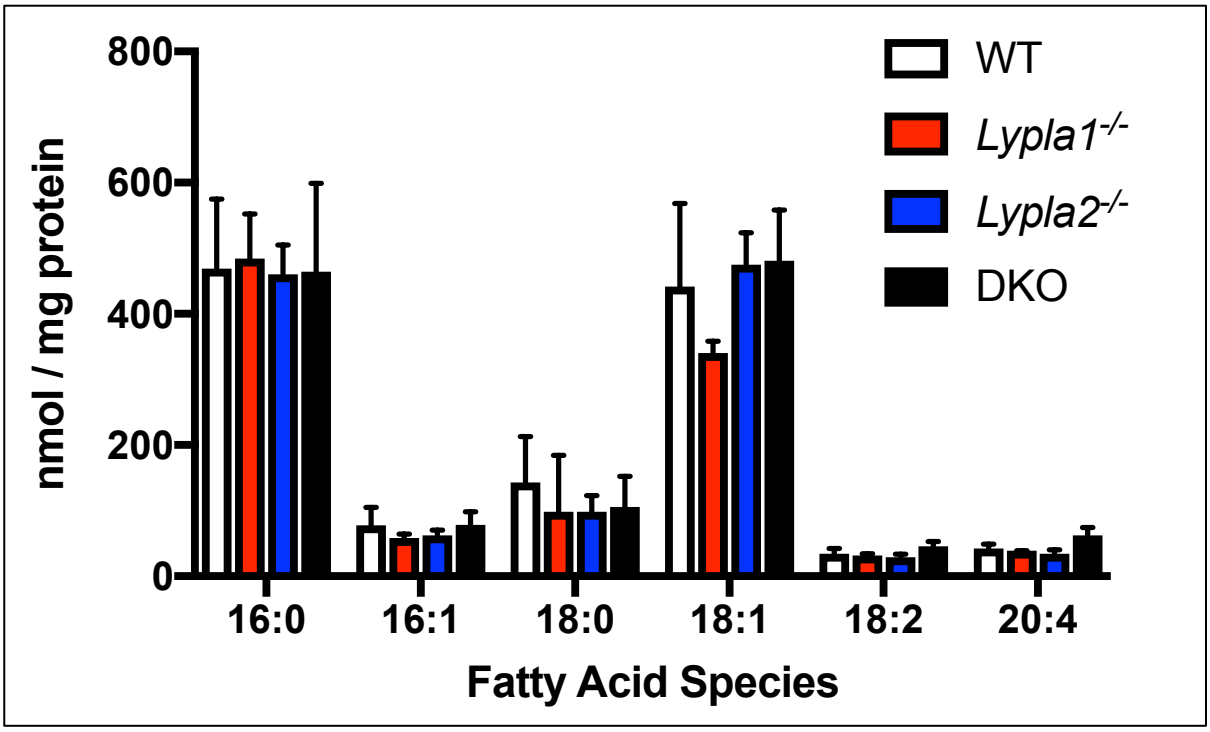

Figure 4.4: FA quantification via PFB-Br-derivatization and LC-MS/MS from methanol extracts of WT, *Lypla1*$^{-/-}$, *Lypla2*$^{-/-}$, and DKO neuro2a cells. FAs were quantified using an exogenous 16:0-d_{31} internal standard and normalized to total protein content (N=6).

Notably, while these large changes in LysoPLs were observed, FA levels in the lipid extracts were quantified via PFB-derivatization, as described above, and no significant differences were seen in the knockout cells (Figure 4.4). This is not surprising as cellular LysoPL levels are roughly 1000-fold lower than those of free FAs; therefore, LysoPL-hydrolysis is unlikely to be a major contributor to the levels of cellular FAs. Together, the data suggest that LYPLA2 makes a greater contribution to LysoPL hydrolysis than LYPLA1 and/or can fully compensate for the loss of LYPLA1. However, the loss of both enzymes appears to unmask a role for LYPLA1 that is not revealed by the single knockout cells.

Interestingly, while lipids in each of the LysoPL classes exhibited significant increases in the DKO cells, albeit at varying magnitudes, there was no consistent pattern in the exact species (as designated by the acyl chain) most affected. This suggests that LYPLA substrate specificity is more dependent on LysoPL class than acyl chain identity, with LPC, LPE, and LPI species in the DKO cells increasing by >300% on average compared to WT cells. Furthermore, in contrast to *in vitro* studies where LYPLA2 has been shown to prefer fully saturated LysoPL substrates, unsaturated LysoPLs of each class in the DKO cells are significantly increased, especially in the LPC, LPE, and LPI classes (66). Indeed, the highest –fold changes between DKO and WT cells occurred in the polyunsaturated LPCs, although these were mostly minor species. Of course, it is possible that neither LYPLA1 nor LYPLA2 plays a direct role in changing some LysoPL levels. It is possible that genetic deletions of multiple lipases involved in the Lands Cycle alter lipid-remodeling pathways, leading to indirect increases of specific LysoPL species that may not necessarily be directly hydrolyzed by either enzyme. Such remodeling might also occur through the compensatory overexpression of other enzymes in response to the deletion. Nevertheless, these data demonstrate that the *in vivo* impact of a specific serine hydrolase cannot be easily

predicted by *in vitro* studies of its substrate selectivity, stressing the importance of cellular models in studying enzymatic activity.

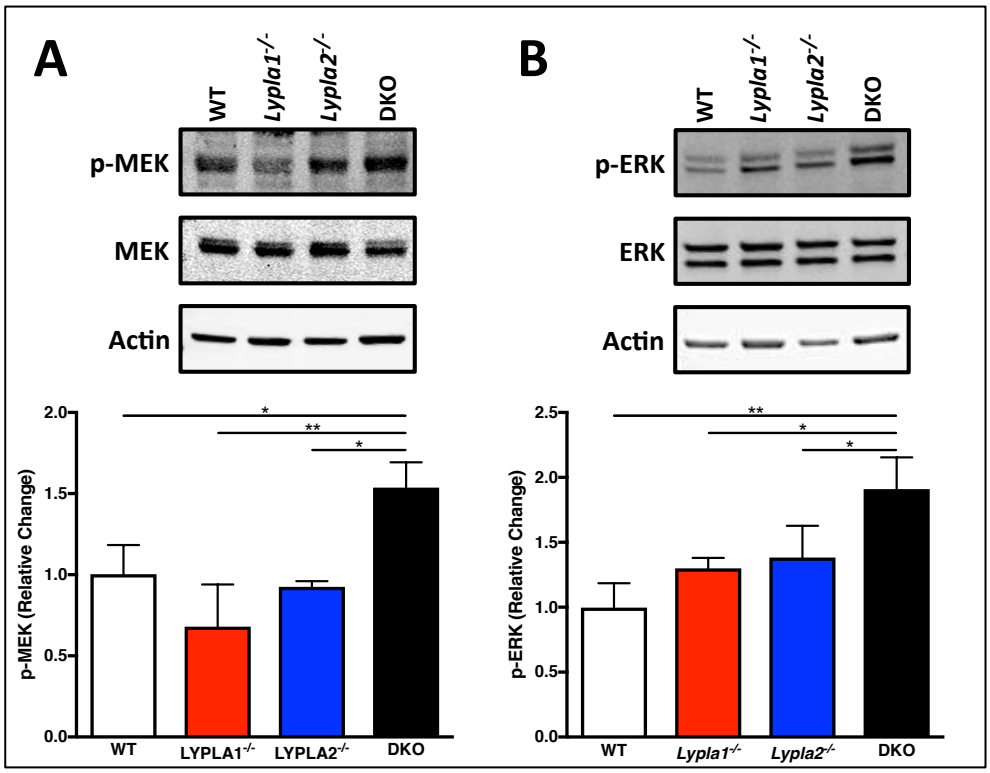

Figure 4.5: Western blotting of Neuro2a lysates from WT, *Lypla1*$^{-/-}$, *Lypla2*$^{-/-}$, and DKO cells. Relative changes were quantified in triplicate analysis and representative lanes are shown. **(A)** Phospho-MEK1/2 is significantly increased in DKO cells. **(B)** Phospho-ERK1/2 is significantly increased in DKO cells. ** $P<0.05$, ** $P<0.01$*

MAPK Signaling Pathway Activity is Increased in DKO Cells

The above data indicated that *Lypla* knockout leads to increases in LysoPLs, which are well-characterized signaling molecules. As activation of the MAPK pathway is commonly associated with LysoPL signaling, we evaluated the phosphorylation states of individual kinases within the MAPK cascade using phospho-specific antibodies and compared them between WT and *Lypla* knockout cells. When normalized to total MAPK/ERK kinase (MEK)1/2,

phosphorylated MEK1/2 was significantly higher in DKO than WT or either single knockout cell lines (Figure 4.5A). Additionally, when normalized to total ERK1/2, phosphorylated ERK1/2 demonstrated this same trend with significant increases observed in DKO cells (Figure 4.5B). The increased phosphorylation states of these proteins suggest that the elevated LysoPLs in DKO cells are activating the MAPK signaling pathway.

Neuronal Differentiation is Increased in LYPLA Knockout Cells

The consequences of ERK phosphorylation have been extensively studied and are dependent on cell type. In neuroblastoma cells, the MAPK signaling pathway is known to induce neuronal differentiation, increasing neurite outgrowth and cell area, and initiating gap junction intracellular communication (139,146,151,243). To assess the impact of MAPK signaling pathway activation in the context of LYPLA deficiency, we utilized immunocytochemistry and high-throughput imaging to compare the morphology and degree of neuronal differentiation between the WT and *Lypla* knockout neuro2a cells. Retinoic acid was also used as a positive control to induce differentiation in WT cells. After fixing and permeabilizing the cells in 96-well plates, the overall shape of each cell was visualized using an antibody directed toward βIII-tubulin (green). Each cell was identified using the nuclear stain DAPI to enable cell counting and normalization between samples (Figure 4.6A). Multiple 10x magnification images were "stitched together" to create one composite image for each well (1 replicate), and images were processed with MetaXpress software using the neurite outgrowth application. This technology allowed us to take large-scale images of entire cell populations in 96-well plates and quickly convert them into quantitative outputs of cell sizes and morphologies as an established method of measuring neuronal differentiation (271,272). Parameters quantified with this application include number of

cells, cell body area, straightness of processes, numbers of processes and branches, and a total outgrowth measurement incorporating the lengths of all processes and branches. These parameters were normalized first to the number of cells in each sample and then to the corresponding values of WT cells to give -fold changes (Figure 4.6B-D). While the straightness of the processes of each cell line was unchanged (data not shown), both the average cell body area and the average total outgrowth of the *Lypla1*$^{-/-}$, *Lypla2*$^{-/-}$, and DKO cells were significantly increased compared to those of WT cells. Furthermore, the average number of processes/cell was significantly increased in the DKO cells to levels comparable to that of WT cells treated with retinoic acid. Additionally, the average total outgrowth of each LYPLA knockout was comparable to that of the WT cells treated with retinoic acid.

Previous studies have shown that some LysoPLs can induce or suppress neuronal differentiation (16:0 LPC and 16:0 LPA, respectively) in neuro2a cells (151). Both of these species are present in FBS, suggesting the possibility that the conditions used to induce differentiation in the cells (a decrease in FBS content in the culture medium from 10% to 2%) resulted in changes in their levels that contributed to the differentiation process. We confirmed the presence of ~800 nM 16:0 LPC and ~30 nM 16:0 LPA in medium containing 2% FBS, suggesting starting concentrations of ~4 μM 16:0 LPC and ~150 nM 16:0 LPA in medium containing 10% FBS. To directly assess the effects of these lipids on Neuro2a differentiation, we conducted experiments in which each lipid was added to differentiation medium (containing 2% FBS) at a concentration of 1 μM. The cells were not viable in the absence of serum, precluding carrying out these experiments under serum-free conditions.

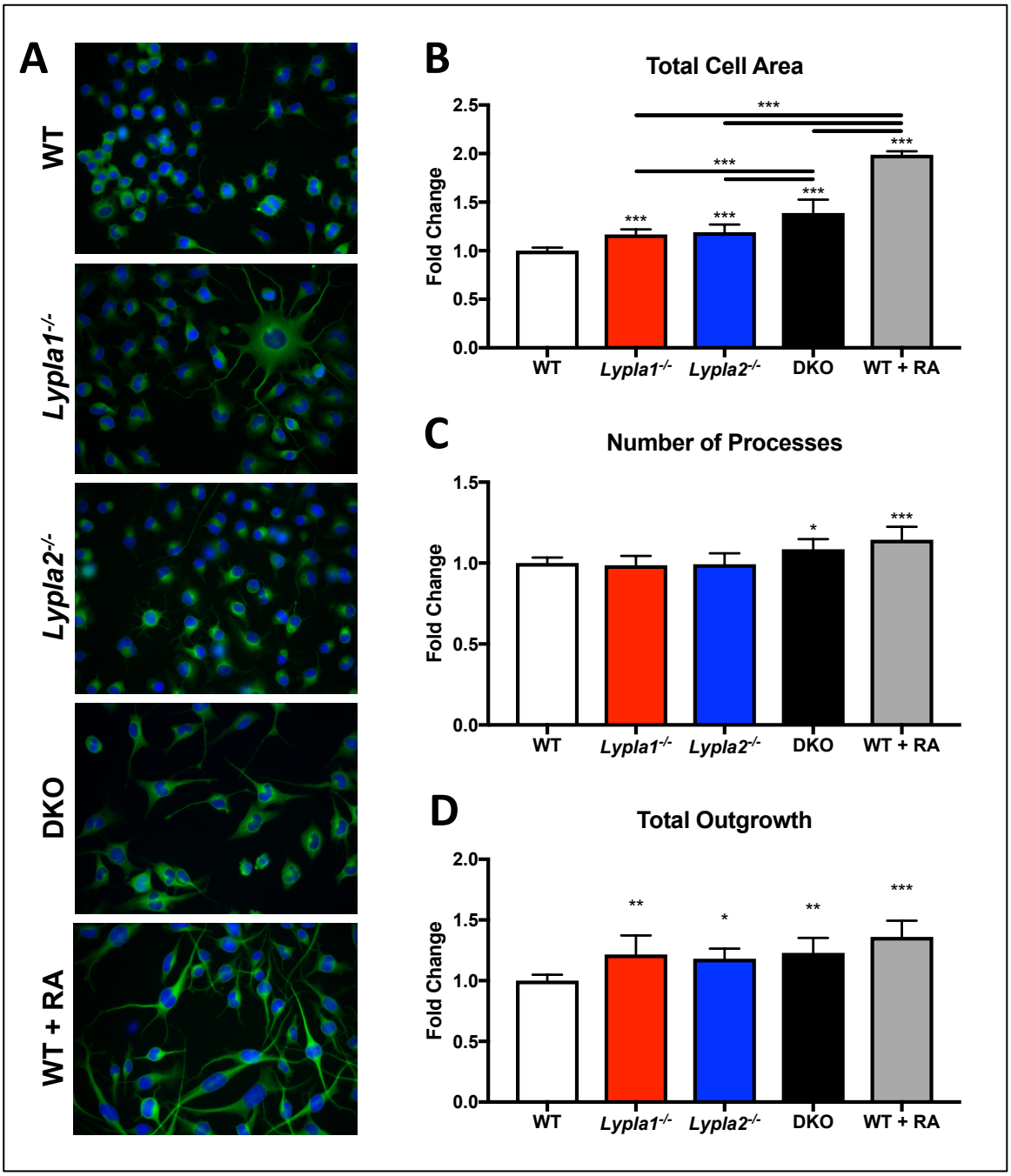

Figure 4.6: Knockouts of *Lypla* genes induce neural differentiation. Representative images were taken from coverslips; data was quantified from images taken of 96-well plates. N=24 (A) Detection of β-III Tubulin (green) and nuclei (blue) in WT, *Lypla1*$^{-/-}$, *Lypla2*$^{-/-}$, and DKO Neuro2a cells by immunocytochemistry. Cells were cultured in DMEM with 2% FBS for 48 hours to induce differentiation prior to morphometric analyses using MetaXPress Imaging software. (B) Average cell area normalized to WT values and represented as fold changes. (C) Average number of processes per cell normalized to WT values and represented as fold changes. (D) Average total outgrowth of cells normalized to WT values and represented as fold changes. **P<0.05, **P<0.001, ***P<0.0001.*

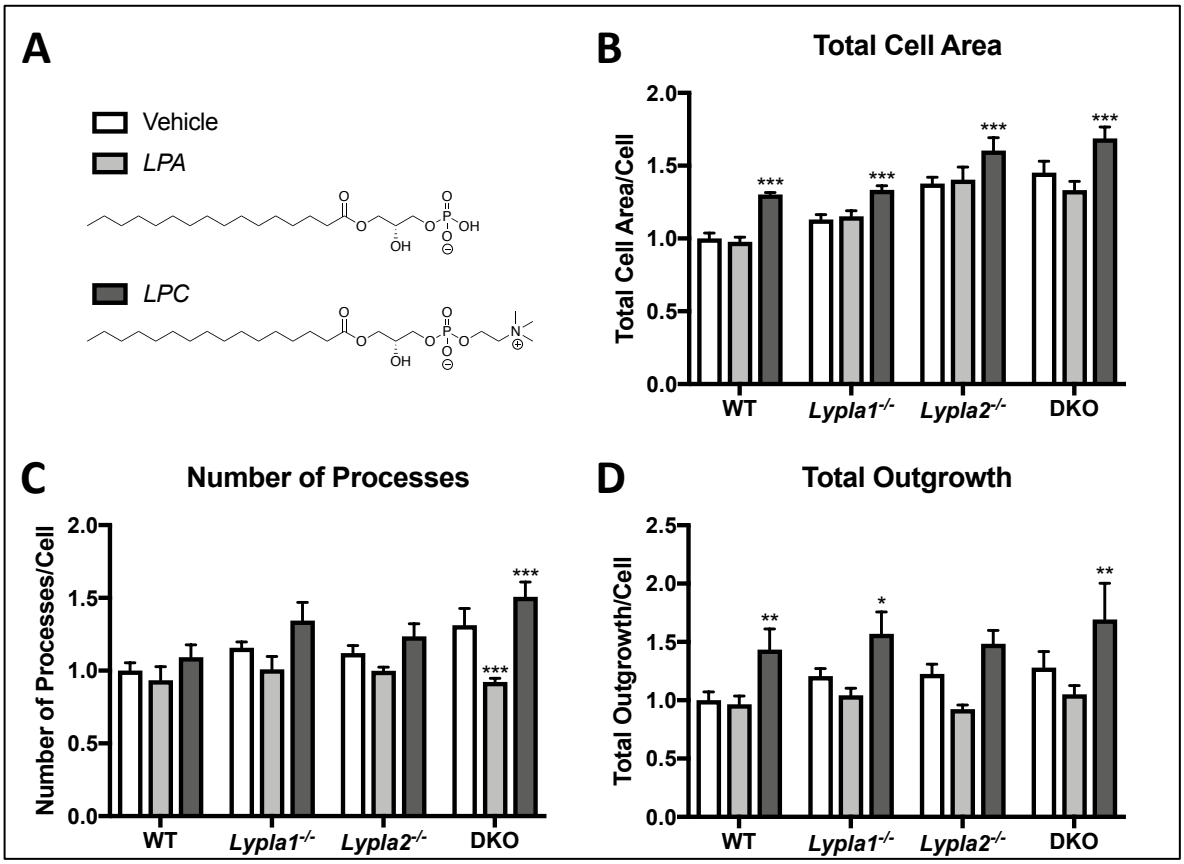

Figure 4.7: Exogenous addition of LysoPLs demonstrate effects of *Lypla*–mediated LPA and LPC hydrolysis on neuronal differentiation. Data was quantified from images taken of 96-well plates (N=8). (A) Legend of each cohort – Vehicle (white), 16:0 LPA (light grey), 16:0 LPC (dark grey). (B) Average cell area normalized to vehicle-treated WT values and represented as fold changes. (C) Average number of processes per cell normalized to vehicle-treated WT values and represented as fold changes. (D) Average total outgrowth of cells normalized to vehicle-treated WT values and represented as fold changes. **P<0.05, **P<0.001, ***P<0.0001.*

As shown in Figure 4.7, the addition of 16:0 LPC significantly increased neuronal differentiation in each cell line, whereas the addition of 16:0 LPA had only modest effects on the average number of processes in DKO cells. These data suggest that the relatively low concentrations of LysoPLs in the 2% FBS-containing medium may be an external source of LYPLA substrates that mediate neuronal differentiation. However, the fact that concentrations of these lipids are actually decreased when the serum concentration is reduced to induce differentiation under our conditions suggests that they are unlikely to be playing a major role in

the phenomena that we observe. Thus, it is most likely that higher levels of basal neuronal differentiation observed in DKO cells, which is comparable to those of WT cells treated with a differentiation agent, are due to increased endogenous LysoPL levels.

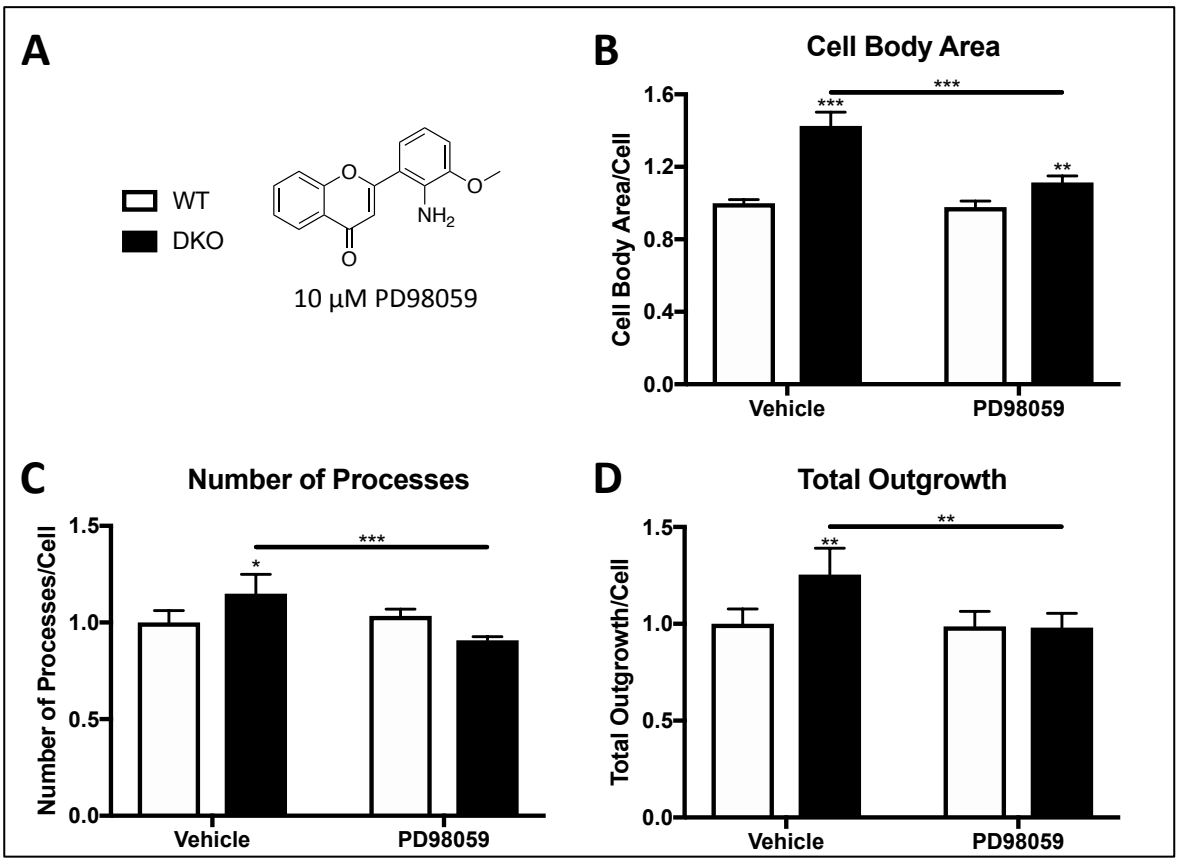

Figure 4.8: PD98059 inhibition of MAPK activation reduces impact of *Lypla* knockout on neuronal differentiation. Data were quantified from images taken of 96-well plates (N=8). (A) Legend of each cohort – WT cells (white), DKO cells (black), treated with DMSO vehicle or 10 µM PD98059. (B) Average cell area normalized to vehicle-treated WT values and represented as fold changes. (C) Average number of processes per cell normalized to vehicle-treated WT values and represented as fold changes. (D) Average total outgrowth of cells normalized to vehicle-treated WT values and represented as fold changes. **P<0.05, **P<0.001, ***P<0.0001.*

To further verify that the increased levels of neuronal differentiation were due to increased MAPK activation, WT and DKO cells were treated with a MEK inhibitor, PD98059, and neurite outgrowth parameters were quantified (Figure 4.8). While outgrowth parameters in

cells treated with the DMSO vehicle were consistent with basal neuronal differentiation in each cell line (Figure 4.6), the cell body area, number of processes, and total outgrowth of DKO cells treated with PD98059 were all significantly reduced. Furthermore, the average number of processes and total outgrowth of PD98059-treated DKO cells was comparable to that of untreated WT cells (Figure 4.8C-D). These data suggest that inhibiting MAPK activation with a MEK antagonist in DKO cells counteracts the effects of increased LysoPLs on neuronal differential. The phenotypic changes to neuritogenesis, especially the increased total outgrowth of DKO cells, are likely due to the increased LysoPL levels and their role in the activation of the MAPK signaling cascade. If this is the case, LYPLAs are demonstrably important in maintaining LysoPL homeostasis and modulating their effects on signaling processes in cells.

4.4 Discussion

LysoPL metabolism is a significant component of the Lands cycle, modulating the levels of potent bioactive signaling molecules and preventing membrane disruption (102,104). LYPLA1 and LYPLA2 are responsible for a substantial fraction of this activity, and, consequentially, for regulating the signaling effects of their respective LysoPL substrates (209). While past work has suggested LYPLA1 and LYPLA2 display relative substrate specificity in terms of LysoPL hydrolysis, these studies have been done using recombinant enzyme and fail to accurately portray the roles of LYPLAs in cellular settings. To compare the activities of these two enzymes, we have taken a multifaceted approach using *in vitro* and cellular assays to determine how LYPLAs maintain LysoPL homeostasis.

We have characterized the roles of LYPLA1 and LYPLA2 in LysoPL hydrolysis in a neuroblastoma cell model in which *Lypla1*, *Lypla2*, or both genes were deleted. The results demonstrated minimal effects of *Lypla1* deletion on LysoPL levels, although it interesting to note that the only LysoPL species that increased in *Lypla1*$^{-/-}$ cells contained 20:4, suggesting that LYPLA1, specifically, may play a role in regulating arachidonate levels and eicosanoid biosynthesis. In contrast, *Lypla2* deletion affected a greater number and broader diversity of lipid species than *Lypla1* deletion, and substantial LysoPL elevation occurred only with knockout of both enzymes (Figure 4.3, Table 4.3). In general, the data suggest that the two enzymes act cooperatively, with apparent compensation of one isoform for the loss of the other, although that occurs without substantial changes in protein expression (Figure 4.2A). The consistent levels of protein expression in the knockout cells suggest the enzymes are constitutively expressed to modulate LysoPL levels. However, it is possible that the enzymes could undergo activation via post-translational modification; both LYPLA1 and LYPLA2 are palmitoylated in cells at conserved Cys2, LYPLA1 is acetylated at Lys224 and LYPLA2 is phosphorylated at Ser82 (186,235,273). Nevertheless, it appears that LYPLA1 and LYPLA2 are able to hydrolyze the majority of LysoPLs in cells despite the differential preferences for LysoPL classes observed *in vitro*. One must interpret these data with caution, however, as lysates from DKO cells retained substantial hydrolytic activity (Figure 4.2B). The specific nature of this activity is not known, but it almost certainly has an impact on the ultimate pattern of LysoPL changes observed in the various cell lines that we explored.

In neuroblastoma cells lacking both *Lypla1* and *Lypla2*, lysophospholipase activity is sufficiently compromised to lead to increased LysoPL levels (Figure 4.3) and increased activation of the MAPK signaling pathway (Figure 4.5). Correspondingly, these data suggest that

LYPLA1 and LYPLA2 are able to modulate cell differentiation and neuritogenesis in neuroblastoma cells through their hydrolytic metabolism of LysoPLs (Figure 4.6). The role of lysophospholipase-dependent modulation of LysoPL levels in physiological models of neurodifferentiation will be an interesting subject for further study.

In summary, we have closely compared the activities of LYPLA1 and LYPLA2 and determined that the two proteins have significant overlap in their cellular functions. Both enzymes cooperate to maintain lipid homeostasis in cells; however, losing the activity of only one of these enzymes seems to have modest to no effect on LysoPL levels, suggesting the counterpart lysophospholipase is able to compensate for that loss. However, when both enzymes are knocked out, the cells are unable to regulate levels of LysoPLs, leading to aberrant LysoPL-dependent signaling, an unregulated Lands cycle, and associated phenotypic and morphological changes to the cells. This work is one of the first documented studies of LYPLA activity in a cellular setting and gives a clear answer to why inhibiting only LYPLA1 or LYPLA2 seems to have little to no effect (222,274). We have focused here on the role of these proteins in maintaining LysoPL homeostasis, but their redundancy in substrate specificity may also apply to their other major function, namely the thioesterase activity that results in the depalmitoylation of protein substrates (172). While relatively few palmitoylated proteins have been identified as specific substrates for either LYPLA, it has been shown that incomplete knockdown or inhibiting only one LYPLA is ineffective, and dual inhibition of LYPLA1 and LYPLA2 with palmostatin B is often required to affect global protein palmitoylation (190,222,274). These trends are consistent with our findings that LYPLA1 and LYPLA2 seem to share LysoPL substrates in cells and offer credence to a dual inhibition/knockout approach to further study their physiological and pathophysiological functions.

5

Lysophospholipases Regulate Dynamic Protein S-Palmitoylation as Acyl-Protein Thioesterases

5.1 Introduction

In addition to their role in the degradation of LysoPLs, LYPLAs display other activities (Figure 5.1). For example, the monoacylglycerol and endocannabinoid, 2-AG, is oxygenated by COX-2 to generate PG-Gs (47,221). Our previous work has identified LYPLA2 as a PG-G hydrolase, converting PG-Gs to free PGs (66). Furthermore, LYPLA1 and LYPLA2 are among a small pool of enzymes known to exhibit thioesterase activity on palmitoylated proteins such as the $G_{5\alpha}$ subunit of heterotrimeric G proteins and Ras (183,190,222). This post-translational modification serves to alter protein conformation and/or tether a cytosolic protein to a lipid membrane with the addition of a lipophilic acyl moiety covalently bound to cysteine residues via a thioester linkage (168,177,184,275). LYPLA1 and LYPLA2 act to remove these acyl modifications as part of a dynamic palmitoylation process, regulating the subcellular location and conformation of a variety of cellular proteins (183,184,186,222).

While LYPLA1 and LYPLA2 have demonstrated acyl-protein thioesterase activity in cellular settings, most of this work was done using general thioesterase inhibitors, such as palmostatin B (186,190,276). Resulting global changes to protein palmitoylation is likely due to the inhibition of LYPLAs in addition to numerous other enzymes, such as ABHD17 or a plethora of unidentified acyl-protein thioesterases. Some studies have isolated specific lipoprotein

substrates of LYPLA1 and LYPLA2, specifically, using their appropriate inhibitors, ML348 and ML349, respectively (222,233). However, we have shown that the IC_{50} of these inhibitors is relatively high, and inhibiting LYPLAs in cells would require concentrations of these compounds well above levels at which they remain selective (66). Alternatively, we used CRISPR/Cas9 genome editing to generate knockout neuro2a cells, an established cell model of dynamic palmitoylation processes (277,278), lacking the genes for *Lypla1*, *Lypla2* or both to prevent their specific acyl-protein thioesterase activity and determine individual lipoprotein substrates of each respective enzyme.

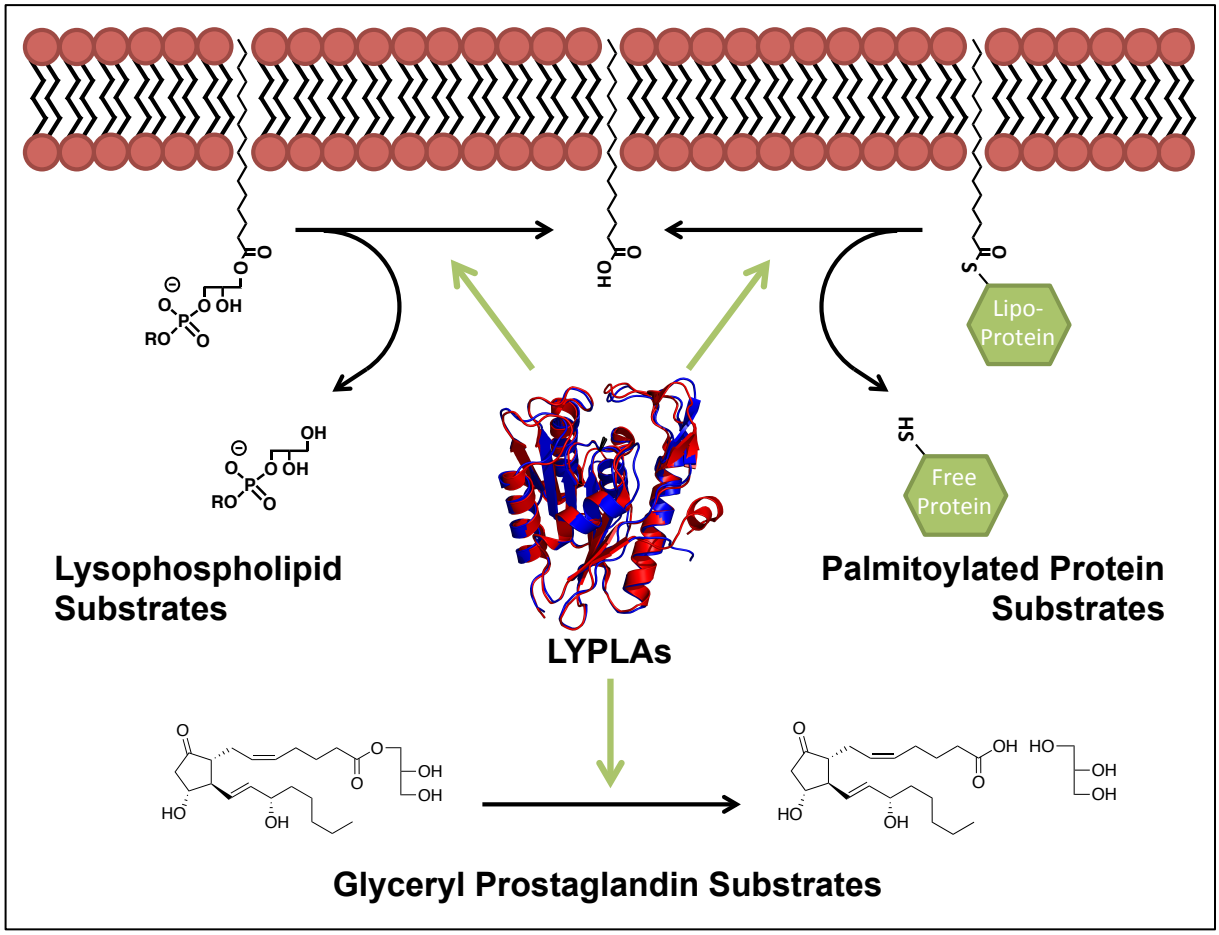

Figure 5.1: LYPLAs hydrolyze three different classes of substrates: LysoPL substrates, palmitoylated protein substrates, and PG-G substrates.

To determine changes in protein palmitoylation, we utilized a chemical reporter with an alkyne tag, *a*PA, a common tool used to visualize protein palmitoylation in cells (166,279). The presence of the bioorthogonal alkyne functional group enables fluorescent labeling and visualization or biotin labeling and streptavidin enrichment via click chemistry. These tools, in conjunction with our genetic knockout cell lines and SILAC, enable us to determine global and individual changes of palmitoylated protein substrates of LYPLA1 and LYPLA2, as well as common lipoprotein substrates between the two acyl-protein thioesterases. This work represents the first examples of coupling CRISPR technology with global palmitoylation changes, and clarifies the mechanisms of dynamic protein palmitoylation in a cellular setting.

5.2 Materials and Methods

Chemicals, Cells, and Reagents

All reagents were purchased from Sigma Aldrich (St. Louis, MO), unless otherwise stated. aPA was synthesized by Ned Porter's lab. ML349 was synthesized as described above. LC-MS solvents were from Fisher (Pittsburgh, PA). Recombinant enzyme was expressed and purified as described above. RAW264.7 macrophages were obtained from the American Type Culture Collection (ATCC, Manassas, VA). Genetically edited neuro2a cells were generated as described above. Cell culture reagents were purchased from Invitrogen (Grand Island, NY). All experiments were performed twice in triplicate, unless otherwise noted, and statistical significance was determined using one-way analysis of variance, unless otherwise noted.

Cell Culture

Neuro2a cells were maintained as adherent cultures in DMEM supplemented with 10% FBS from Atlas Biologicals (Fort Collins, CO). Cells were cultured at 37ºC, 5% CO_2, grown to no more than 75% confluency, and trypsinized to passage. For SILAC experiments, WT neuro2a cells were cultured in isotopically labeled light media (0.1 g/L natural abundance isotope amino acids) from Fisher Scientific (Pittsburgh, PA) with 10% dialyzed FBS from Fisher Scientific and DKO neuro2a cells were cultured in isotopically labeled heavy media (0.1 g/L $^{13}C_6{}^{15}N_2$ Lys and $^{13}C_6{}^{15}N_4$ Arg) with 10% dialyzed FBS. Each cell line was passaged at least 6 times, until all Lys and Arg were replaced by the labeled amino acids.

***a*FA Enrichment**

WT, *Lypla1*$^{-/-}$, *Lypla2*$^{-/-}$, or DKO neuro2a cells or RAW264.7 macrophages (1 x 10^6) were plated in 8 mL DMEM with 10% FBS and incubated at 37ºC with 5% CO_2. After 24 h, media was replaced with DMEM without FBS or supplemented with 10% FBS containing EtOH vehicle, 1 μM *a*FAs (*a*AA, *a*LA, *a*PA), or 0.1, 1, 10, 50, or 100 μM *a*PA. In experiments with RAW264.7 cells, DMSO vehicle or 10 μM ML349 were also added with *a*FAs. After another 24 h, media was aspirated, cells were washed with 3 mL ice-cold PBS, and harvested into 3 mL ice-cold PBS.

LC-MS/MS Analysis

Analysis of *a*FAs was accomplished by reverse phase chromatography followed by mass spectrometric detection by selected reaction monitoring (SRM) with low collision energy (-5 V) and using the same mass for Q1 and Q3. The instrument was a Shimadzu LC-20 HPLC system

coupled to an Applied Biosystems 3200 QTrap mass spectrometer. Separation of FAs was achieved by gradient elution of a Phenomenex Luna C18 column (50 mm x 2.0 mm, 3 μm particle size). Solvent A was HPLC grade water with 0.1% formic acid, and solvent B was ACN with 0.1% formic acid. Samples were injected onto the column with a starting condition of 50% solvent A and 50% solvent B at a flow rate of 0.5 mL/min. After 0.5 min, a linear gradient of increasing solvent B to 99% was run over 2 min and then held for 4 min before returning to 50% B over 0.1 min. SRM transitions were as follows: *a*AA transition m/z 300.4→300.4; *a*LA m/z 276.4→276.4; *a*PA m/z 251.1→251.1; 17:0 m/z 269.5→269.5.

Click Chemistry Labeling of *a*FAs

Cell pellets were lysed in 200 μL ice-cold PBS containing protease inhibitor tablet (0.2 mg/mL) via sonication (2 rounds of 10 x 10 sec pulses). Insolubles were removed via centrifugation at 15,000 *x g* for 10 min, and soluble protein concentration in the supernatant was determined via Pierce™ BCA protein assay. 1 mg of protein from each cell lysate was diluted to 300 μL solutions, and the following click reagents were added: 0.5 μL of 50 mM CuSO4 (aq), 0.5 μL of 50 mM TCEP (aq), 1.5 μL of 1.7 mM TBTA (DMSO), 0.5 μL of 1 mM N_3-AlexaFluor or 0.5 μL of 10 mM N_3-biotin. In the case of biotin conjugation, lysates were "pre-cleared" by incubating with streptavidin beads to remove any endogenously biotinylated proteins prior to the click chemistry reaction. Each solution was vortexed and incubated at room temperature for 1 h while protected from light.

SDS-PAGE Analysis and Protein Visualization

Protein expression was determined by western blot analysis as described above. Protein

palmitoylation levels were determined by fluorescent labeling (AlexaFluor labeled protein) or IR-streptavidin visualization (biotin-labeled protein). 20 μg of protein were loaded into each well of a 12% SDS-PAGE gel and gel was run at 100 V for ~2 hr. In the case of AlexaFluor labeling, gels were imaged on fluorescent scanner (590 nm excitation/ 617 nm emission). Each lane of palmitoylated protein was normalized to total protein levels determined by Coomassie staining as described above immediately after fluorescent imaging. In the case of IR-streptavidin visualization, protein was transferred to nitrocellulose for Western blot analysis as described above. Actin was used as a loading control, and biotinylated protein corresponding to *a*FA-labeling was visualized using 700 nm IR-streptavidin (1:10000 in 1:1 TBS-T:Odyssey Blocking Buffer).

Immunocytochemistry

WT, *Lypla1*$^{-/-}$, *Lypla2*$^{-/-}$, or DKO Neuro2a cells (4 x 10^3) were plated in 100 μL DMEM with 10% FBS in a 96-well plate. After 48 h, the medium was replaced with 100 μL DMEM containing 10% FBS and DMSO control or various concentrations of *a*PA. Cells were cultured for 24 h to promote *a*FA enrichment and protein labeling. Cells were then washed 2 x with 100 μL PBS and fixed with the addition of 3.7% formaldehyde in PBS, followed by shaking at room temperature for 20 min. Cells were then washed 2 x with PBS and permeabilized with 0.15% Triton X-100 in PBS for 10 min at room temperature. Cells were again washed 2 x with PBS and blocked with Odyssey Blocking Buffer by shaking for 1 h at room temperature. Cells were then labeled with N_3-AlexaFluor via click chemistry by adding a master-mix of $CuSO_4$, TCEP, TBTA, and N_3-AlexaFluor to give the same final concentrations as used in gel visualization experiments as described above, and shaking at room temperature for 1 h. Cells were then

washed 3 x with TBS containing 0.1% (v/v) Tween (TBS-T) for 10 min while shaking at room temperature, prior to the addition of 4',6-diamidino-2-phenylindole (DAPI) (1:1000 v/v, Invitrogen) for 1 h while shaking at room temperature. Cells were then washed again 3 x with TBS-T and rinsed 3 x with PBS. Stained cells were imaged at 10x power in a 5 x 5 array, and the data were processed using a MetaXpress Micro XL automated microscope imager, which generated a single composite image per well.

Streptavidin Enrichment of *a*PA-labeled Proteins

WT and DKO neuro2a cells (5 x 10^6) were cultured in isotopically-labeled light and heavy media, respectively, and plated in 20 mL DMEM with 10% FBS and enriched with 50 μM *a*PA as described above. Cells were lysed and protein concentrations were determined as described above. 2.5 mg of protein from WT cells (light) was combined 1:1 with 2.5 mg of protein from DKO cells (heavy) and UV-cleavable N_3-biotin labeling of the combined protein samples was performed as described previously, though without exposing samples to any light. Biotinylated protein was enriched using 50 μL streptavidin beads washed with PBS per sample using the following wash steps: 2 each of 1% SDS in PBS, 4 M Urea in PBS, 1 M NaCl in PBS, PBS, H_2O. Enriched protein was eluted from beads by stirring in glass tubes under 360 nm light for 1 h. Eluted protein was concentrated in speed-vac for 16 h and dried protein eluates were analysed by Vanderbilt University Mass Spectrometry Research Center Proteomics Lab.

5.3 Results

Cells Utilize aFAs from Media with or without FBS

The ability of neuro2a cells to utilize exogenous *a*FAs was assessed by quantifying the percentage of *a*FAs remaining in media after a 24 h enrichment period (Figure 5.2). Whereas *a*LA is the most depleted (17 ± 0.7%) and presumably incorporated into the cells, smaller fractions of *a*AA and *a*PA are incorporated, leaving just over 60% in the medium after 24 h. Additionally, the removal of serum had a modest effect on *a*PA enrichment, reducing the remaining amount by about 10%, though this effect was insignificant. These data suggest that removing serum from the media did not have a significant effect on *a*FA enrichment, and the deleterious effects on cell growth that result from removing serum were not warranted in the interest of increasing *a*FA uptake.

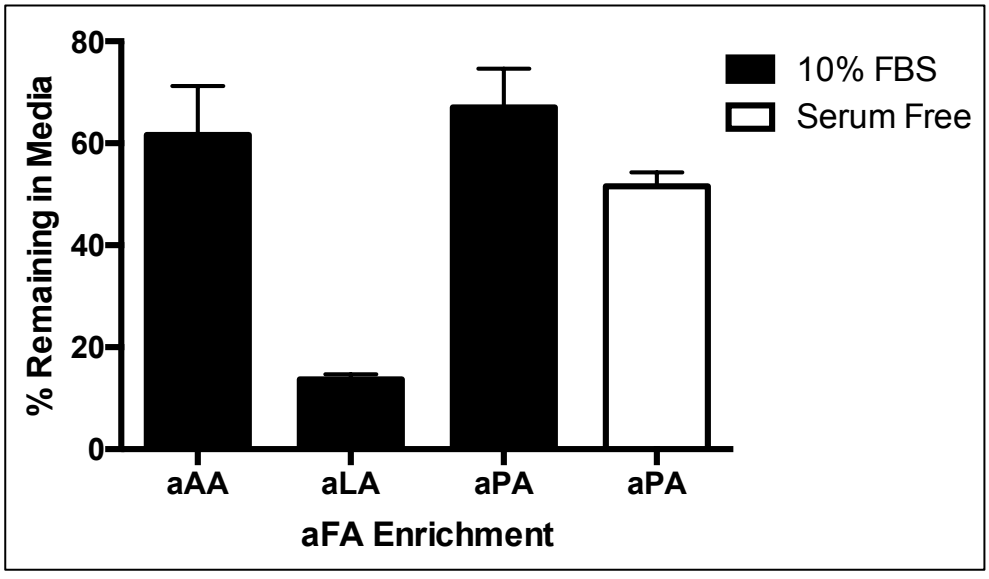

Figure 5.2: aFAs are depleted in cell media after a 24 h enrichment period. Removing serum from media slightly increases the amount of aPA enrichment into cells.

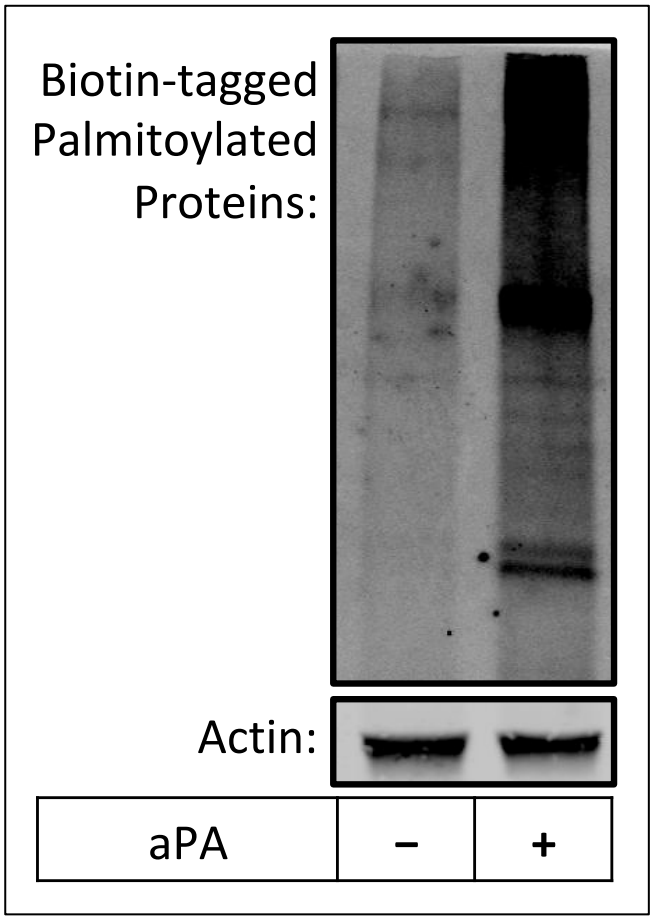

Figure 5.3: Proteins labeled with *a*PA can be identified by covalently attaching an azido-biotin moiety via click chemistry and visualizing with Western blotting analysis with IR-active streptavidin.

ML349 Inhibition of LYPLA2 Increases Global Protein Palmitoylation

After ensuring the neuro2a cells were able to take up exogenous *a*FAs from media, the ability of the cells to utilize these reporters as FA mimetics for protein acylation studies was assessed via click chemistry and western blotting analysis (Figure 5.3). After using click chemistry to covalently label modified proteins from cells enriched with an EtOH vehicle or 50 μM *a*PA, streptavidin visualization via Western blotting revealed clear differences between treated and control cells. These data suggest *a*PA can be used to identify protein substrates of dynamic palmitoylation processes in cells.

We have shown that ML349 treatment of RAW264.7 macrophage cells inhibits cellular LYPLA2 and prevents PG-G hydrolysis (Figure 2.11) (66). To determine the effects of ML349 on protein palmitoylation in these cells, RAW264.7 cells were enriched with 50 μM *a*PA to promote endogenous protein palmitoylation with an alkyne reporter tag as demonstrated in Figure 5.3. Simultaneously, cells were treated with 10 μM ML349 to inhibit LYPLA2 hydrolytic activity and prevent depalmitoylation of its specific lipoprotein substrates. As shown in Figure 5.4, protein palmitoylation was drastically increased in *a*PA-enriched RAW264.7 cells treated with the LYPLA2 inhibitor, ML349. Furthermore, neither *a*PA enrichment nor ML349 treatment affected LYPLA2 expression, suggesting these changes in protein palmitoylation were directly resulting from inhibiting LYPLA2 activity. While some protein bands were present in the unenriched control samples, these proteins are likely to be endogenously biotinylated background. Additionally, proteins in the LYPLA2-inhibited sample appear as an unresolved smear, suggesting a much higher quantity of protein palmitoylation. These results suggest that despite only GAP-43 being validated as a substrate of LYPLA2, a plethora of unidentified lipoprotein substrates of the acyl-protein thioesterase exist (172,186,187,190,222,226,227).

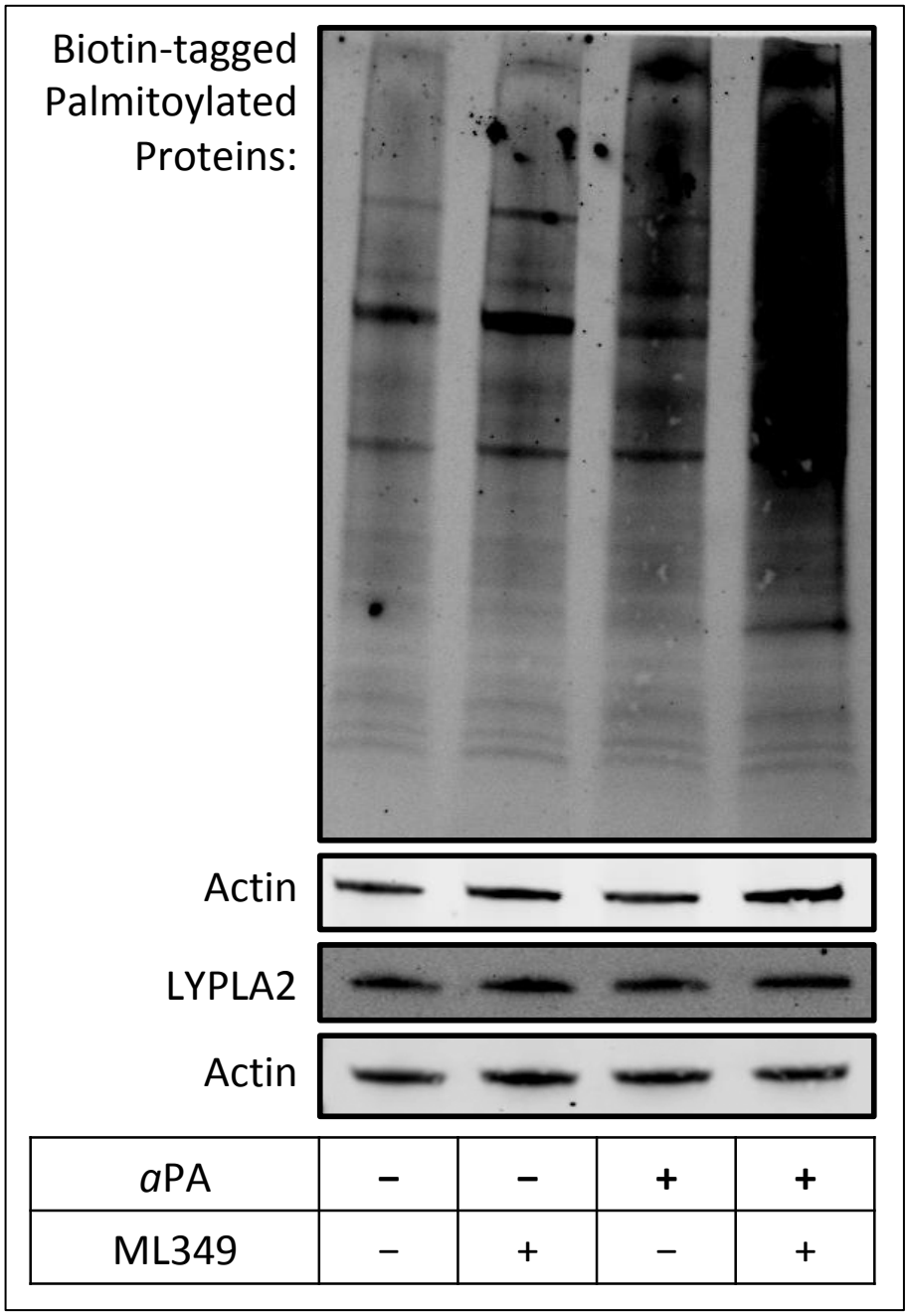

Figure 5.4: Western blot analysis of RAW264.7 cells enriched with 50 μM *a*PA demonstrates increased protein palmitoylation after inhibiting LYPLA2 depalmitoylation with 10 μM ML349. Actin was used as a loading control for palmitoylated protein levels and for LYPLA2 expression in a separate Western blot.

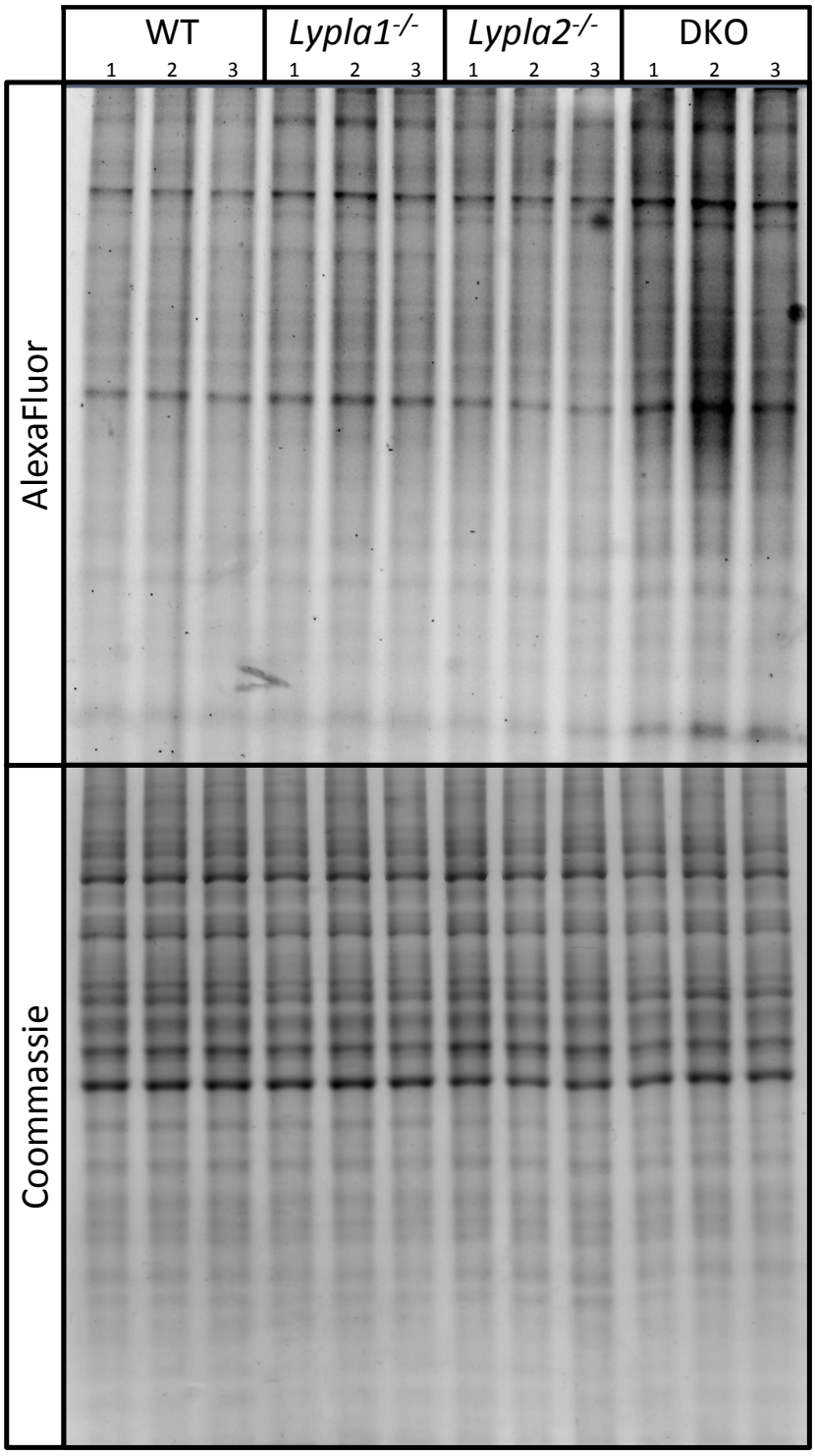

Figure 5.5: Gel imaging analysis of WT, *Lypla1*$^{-/-}$, *Lypla2*$^{-/-}$, and DKO neuro2a cells enriched with 50 µM *a*PA demonstrates increased protein palmitoylation only in cells lacking both *Lypla1* and *Lypla2* genes. Protein palmitoylation was visualized with azidoAlexaFluor via click chemistry cycloaddition. Total protein staining with Coomassie was used as a loading control for the palmitoylated protein levels.

Protein Palmitoylation is Increased in DKO Neuro2a Cells

LYPLA2-specific inhibition with ML349 in RAW264.7 macrophages results in increased protein palmitoylation (Figure 5.4). These data suggest dynamic protein palmitoylation can be modulated with the use of LYPLA-specific inhibition or preventing acyl-protein thioesterase expression with genome editing. To evaluate the effects of LYPLA1 and LYPLA2 knockouts on protein palmitoylation, previously generated genetic knockouts of *Lypla1*, *Lypla2*, and DKO neuro2a cells were utilized (Figure 4.2A). WT neuro2a cells and each knockout cell line were enriched with 50 μM *a*PA prior to harvesting and cell lysates were labeled with azido-AlexaFluor via click chemistry (Figure 5.5). Interestingly, individual knockouts of *Lypla1* or *Lypla2* had no discernable effect on protein palmitoylation compared to WT cells. However, DKO cells lacking both enzymes had higher levels of protein palmitoylation than the other cohorts.

For a more quantitative approach to comparing protein palmitoylation between cells, we utilized immunocytochemistry and high-throughput imaging to compare AlexaFluor fluorescence in clicked neuro2a cells after enriching with various concentrations of *a*PA (Figure 5.6). Total intensity of fluorescence of the AlexaFluor-labeled palmitoylated proteins was quantified in each well and normalized to the number of cells in each well, determined by nuclear staining with DAPI. These values were then normalized to vehicle-treated WT fluorescence to compare each cell line with different concentrations. Significant increases in palmitoylation were observed in DKOs at *a*PA enrichment concentrations of 10 μM and higher. Additionally, slight, though significant, increases were also seen in *Lypla2*$^{-/-}$ cells at *a*PA enrichment concentrations of 50 μM and higher. These data confirmed that it is possible to quantify changes in protein palmitoylation resulting from preventing the expression of LYPLAs.

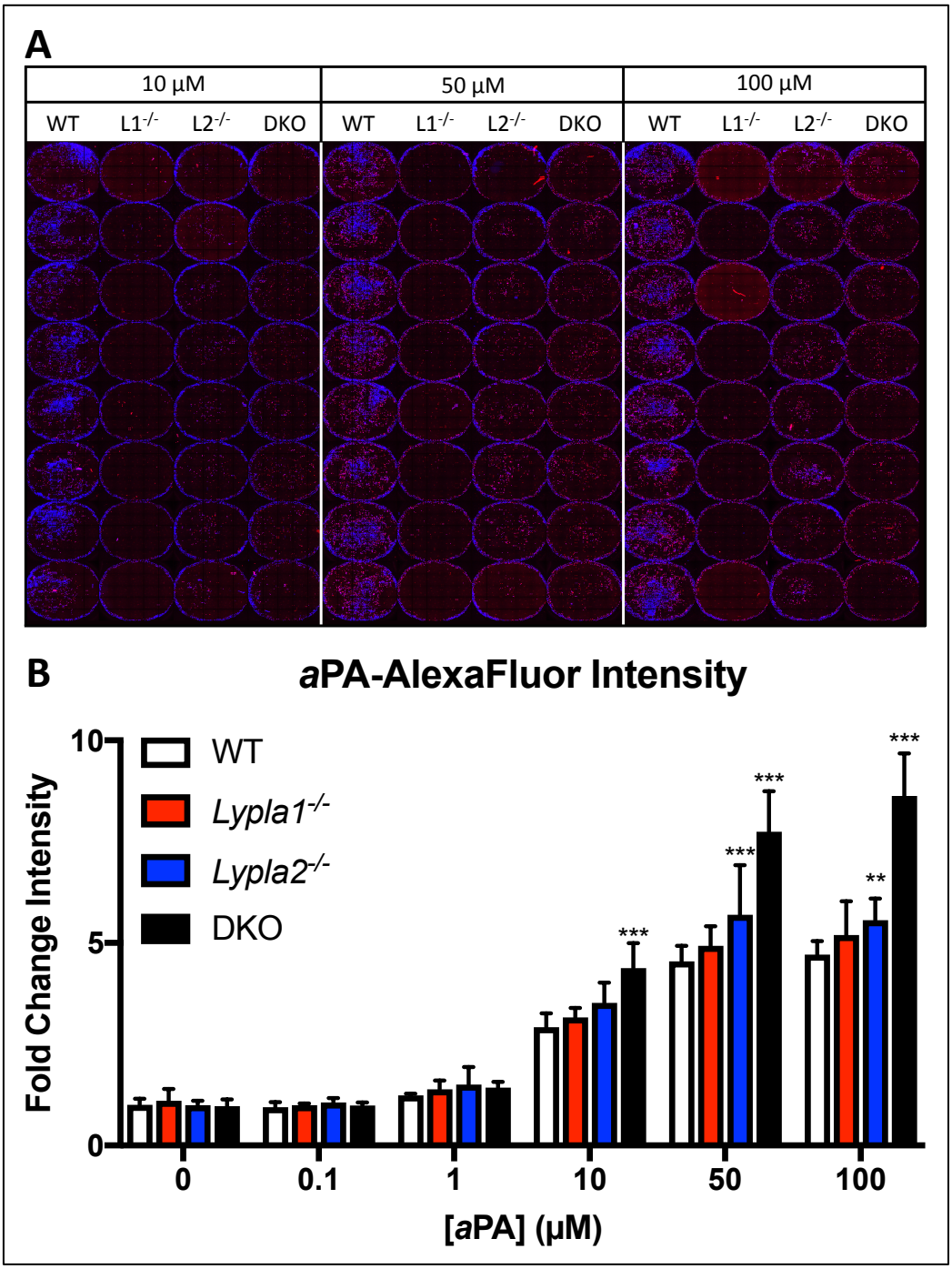

Figure 5.6: Protein palmitoylation is significantly increased in DKO cells and is slightly increased in *Lypla2*$^{-/-}$ cells at higher concentrations of *a*PA. (**A**) Fluorescence imaging analysis of individual WT, *Lypla1*$^{-/-}$, *Lypla2*$^{-/-}$, and DKO neuro2a cells enriched with 50 µM *a*PA demonstrates sensitive changes in protein palmitoylation between cell lines. Representative plate shown with concentrations of *a*PA at 10, 50, and 100 µM. (**B**) Total intensity of *a*PA-AlexaFluor fluorescence in each well was normalized to the number of cells counted with DAPI nuclear staining to give average intensity of fluorescence/cell, and normalized to WT levels. (N=16) ***P<0.001, ***P<0.0001.*

Together, the results suggest that a similar mechanism of cooperation between LYPLA1 and LYPLA2 to mediate dynamic protein palmitoylation exists as seen with LysoPL hydrolysis as described above. In this case, both LYPLA1 and LYPLA2 are able to account for the loss of activity in the opposite single knockout cells, but when both genes are deleted, protein palmitoylation is significantly increased. Contrastingly, protein palmitoylation was increased in the ML349-treated RAW264.7 cells (Figure 5.4); however, it seems more likely that ML349 is no longer specifically inhibiting LYPLA2 at 10 μM, and instead both LYPLA1 and LYPLA2 are being inhibited, along with multiple other acyl-protein thioesterases, to increase protein palmitoylation levels. In this case, it would make sense that LYPLA1 and LYPLA2 actually do share a number of lipoprotein substrates, which would explain why specific inhibition of either protein does not drastically alter dynamic protein palmitoylation.

Dynamic Palmitoylation States of Specific Proteins are Altered in DKO Neuro2a Cells

Global protein palmitoylation was increased in DKO cells relative to WT cells as demonstrated in Figures 5.5-6. For precise identification and accurate quantification of individual proteins with altered palmitoylation in DKO cells, SILAC was used to differentiate proteins derived from WT or DKO neuro2a cells in proteomics experiments. After combining equivalent quantities of protein from *a*PA-enriched light WT lysates and heavy DKO lysates, click chemistry was used to attach a UV-cleavable biotin moiety to all *a*PA-modified proteins, allowing for streptavidin-based enrichment of palmitoylated proteins and subsequent proteolytic digestion. Then, proteomic analysis of the enriched peptides derived from palmitoylated proteins enabled the identification and quantification of proteins whose palmitoylation state was altered in the DKO cells.

DKO:WT		UniProt Accession	Protein ID
> 20% Increase	1.21	P09405	nucleolin(Ncl)
	1.21	Q7TPV4	MYB binding protein (P160) 1a(Mybbp1a)
	1.21	P0CG50	ubiquitin C(Ubc)
	1.22	P63038	heat shock protein 1 (chaperonin)(Hspd1)
	1.23	P49312	heterogeneous nuclear ribonucleoprotein A1(Hnrnpa1)
	1.23	Q99PL5	ribosome binding protein 1(Rrbp1)
	1.24	Q9JKR6	hypoxia up-regulated 1(Hyou1)
	1.24	Q9DCN2	cytochrome b5 reductase 3(Cyb5r3)
	1.24	P62242	ribosomal protein S8(Rps8)
	1.25	Q8VEK3	heterogeneous nuclear ribonucleoprotein U(Hnrnpu)
	1.25	P63101	tyr 3-monooxygenase/trp 5-monooxygenase activation protein, zeta polypeptide(Ywhaz)
	1.26	Q61656	DEAD (Asp-Glu-Ala-Asp) box polypeptide 5(Ddx5)
	1.26	P06837	growth associated protein 43(Gap43)
	1.29	Q9CZU6	citrate synthase(Cs)
	1.29	P34022	RAN binding protein 1(Ranbp1)
	1.30	P51150	RAB7, member RAS oncogene family(Rab7)
	1.31	P14211	calreticulin(Calr)
	1.32	P61982	tyr 3-monooxygenase/trp 5-monooxygenase activation protein, gamma polypeptide(Ywhag)
	1.33	P17225	polypyrimidine tract binding protein 1(Ptbp1)
	1.35	P38647	heat shock protein 9(Hspa9)
	1.35	P08249	malate dehydrogenase 2, NAD (mitochondrial)(Mdh2)
	1.37	Q9Z127	solute carrier family 7 (cationic amino acid transporter, y+ system), member 5(Slc7a5)
	1.38	P20152	vimentin(Vim)
	1.39	Q9Z1N5	DEAD (Asp-Glu-Ala-Asp) box polypeptide 39B(Ddx39b)
	1.43	Q9CQM2	KDEL (Lys-Asp-Glu-Leu) endoplasmic reticulum protein retention receptor 2(Kdelr2)
	1.48	Q6IRU2	tropomyosin 4(Tpm4)
	1.48	P14148	ribosomal protein L7(Rpl7)
	1.53	P10852	solute carrier family 3 (activators of dibasic and neutral amino acid transport), member 2(Slc3a2)
	1.55	Q6NZJ6	eukaryotic translation initiation factor 4, gamma 1(Eif4g1)
	1.56	P09103	prolyl 4-hydroxylase, beta polypeptide(P4hb)
	1.58	P46061	RAN GTPase activating protein 1(Rangap1)
	1.63	P08113	heat shock protein 90, beta (Grp94), member 1(Hsp90b1)
	1.68	Q07409	contactin 3(Cntn3)
	1.78	Q9WVA4	transgelin 2(Tagln2)
	1.82	P21107	tropomyosin 3, gamma(Tpm3)
	1.85	O35114	scavenger receptor class B, member 2(Scarb2)
	1.86	Q922R8	protein disulfide isomerase associated 6(Pdia6)
	2.34	Q8CGK3	lon peptidase 1, mitochondrial(Lonp1)
> 20% Decrease	0.38	Q9EQU5	SET nuclear oncogene(Set)
	0.39	P21995	embigin(Emb)
	0.46	P05202	glutamatic-oxaloacetic transaminase 2, mitochondrial(Got2)
	0.54	P06151	lactate dehydrogenase A(Ldha)
	0.55	Q9JLV1	BCL2-associated athanogene 3(Bag3)
	0.59	P57787	solute carrier family 16 (monocarboxylic acid transporters), member 3(Slc16a3)
	0.59	P14873	microtubule-associated protein 1B(Map1b)
	0.60	P14152	malate dehydrogenase 1, NAD (soluble)(Mdh1)
	0.61	Q8R191	synaptogyrin 3(Syngr3)
	0.65	P52480	pyruvate kinase, muscle(Pkm)
	0.67	Q7TQ95	ER junction formation factor 1(Lnpk1)
	0.69	Q91XV3	brain abundant, membrane attached signal protein 1(Basp1)
	0.69	Q05816	fatty acid binding protein 5, epidermal(Fabp5)
	0.70	P80315	chaperonin containing Tcp1, subunit 4 (delta)(Cct4)
	0.70	Q03265	ATP synthase, H+ transporting, mitochondrial F1 complex, alpha subunit 1(Atp5a1)
	0.70	Q9CQX2	cytochrome b5 type B(Cyb5b)
	0.70	Q9WTQ5	A kinase (PRKA) anchor protein (gravin) 12(Akap12)
	0.73	P17751	triosephosphate isomerase 1(Tpi1)
	0.74	P80314	chaperonin containing Tcp1, subunit 2 (beta)(Cct2)
	0.75	O70251	eukaryotic translation elongation factor 1 beta 2(Eef1b2)
	0.76	P62821	RAB1A, member RAS oncogene family(Rab1a)
	0.76	Q8BK64	AHA1, activator of heat shock protein ATPase 1(Ahsa1)
	0.78	O55143	ATPase, Ca++ transporting, cardiac muscle, slow twitch 2(Atp2a2)

Table 5.1: Proteins identified as palmitoylated with a 20% increase or decrease in palmitoylation in DKO cells compared to WT cells, with $P<0.05$.

For identification of palmitoylated proteins, tandem mass spectra were searched with Sequest (Thermo Fisher Scientific) against a mouse subset database created from the UniprotKB protein database. Only proteins with two or more peptides present were identified as present in the neuro2a cells. Ratios of the light and heavy peptides were quantified to give relative changes in protein palmitoylation between WT and DKO cells, resulting in 129 identified palmitoylated proteins present in both cohorts (Figure 5.7). Palmitoylated proteins that significantly increased or decreased by greater than 20% in DKO cells compared to WT cells were identified and added to Table 5.1.

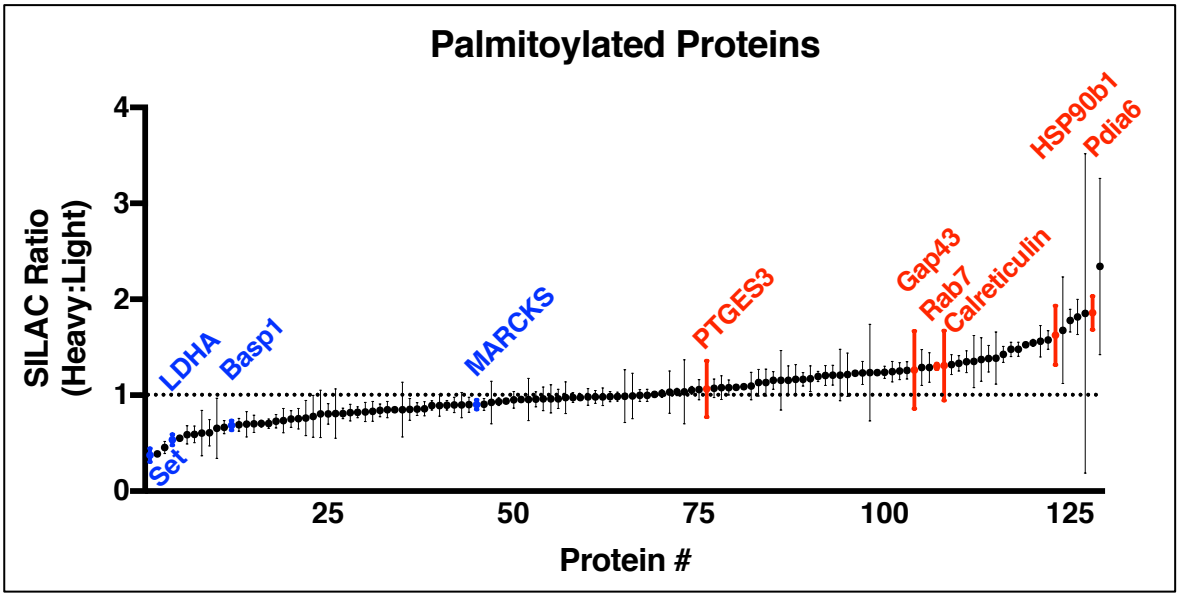

Figure 5.7: Palmitoylated proteins with multiple peptides identified in DKO and WT neuro2a cells. Proteins highlighted in blue (decreased in DKO cells) and red (increased in DKO cells) are some of the known targets of palmitoylation. Proteins significantly increased or decreased in DKO cells that change by over 20% are described in Table 5.1.

Many proteins identified in these experiments are known targets of palmitoylation (highlighted in blue or red for decreases or increases in DKO cells, respectively), validating these methodologies were able to isolate known lipoproteins from cell lysates (Figure 5.7)

(161,223,280-283). For example, GAP-43 was increased in DKO cells by 26% in DKO cells, and is a known substrate of LYPLA2 depalmitoylation (172,183,186,187,190,222,224-227). Importantly, any proteins with increased palmitoylation in DKO cells are potential substrates of specifically LYPLA1, specifically LYPLA2, or both LYPLA1 and LYPLA2, and determination of the exact acyl-protein thioesterase responsible for depalmitoylating the lipoprotein of interest would require further validation studies.

5.4 Discussion

Protein acylation is an abundant and long-lived PTM, with almost 15% of proteins in eukaryotic cells undergoing the modification (164). Protein palmitoylation is an important mechanism in regulating the activity and subcellular location of protein substrates (160,166,168,177,227). This dynamic cysteine modification is regulated by acyl-protein thioesterase enzymes, which remove the S-palmitoyl moieties by hydrolyzing the thioester bonds (172,183,184,186,275). However, only three acyl-protein thioesterase enzymes have been identified: LYPLA1, LYPLA2, and ABHD17. Furthermore, relatively few lipoprotein substrates of these enzymes have been identified, with GAP-43 being the only known protein substrate of LYPLA2, specifically (187,284).

To characterize the roles of LYPLA1 and LYPLA2 as acyl-protein thioesterases, we utilized a chemical probe, *a*PA, to label all palmitoylated proteins with an alkyne moiety. This reporter molecule allowed for bioorthogonal labeling of palmitoylated proteins with fluorescent or biotin tags to allow for visualization and enrichment, as demonstrated in Figure 5.3. This

qualitative approach allowed for comparing different cell samples to evaluate the effects of LYPLA1 and LYPLA2 activity on dynamic protein palmitoylation. For example, when cells were inhibited with ML349, a LYPLA2-specific small molecule inhibitor, protein palmitoylation was increased relative to vehicle-treated cells (Figure 5.4), suggesting many more lipoprotein substrates of LYPLA2 exist in cells.

Alternatively, genetic knockouts of LYPLA1 or LYPLA2, individually, did not have a drastic effect on palmitoylation levels. However, knocking out both genes caused an increase in protein palmitoylation (Figure 5.5). Additionally, these same trends were seen with a quantitative immunofluorescence approach to compare palmitoylation between cell lines (Figure 5.6). These results are consistent with the effects of the genetic knockouts on LysoPLs (Figure 4.3), and suggest the enzymes share a wide range of LysoPL and lipoprotein substrates in cells, despite minor distinct substrate preferences with recombinant protein assays. These results also explain why approaches that inhibit only LYPLA1 or LYPLA2 to modulate protein palmitoylation are often unsuccessful, and dual inhibition of both proteins is generally required to observe changes in dynamic palmitoylation (190,222,274).

Accordingly, lipoprotein content in DKO and WT cells was compared using SILAC and proteomics approaches to identify proteins with higher palmitoylation in DKO cells as substrates of LYPLAs. 129 proteins were identified as changed in DKO cells, though many of these were decreased and changes were, therefore, likely indirect effects of deleting *Lypla1* and *Lypla2*. Of the 129 proteins, 61 were increased, 38 of which were increased by more than 20% (Table 5.1). Interestingly, many of the proteins identified were chaperone proteins, responsible for folding/unfolding proteins that have been denatured due to cellular stress or routine denaturing. Specifically, 8 heat shock proteins demonstrated significant changes in protein palmitoylation.

These data suggest that LYPLAs are important in regulating the activity of protein chaperones responsible for maintaining the structure of numerous other enzymes in cells over time.

In contrast, 23 proteins displayed decreased palmitoylation in DKO cells. As with the LysoPL data from *Lypla* KO cells, it is important to consider indirect effects of the genetic knockouts. While LYPLA1 and LYPLA2 are no longer present, other thioesterases are still expressed and can account for the resultant substantial changes to palmitoylation. If the expression of any of these thioesterases is increased in the DKO cells, palmitoylation of their normal substrates could be excessively decreased as a consequence of attempting to modulate the increased global palmitoylation. Furthermore, LYPLAs depalmitoylate each other and are likely to regulate the acylation state of other acyl-protein thioesterases themselves. If these proteins are stuck in a palmitoylated state because LYPLAs are knocked out, they would remain active and continue to depalmitoylate their own substrates, explaining significant decreases in certain palmitoylated proteins in the DKO cells.

In summary, we have preliminarily characterized the roles of LYPLA1 and LYPLA2 in dynamic protein palmitoylation and determined the lipoprotein substrate pools of these enzymes had been vastly underestimated. Global protein palmitoylation was significantly increased in cells lacking both enzymes, which supports the hypothesis that LYPLA1 and LYPLA2 accommodate for the loss of the others' activity, which was also seen in the case of LysoPL substrates. Much like LysoPLs, it is likely that LYPLA1 and LYPLA2 share a wide variety of lipoprotein substrates in cells, and work together to mediate dynamic protein palmitoylation as well as modulating LysoPL substrates in the Lands Cycle.

6

Significance

The main goal of this work has been to characterize the relatively unstudied LYPLA enzymes. These two similar serine hydrolases were preliminarily shown to metabolize three distinct classes of substrate: eicosanoids derived from endocannabinoids, lysophospholipid signaling molecules, and palmitoylated proteins. While some activity by LYPLA1 and LYPLA2 toward each of these substrate classes had been reported, most of this work had been done with recombinant enzyme. Furthermore, classifications of the two enzymes' preferences toward their various substrates lacked a significant amount of information. For example, our work was the only example of LYPLA-mediated hydrolysis of PG-Gs to be published; no studies compared activity of LYPLAs toward LysoPLs with various acyl chains or toward LysoPL substrates in a cellular setting where more than one endogenous substrate was available at a given time; and methods to identify lipoprotein substrates of a specific acyl-protein thioesterase were unable to determine more than one substrate for LYPLA2. This work has been successful in addressing the lack of information for each of these fields of study.

First, as described in Chapter 2, after identifying LYPLA2 as a potential PG-G hydrolase, we were able to validate this activity across multiple human cancer cell lines and differentiate the activities of LYPLA1 and LYPLA2 toward this substrate class. Interestingly, this is the only substrate class of LYPLAs where only one of the proteins displays a significant effect on levels of the substrates in cells. We have fully characterized the ability of LYPLA1 and LYPLA2 to perform this activity and have determined that, despite similar activities with recombinant

protein, only LYPLA2 seems to act as a cellular PG-G hydrolase. Furthermore, as described in Chapter 3, we employed x-ray crystallography to solve the first crystal structure of LYPLA2 and utilized the resulting data to generate a possible explanation for these differences in activity. By developing site-directed mutants of LYPLA2 based on contrasting structural features of the two proteins, and by interpreting activity data from hydrolysis assays with these mutants, we were able to posit a model for PG-G substrate binding to LYPLA2. Additionally, as described in Chapter 3, we were able to develop analytical methods to quantify hydrolysis of LysoPL substrates. These substrates are notoriously difficult to work with due to poor solubility and contamination, and our novel techniques that utilize a labeled LysoPL substrate and fatty acid derivatization with PFB-Br enabled us to avoid expensive and inaccurate radiolabeling approaches.

Second, as described in Chapter 4, we generated the first genetic knockout cell lines of *Lypla1*, *Lypla2*, and both genes using CRISPR-Cas9 gene-editing technology. These cell lines were instrumental tools in studying LYPLA1 and LYPLA2 activity in cellular settings. We were able to use these cell models to compare the activities of LYPLAs on LysoPL levels in cells by using extensive LC-MS/MS-based lipidomics to quantify over 30 different LysoPL species in each cell line. The data from these experiments revealed the cellular dynamic between LYPLA1 and LYPLA2 as cooperative and redundant, able to account for the loss of the other's activity in the single knockout cell lines, but instrumental in maintaining lipid homeostasis and modulating LysoPL signaling as demonstrated in the DKO cells. These studies revealed the important roles of LYPLAs in lipid metabolism and characterized the phenotypic effects of these proteins' activities on cellular differentiation.

Finally, as described in Chapter 5, we were able to use the CRISPR cell models again to characterize the roles of the proteins in dynamic palmitoylation processes in cells. By adapting chemical biology techniques using alkyne-labeled reporter tags, we were able to visualize and purify palmitoylated proteins from these cell lines and compare global palmitoylation levels. Furthermore, using SILAC and sensitive MS/MS-based proteomics, we were able to identify a host of palmitoylated proteins affected by LYPLA1 and LYPLA2 activity. Whereas only one reported substrate of LYPLA2 had been identified previously, our methods have highlighted 129 potential lipoprotein substrates of LYPLA1 and LYPLA2. Additionally, the methods we developed can be applied to studying other acyl-protein thioesterase or palmitoyltransferase enzymes.

Together, this dissertation project was successful in determining specific structural determinants of the contrasting activity between LYPLA1 and LYPLA2, as well as in characterizing their role in cellular lipid and lipoprotein metabolism. However, there is still much work that needs to be done to fully understand the contribution of these proteins to these biochemical processes. In-depth lipidomics experiments will need to be continued to further understand the mechanism in which LYPLAs account for each other's loss in activity and the structural determinants that dictate the preferences for LysoPL substrates that increase preferentially in DKO cells. Additionally, lipoprotein candidates need to be validated as LYPLA substrates using new, more sensitive assays to detect small changes in palmitoylation. Collectively, much progress has been made in the characterization of these enzymes, and along with that progress, many more questions have been raised.

References

1. Boyd, S. T. (2006) The endocannabinoid system. *Pharmacotherapy* **26**, 218S-221S
2. De Petrocellis, L., Cascio, M. G., and Di Marzo, V. (2004) The endocannabinoid system: a general view and latest additions. *Br. J. Pharmacol.* **141**, 765-774
3. Battista, N., Di Tommaso, M., Bari, M., and Maccarrone, M. (2012) The endocannabinoid system: an overview. *Front. Behav. Neurosci.* **6**, 9
4. Robson, P. (2001) Therapeutic aspects of cannabis and cannabinoids. *Br. J. Psychiatry* **178**, 107-115
5. Pisanti, S., and Bifulco, M. (2018) Medical Cannabis: A plurimillennial history of an evergreen. *J. Cell. Physiol.*
6. Wang, J., and Ueda, N. (2009) Biology of endocannabinoid synthesis system. *Prostaglandins Other Lipid Mediat.* **89**, 112-119
7. Prescott, S. M., and Majerus, P. W. (1983) Characterization of 1,2-diacylglycerol hydrolysis in human platelets. Demonstration of an arachidonoyl-monoacylglycerol intermediate. *J. Biol. Chem.* **258**, 764-769
8. Sugiura, T., and Waku, K. (2000) 2-Arachidonoylglycerol and the cannabinoid receptors. *Chem. Phys. Lipids* **108**, 89-106
9. Di Marzo, V., Fontana, A., Cadas, H., Schinelli, S., Cimino, G., Schwartz, J. C., and Piomelli, D. (1994) Formation and inactivation of endogenous cannabinoid anandamide in central neurons. *Nature* **372**, 686-691
10. Sugiura, T., Kondo, S., Sukagawa, A., Tonegawa, T., Nakane, S., Yamashita, A., Ishima, Y., and Waku, K. (1996) Transacylase-mediated and phosphodiesterase-mediated synthesis of N-arachidonoylethanolamine, an endogenous cannabinoid-receptor ligand, in

rat brain microsomes. Comparison with synthesis from free arachidonic acid and ethanolamine. *Eur. J. Biochem.* **240**, 53-62

11. Cadas, H., di Tomaso, E., and Piomelli, D. (1997) Occurrence and biosynthesis of endogenous cannabinoid precursor, N-arachidonoyl phosphatidylethanolamine, in rat brain. *J. Neurosci.* **17**, 1226-1242
12. Cadas, H., Gaillet, S., Beltramo, M., Venance, L., and Piomelli, D. (1996) Biosynthesis of an endogenous cannabinoid precursor in neurons and its control by calcium and cAMP. *J. Neurosci.* **16**, 3934-3942
13. Rouzer, C. A., Ghebreselasie, K., and Marnett, L. J. (2002) Chemical stability of 2-arachidonylglycerol under biological conditions. *Chem. Phys. Lipids* **119**, 69-82
14. Munro, S., Thomas, K. L., and Abu-Shaar, M. (1993) Molecular characterization of a peripheral receptor for cannabinoids. *Nature* **365**, 61-65
15. Herkenham, M., Lynn, A. B., Johnson, M. R., Melvin, L. S., de Costa, B. R., and Rice, K. C. (1991) Characterization and localization of cannabinoid receptors in rat brain: a quantitative in vitro autoradiographic study. *J. Neurosci.* **11**, 563-583
16. Reggio, P. H. (2010) Endocannabinoid binding to the cannabinoid receptors: what is known and what remains unknown. *Curr. Med. Chem.* **17**, 1468-1486
17. Griffin, G., Atkinson, P. J., Showalter, V. M., Martin, B. R., and Abood, M. E. (1998) Evaluation of cannabinoid receptor agonists and antagonists using the guanosine-5'-O-(3-[35S]thio)-triphosphate binding assay in rat cerebellar membranes. *J. Pharmacol. Exp. Ther.* **285**, 553-560
18. Pertwee, R. G. (1999) Pharmacology of cannabinoid receptor ligands. *Curr. Med. Chem.* **6**, 635-664

19. Stella, N., Schweitzer, P., and Piomelli, D. (1997) A second endogenous cannabinoid that modulates long-term potentiation. *Nature* **388**, 773-778

20. Svizenska, I., Dubovy, P., and Sulcova, A. (2008) Cannabinoid receptors 1 and 2 (CB1 and CB2), their distribution, ligands and functional involvement in nervous system structures--a short review. *Pharmacol. Biochem. Behav.* **90**, 501-511

21. Basavarajappa, B. S. (2007) Critical enzymes involved in endocannabinoid metabolism. *Protein and peptide letters* **14**, 237-246

22. Di Marzo, V., De Petrocellis, L., and Bisogno, T. (2005) The biosynthesis, fate and pharmacological properties of endocannabinoids. *Handb. Exp. Pharmacol.*, 147-185

23. Dinh, T. P., Carpenter, D., Leslie, F. M., Freund, T. F., Katona, I., Sensi, S. L., Kathuria, S., and Piomelli, D. (2002) Brain monoglyceride lipase participating in endocannabinoid inactivation. *Proc. Natl. Acad. Sci. U. S. A.* **99**, 10819-10824

24. Dinh, T. P., Freund, T. F., and Piomelli, D. (2002) A role for monoglyceride lipase in 2-arachidonoylglycerol inactivation. *Chem. Phys. Lipids* **121**, 149-158

25. Hillard, C. J., Wilkison, D. M., Edgemond, W. S., and Campbell, W. B. (1995) Characterization of the kinetics and distribution of N-arachidonylethanolamine (anandamide) hydrolysis by rat brain. *Biochim. Biophys. Acta* **1257**, 249-256

26. Ueda, N., Kurahashi, Y., Yamamoto, S., and Tokunaga, T. (1995) Partial purification and characterization of the porcine brain enzyme hydrolyzing and synthesizing anandamide. *J. Biol. Chem.* **270**, 23823-23827

27. Cravatt, B. F., Giang, D. K., Mayfield, S. P., Boger, D. L., Lerner, R. A., and Gilula, N. B. (1996) Molecular characterization of an enzyme that degrades neuromodulatory fatty-acid amides. *Nature* **384**, 83-87

28. Savinainen, J. R., Saario, S. M., and Laitinen, J. T. (2012) The serine hydrolases MAGL, ABHD6 and ABHD12 as guardians of 2-arachidonoylglycerol signalling through cannabinoid receptors. *Acta Physiol. (Oxf.)* **204**, 267-276

29. Kozak, K. R., and Marnett, L. J. (2002) Oxidative metabolism of endocannabinoids. *Prostaglandins Leukot. Essent. Fatty Acids* **66**, 211-220

30. Smith, W. L., DeWitt, D. L., and Garavito, R. M. (2000) Cyclooxygenases: structural, cellular, and molecular biology. *Annu Rev Biochem* **69**, 145-182

31. Rouzer, C. A., and Marnett, L. J. (2003) Mechanism of free radical oxygenation of polyunsaturated fatty acids by cyclooxygenases. *Chem Rev* **103**, 2239-2304

32. Rouzer, C. A., and Marnett, L. J. (2009) Cyclooxygenases: structural and functional insights. *J Lipid Res* **50 Suppl**, S29-34

33. Garavito, R. M., Malkowski, M. G., and DeWitt, D. L. (2002) The structures of prostaglandin endoperoxide H synthases-1 and -2. *Prostaglandins Other Lipid Mediat* **68-69**, 129-152

34. Prusakiewicz, J. J., Duggan, K. C., Rouzer, C. A., and Marnett, L. J. (2009) Differential sensitivity and mechanism of inhibition of COX-2 oxygenation of arachidonic acid and 2-arachidonoylglycerol by ibuprofen and mefenamic acid. *Biochemistry* **48**, 7353-7355

35. Gupta, K., Selinsky, B. S., Kaub, C. J., Katz, A. K., and Loll, P. J. (2004) The 2.0 A resolution crystal structure of prostaglandin H2 synthase-1: structural insights into an unusual peroxidase. *J. Mol. Biol.* **335**, 503-518

36. Marnett, L. J. (2000) Cyclooxygenase mechanisms. *Curr. Opin. Chem. Biol.* **4**, 545-552

37. Dong, L., Vecchio, A. J., Sharma, N. P., Jurban, B. J., Malkowski, M. G., and Smith, W. L. (2011) Human cyclooxygenase-2 is a sequence homodimer that functions as a

conformational heterodimer. *J. Biol. Chem.* **286**, 19035-19046

38. Zou, H., Yuan, C., Dong, L., Sidhu, R. S., Hong, Y. H., Kuklev, D. V., and Smith, W. L. (2012) Human cyclooxygenase-1 activity and its responses to COX inhibitors are allosterically regulated by nonsubstrate fatty acids. *J. Lipid Res.* **53**, 1336-1347
39. Kudalkar, S. N., Nikas, S. P., Kingsley, P. J., Xu, S., Galligan, J. J., Rouzer, C. A., Banerjee, S., Ji, L., Eno, M. R., Makriyannis, A., and Marnett, L. J. (2015) 13-Methylarachidonic acid is a positive allosteric modulator of endocannabinoid oxygenation by cyclooxygenase. *J. Biol. Chem.* **290**, 7897-7909
40. Tanabe, T., and Tohnai, N. (2002) Cyclooxygenase isozymes and their gene structures and expression. *Prostaglandins Other Lipid Mediat.* **68-69**, 95-114
41. Crofford, L. J. (1997) COX-1 and COX-2 tissue expression: implications and predictions. *J. Rheumatol. Suppl.* **49**, 15-19
42. O'Neill, G. P., and Ford-Hutchinson, A. W. (1993) Expression of mRNA for cyclooxygenase-1 and cyclooxygenase-2 in human tissues. *FEBS Lett.* **330**, 156-160
43. Eliopoulos, A. G., Dumitru, C. D., Wang, C. C., Cho, J., and Tsichlis, P. N. (2002) Induction of COX-2 by LPS in macrophages is regulated by Tpl2-dependent CREB activation signals. *EMBO J.* **21**, 4831-4840
44. Tsatsanis, C., Androulidaki, A., Venihaki, M., and Margioris, A. N. (2006) Signalling networks regulating cyclooxygenase-2. *Int. J. Biochem. Cell Biol.* **38**, 1654-1661
45. Luong, C., Miller, A., Barnett, J., Chow, J., Ramesha, C., and Browner, M. F. (1996) Flexibility of the NSAID binding site in the structure of human cyclooxygenase-2. *Nat. Struct. Biol.* **3**, 927-933
46. Kozak, K. R., Rowlinson, S. W., and Marnett, L. J. (2000) Oxygenation of the

endocannabinoid, 2-arachidonylglycerol, to glyceryl prostaglandins by cyclooxygenase-2. *J. Biol. Chem.* **275**, 33744-33749

47. Rouzer, C. A., and Marnett, L. J. (2011) Endocannabinoid oxygenation by cyclooxygenases, lipoxygenases, and cytochromes P450: cross-talk between the eicosanoid and endocannabinoid signaling pathways. *Chem. Rev.* **111**, 5899-5921

48. Kozak, K. R., Prusakiewicz, J. J., Rowlinson, S. W., Prudhomme, D. R., and Marnett, L. J. (2003) Amino acid determinants in cyclooxygenase-2 oxygenation of the endocannabinoid anandamide. *Biochemistry* **42**, 9041-9049

49. Kozak, K. R., Crews, B. C., Morrow, J. D., Wang, L. H., Ma, Y. H., Weinander, R., Jakobsson, P. J., and Marnett, L. J. (2002) Metabolism of the endocannabinoids, 2-arachidonylglycerol and anandamide, into prostaglandin, thromboxane, and prostacyclin glycerol esters and ethanolamides. *J. Biol. Chem.* **277**, 44877-44885

50. Funk, C. D. (2001) Prostaglandins and leukotrienes: advances in eicosanoid biology. *Science* **294**, 1871-1875

51. Needleman, P., Marshall, G. R., and Sobel, B. E. (1975) Hormone interactions in the isolated rabbit heart. Synthesis and coronary vasomotor effects of prostaglandins, angiotensin, and bradykinin. *Circ. Res.* **37**, 802-808

52. Brown, K. L., Davidson, J., and Rotondo, D. (2013) Characterisation of the prostaglandin E2-ethanolamide suppression of tumour necrosis factor-alpha production in human monocytic cells. *Biochim. Biophys. Acta* **1831**, 1098-1107

53. Ross, R. A., Craib, S. J., Stevenson, L. A., Pertwee, R. G., Henderson, A., Toole, J., and Ellington, H. C. (2002) Pharmacological characterization of the anandamide cyclooxygenase metabolite: prostaglandin E2 ethanolamide. *J. Pharmacol. Exp. Ther.*

301, 900-907

54. Gatta, L., Piscitelli, F., Giordano, C., Boccella, S., Lichtman, A., Maione, S., and Di Marzo, V. (2012) Discovery of prostamide F2alpha and its role in inflammatory pain and dorsal horn nociceptive neuron hyperexcitability. *PLoS One* **7**, e31111

55. Kozak, K. R., Crews, B. C., Ray, J. L., Tai, H. H., Morrow, J. D., and Marnett, L. J. (2001) Metabolism of prostaglandin glycerol esters and prostaglandin ethanolamides in vitro and in vivo. *The Journal of biological chemistry* **276**, 36993-36998

56. Nirodi, C. S., Crews, B. C., Kozak, K. R., Morrow, J. D., and Marnett, L. J. (2004) The glyceryl ester of prostaglandin E2 mobilizes calcium and activates signal transduction in RAW264.7 cells. *Proc. Natl. Acad. Sci. U. S. A.* **101**, 1840-1845

57. Richie-Jannetta, R., Nirodi, C. S., Crews, B. C., Woodward, D. F., Wang, J. W., Duff, P. T., and Marnett, L. J. (2010) Structural determinants for calcium mobilization by prostaglandin E2 and prostaglandin F2alpha glyceryl esters in RAW 264.7 cells and H1819 cells. *Prostaglandins Other Lipid Mediat.* **92**, 19-24

58. Hu, S. S., Bradshaw, H. B., Chen, J. S., Tan, B., and Walker, J. M. (2008) Prostaglandin E2 glycerol ester, an endogenous COX-2 metabolite of 2-arachidonoylglycerol, induces hyperalgesia and modulates NFkappaB activity. *Br. J. Pharmacol.* **153**, 1538-1549

59. Bruser, A., Zimmermann, A., Crews, B. C., Sliwoski, G., Meiler, J., Konig, G. M., Kostenis, E., Lede, V., Marnett, L. J., and Schoneberg, T. (2017) Prostaglandin E2 glyceryl ester is an endogenous agonist of the nucleotide receptor P2Y6. *Sci. Rep.* **7**, 2380

60. Yu, M., Ives, D., and Ramesha, C. S. (1997) Synthesis of prostaglandin E2 ethanolamide from anandamide by cyclooxygenase-2. *J. Biol. Chem.* **272**, 21181-21186

61. Rouzer, C. A., Tranguch, S., Wang, H., Zhang, H., Dey, S. K., and Marnett, L. J. (2006)

Zymosan-induced glycerylprostaglandin and prostaglandin synthesis in resident peritoneal macrophages: roles of cyclo-oxygenase-1 and -2. *Biochem. J.* **399**, 91-99

62. Mitchener, M. M., Hermanson, D. J., Shockley, E. M., Brown, H. A., Lindsley, C. W., Reese, J., Rouzer, C. A., Lopez, C. F., and Marnett, L. J. (2015) Competition and allostery govern substrate selectivity of cyclooxygenase-2. *Proc. Natl. Acad. Sci. U. S. A.* **112**, 12366-12371

63. Vila, A., Rosengarth, A., Piomelli, D., Cravatt, B., and Marnett, L. J. (2007) Hydrolysis of prostaglandin glycerol esters by the endocannabinoid-hydrolyzing enzymes, monoacylglycerol lipase and fatty acid amide hydrolase. *Biochemistry* **46**, 9578-9585

64. Xie, S., Borazjani, A., Hatfield, M. J., Edwards, C. C., Potter, P. M., and Ross, M. K. (2010) Inactivation of lipid glyceryl ester metabolism in human THP1 monocytes/macrophages by activated organophosphorus insecticides: role of carboxylesterases 1 and 2. *Chem. Res. Toxicol.* **23**, 1890-1904

65. Wang, R., Borazjani, A., Matthews, A. T., Mangum, L. C., Edelmann, M. J., and Ross, M. K. (2013) Identification of palmitoyl protein thioesterase 1 in human THP1 monocytes and macrophages and characterization of unique biochemical activities for this enzyme. *Biochemistry* **52**, 7559-7574

66. Manna, J. D., Wepy, J. A., Hsu, K., Chang, J. W., Cravatt, B. F., and Marnett, L. J. (2014) Identification of the Major Prostaglandin Glycerol Ester Hydrolase in Human Cancer Cells. *J. Biol. Chem.* **289**, 33741-33753

67. Laitinen, T., Navia-Paldanius, D., Rytilahti, R., Marjamaa, J. J., Karizkova, J., Parkkari, T., Pantsar, T., Poso, A., Laitinen, J. T., and Savinainen, J. R. (2014) Mutation of Cys242 of human monoacylglycerol lipase disrupts balanced hydrolysis of 1- and 2-

monoacylglycerols and selectively impairs inhibitor potency. *Mol. Pharmacol.* **85**, 510-519

68. Savinainen, J. R., Kansanen, E., Pantsar, T., Navia-Paldanius, D., Parkkari, T., Lehtonen, M., Laitinen, T., Nevalainen, T., Poso, A., Levonen, A. L., and Laitinen, J. T. (2014) Robust Hydrolysis of Prostaglandin Glycerol Esters by Human Monoacylglycerol Lipase (MAGL). *Mol. Pharmacol.* **86**, 522-535

69. Xie, S., Borazjani, A., Hatfield, M. J., Edwards, C. C., Potter, P. M., and Ross, M. K. (2010) Inactivation of lipid glyceryl ester metabolism in human THP1 monocytes/macrophages by activated organophosphorus insecticides: role of carboxylesterases 1 and 2. *Chem. Res. Toxicol.* **23**, 1890-1904

70. Ross, M. K., Borazjani, A., Wang, R., Crow, J. A., and Xie, S. (2012) Examination of the carboxylesterase phenotype in human liver. *Arch. Biochem. Biophys.* **522**, 44-56

71. Quiroga, A. D., and Lehner, R. (2011) Role of endoplasmic reticulum neutral lipid hydrolases. *Trends in endocrinology and metabolism: TEM* **22**, 218-225

72. Ghosh, S. (2000) Cholesteryl ester hydrolase in human monocyte/macrophage: cloning, sequencing, and expression of full-length cDNA. *Physiol. Genomics* **2**, 1-8

73. Lu, J. Y., and Hofmann, S. L. (2006) Thematic review series: lipid posttranslational modifications. Lysosomal metabolism of lipid-modified proteins. *J. Lipid Res.* **47**, 1352-1357

74. Lu, J. Y., and Hofmann, S. L. (2006) Inefficient cleavage of palmitoyl-protein thioesterase (PPT) substrates by aminothiols: implications for treatment of infantile neuronal ceroid lipofuscinosis. *J. Inherited Metab. Dis.* **29**, 119-126

75. Crow, J. A., Bittles, V., Herring, K. L., Borazjani, A., Potter, P. M., and Ross, M. K.

(2012) Inhibition of recombinant human carboxylesterase 1 and 2 and monoacylglycerol lipase by chlorpyrifos oxon, paraoxon and methyl paraoxon. *Toxicol. Appl. Pharmacol.* **258**, 145-150

76. Nomura, D. K., Lombardi, D. P., Chang, J. W., Niessen, S., Ward, A. M., Long, J. Z., Hoover, H. H., and Cravatt, B. F. (2011) Monoacylglycerol lipase exerts dual control over endocannabinoid and fatty acid pathways to support prostate cancer. *Chem. Biol.* **18**, 846-856

77. Nomura, D. K., Long, J. Z., Niessen, S., Hoover, H. S., Ng, S. W., and Cravatt, B. F. (2010) Monoacylglycerol lipase regulates a fatty acid network that promotes cancer pathogenesis. *Cell* **140**, 49-61

78. Simon, G. M., and Cravatt, B. F. (2010) Activity-based proteomics of enzyme superfamilies: serine hydrolases as a case study. *J. Biol. Chem.* **285**, 11051-11055

79. Long, J. Z., and Cravatt, B. F. (2011) The metabolic serine hydrolases and their functions in mammalian physiology and disease. *Chem. Rev.* **111**, 6022-6063

80. Dodson, G., and Wlodawer, A. (1998) Catalytic triads and their relatives. *Trends Biochem. Sci.* **23**, 347-352

81. Ollis, D. L., Cheah, E., Cygler, M., Dijkstra, B., Frolow, F., Franken, S. M., Harel, M., Remington, S. J., Silman, I., Schrag, J., and et al. (1992) The alpha/beta hydrolase fold. *Protein Eng.* **5**, 197-211

82. Nardini, M., and Dijkstra, B. W. (1999) Alpha/beta hydrolase fold enzymes: the family keeps growing. *Curr. Opin. Struct. Biol.* **9**, 732-737

83. Ordentlich, A., Barak, D., Kronman, C., Ariel, N., Segall, Y., Velan, B., and Shafferman, A. (1998) Functional characteristics of the oxyanion hole in human acetylcholinesterase.

J. Biol. Chem. **273**, 19509-19517

84. Kidd, D., Liu, Y., and Cravatt, B. F. (2001) Profiling serine hydrolase activities in complex proteomes. *Biochemistry* **40**, 4005-4015

85. Holmquist, M. (2000) Alpha/Beta-hydrolase fold enzymes: structures, functions and mechanisms. *Curr Protein Pept Sci* **1**, 209-235

86. Kucerka, N., Nagle, J. F., Sachs, J. N., Feller, S. E., Pencer, J., Jackson, A., and Katsaras, J. (2008) Lipid bilayer structure determined by the simultaneous analysis of neutron and X-ray scattering data. *Biophys. J.* **95**, 2356-2367

87. Nagle, J. F., and Tristram-Nagle, S. (2000) Lipid bilayer structure. *Curr. Opin. Struct. Biol.* **10**, 474-480

88. Nagle, J. F., and Tristram-Nagle, S. (2000) Structure of lipid bilayers. *Biochim. Biophys. Acta* **1469**, 159-195

89. Seddon, A. M., Curnow, P., and Booth, P. J. (2004) Membrane proteins, lipids and detergents: not just a soap opera. *Biochim. Biophys. Acta* **1666**, 105-117

90. Grisshammer, R. (2017) New approaches towards the understanding of integral membrane proteins: A structural perspective on G protein-coupled receptors. *Protein Sci.* **26**, 1493-1504

91. Simons, K., and Ikonen, E. (1997) Functional rafts in cell membranes. *Nature* **387**, 569-572

92. Chiu, M. L. (2012) Introduction to membrane proteins. *Curr Protoc Protein Sci* **Chapter 29**, Unit 29 21

93. Pennington, E. R., Fix, A., Sullivan, E. M., Brown, D. A., Kennedy, A., and Shaikh, S. R. (2017) Distinct membrane properties are differentially influenced by cardiolipin content

and acyl chain composition in biomimetic membranes. *Biochim Biophys Acta Biomembr* **1859**, 257-267

94. Eder, A. E., Munir, S. A., Hobby, C. R., Anderson, D. M., Herndon, J. L., Siv, A. W., Symes, S. J. K., and Giles, D. K. (2017) Exogenous polyunsaturated fatty acids (PUFAs) alter phospholipid composition, membrane permeability, biofilm formation and motility in Acinetobacter baumannii. *Microbiology* **163**, 1626-1636

95. Tse, C. H., Comer, J., Wang, Y., and Chipot, C. (2018) Link between Membrane Composition and Permeability to Drugs. *J. Chem. Theory Comput.* **14**, 2895-2909

96. Seo, P. R., Teksin, Z. S., Kao, J. P., and Polli, J. E. (2006) Lipid composition effect on permeability across PAMPA. *Eur. J. Pharm. Sci.* **29**, 259-268

97. Heden, T. D., Neufer, P. D., and Funai, K. (2016) Looking Beyond Structure: Membrane Phospholipids of Skeletal Muscle Mitochondria. *Trends Endocrinol. Metab.* **27**, 553-562

98. Dawaliby, R., Trubbia, C., Delporte, C., Noyon, C., Ruysschaert, J. M., Van Antwerpen, P., and Govaerts, C. (2016) Phosphatidylethanolamine Is a Key Regulator of Membrane Fluidity in Eukaryotic Cells. *J. Biol. Chem.* **291**, 3658-3667

99. Arisawa, K., Mitsudome, H., Yoshida, K., Sugimoto, S., Ishikawa, T., Fujiwara, Y., and Ichi, I. (2016) Saturated fatty acid in the phospholipid monolayer contributes to the formation of large lipid droplets. *Biochem. Biophys. Res. Commun.* **480**, 641-647

100. Niebylski, C. D., and Salem, N., Jr. (1994) A calorimetric investigation of a series of mixed-chain polyunsaturated phosphatidylcholines: effect of sn-2 chain length and degree of unsaturation. *Biophys. J.* **67**, 2387-2393

101. Huang, C. H. (2001) Mixed-chain phospholipids: structures and chain-melting behavior. *Lipids* **36**, 1077-1097

102. Lands, W. E. (1958) Metabolism of glycerolipides; a comparison of lecithin and triglyceride synthesis. *J. Biol. Chem.* **231**, 883-888

103. Shindou, H., Hishikawa, D., Harayama, T., Yuki, K., and Shimizu, T. (2009) Recent progress on acyl CoA: lysophospholipid acyltransferase research. *J. Lipid Res.* **50 Suppl**, S46-51

104. Yamashita, A., Sugiura, T., and Waku, K. (1997) Acyltransferases and transacylases involved in fatty acid remodeling of phospholipids and metabolism of bioactive lipids in mammalian cells. *J. Biochem.* **122**, 1-16

105. Hishikawa, D., Shindou, H., Kobayashi, S., Nakanishi, H., Taguchi, R., and Shimizu, T. (2008) Discovery of a lysophospholipid acyltransferase family essential for membrane asymmetry and diversity. *Proc. Natl. Acad. Sci. U. S. A.* **105**, 2830-2835

106. Astudillo, A. M., Perez-Chacon, G., Balgoma, D., Gil-de-Gomez, L., Ruiperez, V., Guijas, C., Balboa, M. A., and Balsinde, J. (2011) Influence of cellular arachidonic acid levels on phospholipid remodeling and CoA-independent transacylase activity in human monocytes and U937 cells. *Biochim. Biophys. Acta* **1811**, 97-103

107. Kramer, R. M., Pritzker, C. R., and Deykin, D. (1984) Coenzyme A-mediated arachidonic acid transacylation in human platelets. *J. Biol. Chem.* **259**, 2403-2406

108. Davidsen, J., Mouritsen, O. G., and Jorgensen, K. (2002) Synergistic permeability enhancing effect of lysophospholipids and fatty acids on lipid membranes. *Biochim. Biophys. Acta* **1564**, 256-262

109. Fuller, N., and Rand, R. P. (2001) The influence of lysolipids on the spontaneous curvature and bending elasticity of phospholipid membranes. *Biophys. J.* **81**, 243-254

110. Brown, W. J., Chambers, K., and Doody, A. (2003) Phospholipase A2 (PLA2) enzymes

in membrane trafficking: mediators of membrane shape and function. *Traffic* **4**, 214-221

111. Kooijman, E. E., Chupin, V., de Kruijff, B., and Burger, K. N. (2003) Modulation of membrane curvature by phosphatidic acid and lysophosphatidic acid. *Traffic* **4**, 162-174

112. Lessig, J., Glander, H. J., Schiller, J., Petkovic, M., Paasch, U., and Arnhold, J. (2006) Destabilization of the acrosome results in release of phospholipase A2 from human spermatozoa and subsequent formation of lysophospholipids. *Andrologia* **38**, 69-75

113. Hu, J. S., Li, Y. B., Wang, J. W., Sun, L., and Zhang, G. J. (2007) Mechanism of lysophosphatidylcholine-induced lysosome destabilization. *J. Membr. Biol.* **215**, 27-35

114. Riffo, M. S., and Parraga, M. (1997) Role of phospholipase A2 in mammalian sperm-egg fusion: development of hamster oolemma fusibility by lysophosphatidylcholine. *J. Exp. Zool.* **279**, 81-88

115. Henriksen, J. R., Andresen, T. L., Feldborg, L. N., Duelund, L., and Ipsen, J. H. (2010) Understanding detergent effects on lipid membranes: a model study of lysolipids. *Biophys. J.* **98**, 2199-2205

116. Piomelli, D., Astarita, G., and Rapaka, R. (2007) A neuroscientist's guide to lipidomics. *Nat. Rev. Neurosci.* **8**, 743-754

117. Mills, J. K., and Needham, D. (2005) Lysolipid incorporation in dipalmitoylphosphatidylcholine bilayer membranes enhances the ion permeability and drug release rates at the membrane phase transition. *Biochim. Biophys. Acta* **1716**, 77-96

118. Marsh, D. (1989) Water adsorption isotherms and hydration forces for lysolipids and diacyl phospholipids. *Biophys. J.* **55**, 1093-1100

119. Lundbaek, J. A., and Andersen, O. S. (1994) Lysophospholipids modulate channel function by altering the mechanical properties of lipid bilayers. *J. Gen. Physiol.* **104**, 645-

673

120. Zhelev, D. V. (1998) Material property characteristics for lipid bilayers containing lysolipid. *Biophys. J.* **75**, 321-330

121. Golan, D. E., Brown, C. S., Cianci, C. M., Furlong, S. T., and Caulfield, J. P. (1986) Schistosomula of Schistosoma mansoni use lysophosphatidylcholine to lyse adherent human red blood cells and immobilize red cell membrane components. *J. Cell Biol.* **103**, 819-828

122. Tannaes, T., Bukholm, I. K., and Bukholm, G. (2005) High relative content of lysophospholipids of Helicobacter pylori mediates increased risk for ulcer disease. *FEMS Immunol. Med. Microbiol.* **44**, 17-23

123. Makide, K., Uwamizu, A., Shinjo, Y., Ishiguro, J., Okutani, M., Inoue, A., and Aoki, J. (2014) Novel lysophosphoplipid receptors: their structure and function. *J. Lipid Res.* **55**, 1986-1995

124. Pieringer, R. A., Bonner, H., Jr., and Kunnes, R. S. (1967) Biosynthesis of phosphatidic acid, lysophosphatidic acid, diglyceride, and triglyceride by fatty acyltransferase pathways in Escherichia coli. *J. Biol. Chem.* **242**, 2719-2724

125. Vogt, W. (1963) Pharamacologically active acidic phospholipids and glycolipids. *Biochem. Pharmacol.* **12**, 415-420

126. Tokumura, A., Fukuzawa, K., and Tsukatani, H. (1978) Effects of synthetic and natural lysophosphatidic acids on the arterial blood pressure of different animal species. *Lipids* **13**, 572-574

127. Tokumura, A., Fukuzawa, K., Yamada, S., and Tsukatani, H. (1980) Stimulatory effect of lysophosphatidic acids on uterine smooth muscles of non-pregant rats. *Arch. Int.*

Pharmacodyn. Ther. **245**, 74-83

128. Gerrard, J. M., and Robinson, P. (1989) Identification of the molecular species of lysophosphatidic acid produced when platelets are stimulated by thrombin. *Biochim. Biophys. Acta* **1001**, 282-285

129. Durieux, M. E., Salafranca, M. N., Lynch, K. R., and Moorman, J. R. (1992) Lysophosphatidic acid induces a pertussis toxin-sensitive Ca(2+)-activated Cl- current in Xenopus laevis oocytes. *Am. J. Physiol.* **263**, C896-900

130. Hill, C. S., Oh, S. Y., Schmidt, S. A., Clark, K. J., and Murray, A. W. (1994) Lysophosphatidic acid inhibits gap-junctional communication and stimulates phosphorylation of connexin-43 in WB cells: possible involvement of the mitogen-activated protein kinase cascade. *Biochem. J.* **303 (Pt 2)**, 475-479

131. Choi, J. W., Lee, C. W., and Chun, J. (2008) Biological roles of lysophospholipid receptors revealed by genetic null mice: an update. *Biochim. Biophys. Acta* **1781**, 531-539

132. Velasco, M., O'Sullivan, C., and Sheridan, G. K. (2017) Lysophosphatidic acid receptors (LPARs): Potential targets for the treatment of neuropathic pain. *Neuropharmacology* **113**, 608-617

133. Riaz, A., Huang, Y., and Johansson, S. (2016) G-Protein-Coupled Lysophosphatidic Acid Receptors and Their Regulation of AKT Signaling. *Int. J. Mol. Sci.* **17**, 215

134. Gerrard, J. M., Kindom, S. E., Peterson, D. A., Peller, J., Krantz, K. E., and White, J. G. (1979) Lysophosphatidic acids. Influence on platelet aggregation and intracellular calcium flux. *Am. J. Pathol.* **96**, 423-438

135. Lee, H., Liao, J. J., Graeler, M., Huang, M. C., and Goetzl, E. J. (2002) Lysophospholipid

regulation of mononuclear phagocytes. *Biochim. Biophys. Acta* **1582**, 175-177

136. Tokumura, A., Iimori, M., Nishioka, Y., Kitahara, M., Sakashita, M., and Tanaka, S. (1994) Lysophosphatidic acids induce proliferation of cultured vascular smooth muscle cells from rat aorta. *Am. J. Physiol.* **267**, C204-210

137. Abdel-Latif, A., Heron, P. M., Morris, A. J., and Smyth, S. S. (2015) Lysophospholipids in coronary artery and chronic ischemic heart disease. *Curr. Opin. Lipidol.* **26**, 432-437

138. Camejo, G. (2010) Lysophospholipids: effectors mediating the contribution of dyslipidemia to calcification associated with atherosclerosis. *Atherosclerosis* **211**, 36-37

139. Cherif, H., Argaw, A., Cecyre, B., Bouchard, A., Gagnon, J., Javadi, P., Desgent, S., Mackie, K., and Bouchard, J. F. (2015) Role of GPR55 during Axon Growth and Target Innervation. *eNeuro* **2**

140. Harada, K., Kitaguchi, T., Kamiya, T., Aung, K. H., Nakamura, K., Ohta, K., and Tsuboi, T. (2017) Lysophosphatidylinositol-induced activation of the cation channel TRPV2 triggers glucagon-like peptide-1 secretion in enteroendocrine L cells. *J. Biol. Chem.* **292**, 10855-10864

141. Kawamoto, K., Aoki, J., Tanaka, A., Itakura, A., Hosono, H., Arai, H., Kiso, Y., and Matsuda, H. (2002) Nerve growth factor activates mast cells through the collaborative interaction with lysophosphatidylserine expressed on the membrane surface of activated platelets. *J. Immunol.* **168**, 6412-6419

142. Lee, S. Y., Lee, H. Y., Kim, S. D., Shim, J. W., and Bae, Y. S. (2007) Lysophosphatidylglycerol stimulates chemotactic migration and tube formation in human umbilical vein endothelial cells. *Biochem. Biophys. Res. Commun.* **363**, 490-494

143. Li, Y. F., Li, R. S., Samuel, S. B., Cueto, R., Li, X. Y., Wang, H., and Yang, X. F. (2016)

Lysophospholipids and their G protein-coupled receptors in atherosclerosis. *Front Biosci (Landmark Ed)* **21**, 70-88

144. Lourenssen, S., and Blennerhassett, M. G. (1998) Lysophosphatidylserine potentiates nerve growth factor-induced differentiation of PC12 cells. *Neurosci. Lett.* **248**, 77-80

145. Makide, K., Kitamura, H., Sato, Y., Okutani, M., and Aoki, J. (2009) Emerging lysophospholipid mediators, lysophosphatidylserine, lysophosphatidylthreonine, lysophosphatidylethanolamine and lysophosphatidylglycerol. *Prostaglandins Other Lipid Mediat.* **89**, 135-139

146. Nishina, A., Kimura, H., Sekiguchi, A., Fukumoto, R. H., Nakajima, S., and Furukawa, S. (2006) Lysophosphatidylethanolamine in Grifola frondosa as a neurotrophic activator via activation of MAPK. *J. Lipid Res.* **47**, 1434-1443

147. Yea, K., Kim, J., Lim, S., Kwon, T., Park, H. S., Park, K. S., Suh, P. G., and Ryu, S. H. (2009) Lysophosphatidylserine regulates blood glucose by enhancing glucose transport in myotubes and adipocytes. *Biochem. Biophys. Res. Commun.* **378**, 783-788

148. Zhang, Y., Zhang, J. D., Zhu, M. Q., Zhang, M., Xu, Y. J., Cui, L., and Dhalla, N. S. (2017) Effect of lysophosphatidylglycerol on intracellular free Ca(2+) concentration in A10 vascular smooth muscle cells. *Can. J. Physiol. Pharmacol.* **95**, 1283-1288

149. Huang, Y. H., Schafer-Elinder, L., Wu, R., Claesson, H. E., and Frostegard, J. (1999) Lysophosphatidylcholine (LPC) induces proinflammatory cytokines by a platelet-activating factor (PAF) receptor-dependent mechanism. *Clin. Exp. Immunol.* **116**, 326-331

150. Nishi, E., Kume, N., Ueno, Y., Ochi, H., Moriwaki, H., and Kita, T. (1998) Lysophosphatidylcholine enhances cytokine-induced interferon gamma expression in

human T lymphocytes. *Circ. Res.* **83**, 508-515

151. Paoletti, L., Domizi, P., Marcucci, H., Montaner, A., Krapf, D., Salvador, G., and Banchio, C. (2016) Lysophosphatidylcholine Drives Neuroblast Cell Fate. *Mol. Neurobiol.* **53**, 6316-6331

152. Quan, H., Hur, Y. H., Xin, C., Kim, J. M., Choi, J. I., Kim, M. Y., and Bae, H. B. (2016) Stearoyl lysophosphatidylcholine enhances the phagocytic ability of macrophages through the AMP-activated protein kinase/p38 mitogen activated protein kinase pathway. *Int. Immunopharmacol.* **39**, 328-334

153. Khan, S. Y., McLaughlin, N. J., Kelher, M. R., Eckels, P., Gamboni-Robertson, F., Banerjee, A., and Silliman, C. C. (2010) Lysophosphatidylcholines activate G2A inducing G(alphai)(-)(1)-/G(alphaq/)(1)(1)- Ca(2)(+) flux, G(betagamma)-Hck activation and clathrin/beta-arrestin-1/GRK6 recruitment in PMNs. *Biochem. J.* **432**, 35-45

154. Taylor, L. A., Arends, J., Hodina, A. K., Unger, C., and Massing, U. (2007) Plasma lyso-phosphatidylcholine concentration is decreased in cancer patients with weight loss and activated inflammatory status. *Lipids Health Dis.* **6**, 17

155. Hong, C. W., Kim, T. K., Ham, H. Y., Nam, J. S., Kim, Y. H., Zheng, H., Pang, B., Min, T. K., Jung, J. S., Lee, S. N., Cho, H. J., Kim, E. J., Hong, I. H., Kang, T. C., Lee, J., Oh, S. B., Jung, S. J., Kim, S. J., and Song, D. K. (2010) Lysophosphatidylcholine increases neutrophil bactericidal activity by enhancement of azurophil granule-phagosome fusion via glycine.GlyR alpha 2/TRPM2/p38 MAPK signaling. *J. Immunol.* **184**, 4401-4413

156. Matsumoto, T., Kobayashi, T., and Kamata, K. (2007) Role of lysophosphatidylcholine (LPC) in atherosclerosis. *Curr. Med. Chem.* **14**, 3209-3220

157. Jo, S. H., Kim, S. D., Kim, J. M., Lee, H. Y., Lee, S. Y., Shim, J. W., Yun, J., Im, D. S.,

and Bae, Y. S. (2008) Lysophosphatidylglycerol stimulates chemotactic migration in human natural killer cells. *Biochem. Biophys. Res. Commun.* **372**, 147-151

158. Anavi-Goffer, S., Baillie, G., Irving, A. J., Gertsch, J., Greig, I. R., Pertwee, R. G., and Ross, R. A. (2012) Modulation of L-alpha-lysophosphatidylinositol/GPR55 mitogen-activated protein kinase (MAPK) signaling by cannabinoids. *J. Biol. Chem.* **287**, 91-104

159. Wepy, J. A., Galligan, J. J., Kingsley, P. J., Xu, S., Goodman, M. C., Tallman, K. A., Rouzer, C. A., and Marnett, L. J. (2018) Lysophospholipases Cooperate to Mediate Lipid Homeostasis and Lysophospholipid Signaling. *J. Lipid Res.*

160. Chamberlain, L. H., and Shipston, M. J. (2015) The physiology of protein S-acylation. *Physiol. Rev.* **95**, 341-376

161. Resh, M. D. (2016) Fatty acylation of proteins: The long and the short of it. *Prog. Lipid Res.* **63**, 120-131

162. Lanyon-Hogg, T., Faronato, M., Serwa, R. A., and Tate, E. W. (2017) Dynamic Protein Acylation: New Substrates, Mechanisms, and Drug Targets. *Trends Biochem. Sci.* **42**, 566-581

163. Daniotti, J. L., Pedro, M. P., and Valdez Taubas, J. (2017) The role of S-acylation in protein trafficking. *Traffic* **18**, 699-710

164. Blanc, M., David, F., Abrami, L., Migliozzi, D., Armand, F., Burgi, J., and van der Goot, F. G. (2015) SwissPalm: Protein Palmitoylation database. *F1000Res* **4**, 261

165. Seo, J., and Lee, K. J. (2004) Post-translational modifications and their biological functions: proteomic analysis and systematic approaches. *J. Biochem. Mol. Biol.* **37**, 35-44

166. Hannoush, R. N. (2015) Synthetic protein lipidation. *Curr. Opin. Chem. Biol.* **28**, 39-46

167. Salaun, C., Greaves, J., and Chamberlain, L. H. (2010) The intracellular dynamic of protein palmitoylation. *J. Cell Biol.* **191**, 1229-1238

168. Aicart-Ramos, C., Valero, R. A., and Rodriguez-Crespo, I. (2011) Protein palmitoylation and subcellular trafficking. *Biochim. Biophys. Acta* **1808**, 2981-2994

169. Gottlieb, C. D., and Linder, M. E. (2017) Structure and function of DHHC protein S-acyltransferases. *Biochem. Soc. Trans.* **45**, 923-928

170. Ohno, Y., Kihara, A., Sano, T., and Igarashi, Y. (2006) Intracellular localization and tissue-specific distribution of human and yeast DHHC cysteine-rich domain-containing proteins. *Biochim. Biophys. Acta* **1761**, 474-483

171. Gottlieb, C. D., Zhang, S., and Linder, M. E. (2015) The Cysteine-rich Domain of the DHHC3 Palmitoyltransferase Is Palmitoylated and Contains Tightly Bound Zinc. *J. Biol. Chem.* **290**, 29259-29269

172. Zeidman, R., Jackson, C. S., and Magee, A. I. (2009) Protein acyl thioesterases (Review). *Mol. Membr. Biol.* **26**, 32-41

173. Longo, E., Santis, E. D., Hussain, R., van der Walle, C. F., Casas-Finet, J., Uddin, S., Santos, A. D., and Siligardi, G. (2014) The effect of palmitoylation on the conformation and physical stability of a model peptide hormone. *Int. J. Pharm.* **472**, 156-164

174. Misra, C., Restituito, S., Ferreira, J., Rameau, G. A., Fu, J., and Ziff, E. B. (2010) Regulation of synaptic structure and function by palmitoylated AMPA receptor binding protein. *Mol. Cell. Neurosci.* **43**, 341-352

175. Ni, J., Qu, L., Yang, H., Wang, M., and Huang, Y. (2006) Palmitoylation and its effect on the GTPase-activating activity and conformation of RGS2. *Int. J. Biochem. Cell Biol.* **38**, 2209-2218

176. Probst, W. C., Snyder, L. A., Schuster, D. I., Brosius, J., and Sealfon, S. C. (1992) Sequence alignment of the G-protein coupled receptor superfamily. *DNA Cell Biol.* **11**, 1-20

177. Qanbar, R., and Bouvier, M. (2003) Role of palmitoylation/depalmitoylation reactions in G-protein-coupled receptor function. *Pharmacol. Ther.* **97**, 1-33

178. Wieland, T., and Mittmann, C. (2003) Regulators of G-protein signalling: multifunctional proteins with impact on signalling in the cardiovascular system. *Pharmacol. Ther.* **97**, 95-115

179. Salazar, N. C., Chen, J., and Rockman, H. A. (2007) Cardiac GPCRs: GPCR signaling in healthy and failing hearts. *Biochim. Biophys. Acta* **1768**, 1006-1018

180. Lundstrom, K. (2009) An overview on GPCRs and drug discovery: structure-based drug design and structural biology on GPCRs. *Methods Mol. Biol.* **552**, 51-66

181. Huang, K., and El-Husseini, A. (2005) Modulation of neuronal protein trafficking and function by palmitoylation. *Curr. Opin. Neurobiol.* **15**, 527-535

182. Kang, R., Wan, J., Arstikaitis, P., Takahashi, H., Huang, K., Bailey, A. O., Thompson, J. X., Roth, A. F., Drisdel, R. C., Mastro, R., Green, W. N., Yates, J. R., 3rd, Davis, N. G., and El-Husseini, A. (2008) Neural palmitoyl-proteomics reveals dynamic synaptic palmitoylation. *Nature* **456**, 904-909

183. Davda, D., and Martin, B. R. (2014) Acyl protein thioesterase inhibitors as probes of dynamic S-palmitoylation. *Medchemcomm* **5**, 268-276

184. Hernandez, J. L., Majmudar, J. D., and Martin, B. R. (2013) Profiling and inhibiting reversible palmitoylation. *Curr. Opin. Chem. Biol.* **17**, 20-26

185. Lin, D. T., and Conibear, E. (2015) ABHD17 proteins are novel protein depalmitoylases

that regulate N-Ras palmitate turnover and subcellular localization. *Elife* **4**, e11306

186. Kong, E., Peng, S., Chandra, G., Sarkar, C., Zhang, Z., Bagh, M. B., and Mukherjee, A. B. (2013) Dynamic palmitoylation links cytosol-membrane shuttling of acyl-protein thioesterase-1 and acyl-protein thioesterase-2 with that of proto-oncogene H-ras product and growth-associated protein-43. *J. Biol. Chem.* **288**, 9112-9125

187. Tomatis, V. M., Trenchi, A., Gomez, G. A., and Daniotti, J. L. (2010) Acyl-protein thioesterase 2 catalyzes the deacylation of peripheral membrane-associated GAP-43. *PLoS One* **5**, e15045

188. Yeh, D. C., Duncan, J. A., Yamashita, S., and Michel, T. (1999) Depalmitoylation of endothelial nitric-oxide synthase by acyl-protein thioesterase 1 is potentiated by Ca(2+)-calmodulin. *J. Biol. Chem.* **274**, 33148-33154

189. Duncan, J. A., and Gilman, A. G. (1998) A cytoplasmic acyl-protein thioesterase that removes palmitate from G protein alpha subunits and p21(RAS). *J. Biol. Chem.* **273**, 15830-15837

190. Rusch, M., Zimmermann, T. J., Burger, M., Dekker, F. J., Gormer, K., Triola, G., Brockmeyer, A., Janning, P., Bottcher, T., Sieber, S. A., Vetter, I. R., Hedberg, C., and Waldmann, H. (2011) Identification of acyl protein thioesterases 1 and 2 as the cellular targets of the Ras-signaling modulators palmostatin B and M. *Angew. Chem. Int. Ed. Engl.* **50**, 9838-9842

191. Walker, J. M., and Huang, S. M. (2002) Cannabinoid analgesia. *Pharmacol. Ther.* **95**, 127-135

192. Pertwee, R. G. (2001) Cannabinoid receptors and pain. *Prog. Neurobiol.* **63**, 569-611

193. Valenzano, K. J., Tafesse, L., Lee, G., Harrison, J. E., Boulet, J. M., Gottshall, S. L.,

Mark, L., Pearson, M. S., Miller, W., Shan, S., Rabadi, L., Rotshteyn, Y., Chaffer, S. M., Turchin, P. I., Elsemore, D. A., Toth, M., Koetzner, L., and Whiteside, G. T. (2005) Pharmacological and pharmacokinetic characterization of the cannabinoid receptor 2 agonist, GW405833, utilizing rodent models of acute and chronic pain, anxiety, ataxia and catalepsy. *Neuropharmacology* **48**, 658-672

194. Whiteside, G. T., Gottshall, S. L., Boulet, J. M., Chaffer, S. M., Harrison, J. E., Pearson, M. S., Turchin, P. I., Mark, L., Garrison, A. E., and Valenzano, K. J. (2005) A role for cannabinoid receptors, but not endogenous opioids, in the antinociceptive activity of the CB2-selective agonist, GW405833. *Eur. J. Pharmacol.* **528**, 65-72

195. Di Marzo, V., Bisogno, T., and De Petrocellis, L. (2007) Endocannabinoids and related compounds: walking back and forth between plant natural products and animal physiology. *Chem. Biol.* **14**, 741-756

196. Kogan, N. M., and Mechoulam, R. (2006) The chemistry of endocannabinoids. *J. Endocrinol. Invest.* **29**, 3-14

197. Kathuria, S., Gaetani, S., Fegley, D., Valino, F., Duranti, A., Tontini, A., Mor, M., Tarzia, G., La Rana, G., Calignano, A., Giustino, A., Tattoli, M., Palmery, M., Cuomo, V., and Piomelli, D. (2003) Modulation of anxiety through blockade of anandamide hydrolysis. *Nat. Med.* **9**, 76-81

198. Natarajan, V., Schmid, P. C., Reddy, P. V., and Schmid, H. H. (1984) Catabolism of N-acylethanolamine phospholipids by dog brain preparations. *J. Neurochem.* **42**, 1613-1619

199. Schmid, P. C., Zuzarte-Augustin, M. L., and Schmid, H. H. (1985) Properties of rat liver N-acylethanolamine amidohydrolase. *The Journal of biological chemistry* **260**, 14145-14149

200. Maccarrone, M., van der Stelt, M., Rossi, A., Veldink, G. A., Vliegenthart, J. F., and Agro, A. F. (1998) Anandamide hydrolysis by human cells in culture and brain. *The Journal of biological chemistry* **273**, 32332-32339

201. Lichtman, A. H., Hawkins, E. G., Griffin, G., and Cravatt, B. F. (2002) Pharmacological activity of fatty acid amides is regulated, but not mediated, by fatty acid amide hydrolase in vivo. *The Journal of pharmacology and experimental therapeutics* **302**, 73-79

202. Blankman, J. L., Simon, G. M., and Cravatt, B. F. (2007) A comprehensive profile of brain enzymes that hydrolyze the endocannabinoid 2-arachidonoylglycerol. *Chem. Biol.* **14**, 1347-1356

203. Sang, N., Zhang, J., and Chen, C. (2006) PGE2 glycerol ester, a COX-2 oxidative metabolite of 2-arachidonoyl glycerol, modulates inhibitory synaptic transmission in mouse hippocampal neurons. *The Journal of physiology* **572**, 735-745

204. Sang, N., Zhang, J., and Chen, C. (2007) COX-2 oxidative metabolite of endocannabinoid 2-AG enhances excitatory glutamatergic synaptic transmission and induces neurotoxicity. *J. Neurochem.* **102**, 1966-1977

205. Valdeolivas, S., Pazos, M. R., Bisogno, T., Piscitelli, F., Iannotti, F. A., Allara, M., Sagredo, O., Di Marzo, V., and Fernandez-Ruiz, J. (2013) The inhibition of 2-arachidonoyl-glycerol (2-AG) biosynthesis, rather than enhancing striatal damage, protects striatal neurons from malonate-induced death: a potential role of cyclooxygenase-2-dependent metabolism of 2-AG. *Cell Death Dis.* **4**, e862

206. Alhouayek, M., Masquelier, J., Cani, P. D., Lambert, D. M., and Muccioli, G. G. (2013) Implication of the anti-inflammatory bioactive lipid prostaglandin D2-glycerol ester in the control of macrophage activation and inflammation by ABHD6. *Proc. Natl. Acad.*

Sci. U. S. A. **110**, 17558-17563

207. Simon, G. M., and Cravatt, B. F. (2010) Activity-based proteomics of enzyme superfamilies: serine hydrolases as a case study. *The Journal of biological chemistry* **285**, 11051-11055

208. Long, J. Z., and Cravatt, B. F. (2011) The metabolic serine hydrolases and their functions in mammalian physiology and disease. *Chem. Rev.* **111**, 6022-6063

209. Wang, A., and Dennis, E. A. (1999) Mammalian lysophospholipases. *Biochim. Biophys. Acta* **1439**, 1-16

210. Gibson, D. G., Young, L., Chuang, R. Y., Venter, J. C., Hutchison, C. A., 3rd, and Smith, H. O. (2009) Enzymatic assembly of DNA molecules up to several hundred kilobases. *Nat. Methods* **6**, 343-345

211. Studier, F. W. (2005) Protein production by auto-induction in high density shaking cultures. *Protein Expression Purif.* **41**, 207-234

212. Adibekian, A., Martin, B. R., Chang, J. W., Hsu, K. L., Tsuboi, K., Bachovchin, D. A., Speers, A. E., Brown, S. J., Spicer, T., Fernandez-Vega, V., Ferguson, J., Hodder, P. S., Rosen, H., and Cravatt, B. F. (2012) Confirming target engagement for reversible inhibitors in vivo by kinetically tuned activity-based probes. *J. Am. Chem. Soc.* **134**, 10345-10348

213. Di Marzo, V., Bisogno, T., De Petrocellis, L., Melck, D., Orlando, P., Wagner, J. A., and Kunos, G. (1999) Biosynthesis and inactivation of the endocannabinoid 2-arachidonoylglycerol in circulating and tumoral macrophages. *European journal of biochemistry / FEBS* **264**, 258-267

214. Adibekian, A., Martin, B. R., Chang, J. W., Hsu, K. L., Tsuboi, K., Bachovchin, D. A.,

Speers, A. E., Brown, S. J., Spicer, T., Fernandez-Vega, V., Ferguson, J., Hodder, P. S., Rosen, H., and Cravatt, B. F. (2012) Confirming target engagement for reversible inhibitors in vivo by kinetically tuned activity-based probes. *Journal of the American Chemical Society* **134**, 10345-10348

215. Kozak, K. R., Rowlinson, S. W., and Marnett, L. J. (2000) Oxygenation of the endocannabinoid, 2-arachidonylglycerol, to glyceryl prostaglandins by cyclooxygenase-2. *The Journal of biological chemistry* **275**, 33744-33749

216. Navia-Paldanius, D., Savinainen, J. R., and Laitinen, J. T. (2012) Biochemical and pharmacological characterization of human alpha/beta-hydrolase domain containing 6 (ABHD6) and 12 (ABHD12). *J. Lipid Res.* **53**, 2413-2424

217. Long, J. Z., Li, W., Booker, L., Burston, J. J., Kinsey, S. G., Schlosburg, J. E., Pavon, F. J., Serrano, A. M., Selley, D. E., Parsons, L. H., Lichtman, A. H., and Cravatt, B. F. (2009) Selective blockade of 2-arachidonoylglycerol hydrolysis produces cannabinoid behavioral effects. *Nat. Chem. Biol.* **5**, 37-44

218. Garsetti, D. E., Ozgur, L. E., Steiner, M. R., Egan, R. W., and Clark, M. A. (1992) Isolation and characterization of three lysophospholipases from the murine macrophage cell line WEHI 265.1. *Biochim. Biophys. Acta* **1165**, 229-238

219. Sugimoto, H., Hayashi, H., and Yamashita, S. (1996) Purification, cDNA cloning, and regulation of lysophospholipase from rat liver. *J. Biol. Chem.* **271**, 7705-7711

220. Sunaga, H., Sugimoto, H., Nagamachi, Y., and Yamashita, S. (1995) Purification and properties of lysophospholipase isoenzymes from pig gastric mucosa. *Biochem. J.* **308 (Pt 2)**, 551-557

221. Marnett, L. J. (2009) Decoding endocannabinoid signaling. *Nat. Chem. Biol.* **5**, 8-9

222. Vujic, I., Sanlorenzo, M., Esteve-Puig, R., Vujic, M., Kwong, A., Tsumura, A., Murphy, R., Moy, A., Posch, C., Monshi, B., Rappersberger, K., and Ortiz-Urda, S. (2016) Acyl protein thioesterase 1 and 2 (APT-1, APT-2) inhibitors palmostatin B, ML348 and ML349 have different effects on NRAS mutant melanoma cells. *Oncotarget* **7**, 7297-7306

223. Liu, Y., Fisher, D. A., and Storm, D. R. (1993) Analysis of the palmitoylation and membrane targeting domain of neuromodulin (GAP-43) by site-specific mutagenesis. *Biochemistry* **32**, 10714-10719

224. Abdel-Latif, A. A., Smith, J. P., and Akhtar, R. A. (1983) Studies on the mechanism of alteration by propranolol and mepacrine of the metabolism of phosphoinositides and other glycerolipids in the rabbit iris muscle. *Biochem. Pharmacol.* **32**, 3815-3821

225. Berg, V., Rusch, M., Vartak, N., Jungst, C., Schauss, A., Waldmann, H., Hedberg, C., Pallasch, C. P., Bastiaens, P. I., Hallek, M., Wendtner, C. M., and Frenzel, L. P. (2015) miRs-138 and -424 control palmitoylation-dependent CD95-mediated cell death by targeting acyl protein thioesterases 1 and 2 in CLL. *Blood* **125**, 2948-2957

226. Duncan, J. A., and Gilman, A. G. (2002) Characterization of Saccharomyces cerevisiae acyl-protein thioesterase 1, the enzyme responsible for G protein alpha subunit deacylation in vivo. *J. Biol. Chem.* **277**, 31740-31752

227. Rocks, O., Peyker, A., Kahms, M., Verveer, P. J., Koerner, C., Lumbierres, M., Kuhlmann, J., Waldmann, H., Wittinghofer, A., and Bastiaens, P. I. (2005) An acylation cycle regulates localization and activity of palmitoylated Ras isoforms. *Science* **307**, 1746-1752

228. Devedjiev, Y., Dauter, Z., Kuznetsov, S. R., Jones, T. L., and Derewenda, Z. S. (2000)

Crystal structure of the human acyl protein thioesterase I from a single X-ray data set to 1.5 A. *Structure* **8**, 1137-1146

229. Hachey, D. L., Patterson, B. W., Reeds, P. J., and Elsas, L. J. (1991) Isotopic determination of organic keto acid pentafluorobenzyl esters in biological fluids by negative chemical ionization gas chromatography/mass spectrometry. *Anal. Chem.* **63**, 919-923

230. Yao, C. H., Liu, G. Y., Yang, K., Gross, R. W., and Patti, G. J. (2016) Inaccurate quantitation of palmitate in metabolomics and isotope tracer studies due to plastics. *Metabolomics* **12**

231. Chen, R. F. (1967) Removal of fatty acids from serum albumin by charcoal treatment. *J. Biol. Chem.* **242**, 173-181

232. Patterson, B. W., Zhao, G., Elias, N., Hachey, D. L., and Klein, S. (1999) Validation of a new procedure to determine plasma fatty acid concentration and isotopic enrichment. *J. Lipid Res.* **40**, 2118-2124

233. Won, S. J., Davda, D., Labby, K. J., Hwang, S. Y., Pricer, R., Majmudar, J. D., Armacost, K. A., Rodriguez, L. A., Rodriguez, C. L., Chong, F. S., Torossian, K. A., Palakurthi, J., Hur, E. S., Meagher, J. L., Brooks, C. L., 3rd, Stuckey, J. A., and Martin, B. R. (2016) Molecular Mechanism for Isoform-Selective Inhibition of Acyl Protein Thioesterases 1 and 2 (APT1 and APT2). *ACS Chem. Biol.* **11**, 3374-3382

234. Krissinel, E., and Henrick, K. (2004) Secondary-structure matching (SSM), a new tool for fast protein structure alignment in three dimensions. *Acta Crystallogr. D Biol. Crystallogr.* **60**, 2256-2268

235. Lundby, A., Secher, A., Lage, K., Nordsborg, N. B., Dmytriyev, A., Lundby, C., and

Olsen, J. V. (2012) Quantitative maps of protein phosphorylation sites across 14 different rat organs and tissues. *Nat Commun* **3**, 876

236. Valdes-Rives, S. A., and Gonzalez-Arenas, A. (2017) Autotaxin-Lysophosphatidic Acid: From Inflammation to Cancer Development. *Mediators Inflamm.* **2017**, 9173090

237. Drzazga, A., Sowinska, A., Krzeminska, A., Rytczak, P., Koziolkiewicz, M., and Gendaszewska-Darmach, E. (2017) Lysophosphatidylcholine elicits intracellular calcium signaling in a GPR55-dependent manner. *Biochem. Biophys. Res. Commun.* **489**, 242-247

238. D'Souza, K., Paramel, G. V., and Kienesberger, P. C. (2018) Lysophosphatidic Acid Signaling in Obesity and Insulin Resistance. *Nutrients* **10**

239. Lue, H. W., Podolak, J., Kolahi, K., Cheng, L., Rao, S., Garg, D., Xue, C. H., Rantala, J. K., Tyner, J. W., Thornburg, K. L., Martinez-Acevedo, A., Liu, J. J., Amling, C. L., Truillet, C., Louie, S. M., Anderson, K. E., Evans, M. J., O'Donnell, V. B., Nomura, D. K., Drake, J. M., Ritz, A., and Thomas, G. V. (2017) Metabolic reprogramming ensures cancer cell survival despite oncogenic signaling blockade. *Genes Dev.* **31**, 2067-2084

240. Li, P. L., and Gulbins, E. (2018) Bioactive Lipids and Redox Signaling: Molecular Mechanism and Disease Pathogenesis. *Antioxid. Redox Signal.*

241. Tang, X., Wang, X., Zhao, Y. Y., Curtis, J. M., and Brindley, D. N. (2017) Doxycycline attenuates breast cancer related inflammation by decreasing plasma lysophosphatidate concentrations and inhibiting NF-kappaB activation. *Mol. Cancer* **16**, 36

242. Barnes, M. J., and Cyster, J. G. (2018) Lysophosphatidylserine suppression of T-cell activation via GPR174 requires Galphas proteins. *Immunol. Cell Biol.*

243. Callihan, P., Ali, M. W., Salazar, H., Quach, N., Wu, X., Stice, S. L., and Hooks, S. B. (2014) Convergent regulation of neuronal differentiation and Erk and Akt kinases in

human neural progenitor cells by lysophosphatidic acid, sphingosine 1-phosphate, and LIF: specific roles for the LPA1 receptor. *ASN Neuro* **6**

244. Ikeno, Y., Konno, N., Cheon, S. H., Bolchi, A., Ottonello, S., Kitamoto, K., and Arioka, M. (2005) Secretory phospholipases A2 induce neurite outgrowth in PC12 cells through lysophosphatidylcholine generation and activation of G2A receptor. *J. Biol. Chem.* **280**, 28044-28052

245. Zhang, W., and Liu, H. T. (2002) MAPK signal pathways in the regulation of cell proliferation in mammalian cells. *Cell Res.* **12**, 9-18

246. Meloche, S., and Pouyssegur, J. (2007) The ERK1/2 mitogen-activated protein kinase pathway as a master regulator of the G1- to S-phase transition. *Oncogene* **26**, 3227-3239

247. Ge, C., Xiao, G., Jiang, D., and Franceschi, R. T. (2007) Critical role of the extracellular signal-regulated kinase-MAPK pathway in osteoblast differentiation and skeletal development. *J. Cell Biol.* **176**, 709-718

248. Kehat, I., Davis, J., Tiburcy, M., Accornero, F., Saba-El-Leil, M. K., Maillet, M., York, A. J., Lorenz, J. N., Zimmermann, W. H., Meloche, S., and Molkentin, J. D. (2011) Extracellular signal-regulated kinases 1 and 2 regulate the balance between eccentric and concentric cardiac growth. *Circ. Res.* **108**, 176-183

249. Gross, R. W., and Sobel, B. E. (1983) Rabbit myocardial cytosolic lysophospholipase. Purification, characterization, and competitive inhibition by L-palmitoyl carnitine. *J. Biol. Chem.* **258**, 5221-5226

250. Jarvis, A. A., Cain, C., and Dennis, E. A. (1984) Purification and characterization of a lysophospholipase from human amnionic membranes. *J. Biol. Chem.* **259**, 15188-15195

251. Lepage, N., and Roberts, K. D. (1995) Purification of lysophospholipase of human

spermatozoa and its implication in the acrosome reaction. *Biol. Reprod.* **52**, 616-624

252. Ross, B. M., and Kish, S. J. (1994) Characterization of lysophospholipid metabolizing enzymes in human brain. *J. Neurochem.* **63**, 1839-1848

253. Zhang, Y. Y., Deems, R. A., and Dennis, E. A. (1991) Lysophospholipases I and II from P388D1 macrophage-like cell line. *Methods Enzymol.* **197**, 456-468

254. Zhang, Y. Y., and Dennis, E. A. (1988) Purification and characterization of a lysophospholipase from a macrophage-like cell line P388D1. *J. Biol. Chem.* **263**, 9965-9972

255. Siess, W., Zangl, K. J., Essler, M., Bauer, M., Brandl, R., Corrinth, C., Bittman, R., Tigyi, G., and Aepfelbacher, M. (1999) Lysophosphatidic acid mediates the rapid activation of platelets and endothelial cells by mildly oxidized low density lipoprotein and accumulates in human atherosclerotic lesions. *Proc. Natl. Acad. Sci. U. S. A.* **96**, 6931-6936

256. Zhang, C., Baker, D. L., Yasuda, S., Makarova, N., Balazs, L., Johnson, L. R., Marathe, G. K., McIntyre, T. M., Xu, Y., Prestwich, G. D., Byun, H. S., Bittman, R., and Tigyi, G. (2004) Lysophosphatidic acid induces neointima formation through PPARgamma activation. *J. Exp. Med.* **199**, 763-774

257. Wood, P. L. (2012) Lipidomics of Alzheimer's disease: current status. *Alzheimers Res. Ther.* **4**, 5

258. Tsukahara, T., Matsuda, Y., and Haniu, H. (2017) Lysophospholipid-Related Diseases and PPARgamma Signaling Pathway. *Int. J. Mol. Sci.* **18**

259. Hsu, K. L., Tsuboi, K., Adibekian, A., Pugh, H., Masuda, K., and Cravatt, B. F. (2012) DAGLbeta inhibition perturbs a lipid network involved in macrophage inflammatory

responses. *Nat. Chem. Biol.* **8**, 999-1007

260. Hsu, K. L., Tsuboi, K., Chang, J. W., Whitby, L. R., Speers, A. E., Pugh, H., and Cravatt, B. F. (2013) Discovery and optimization of piperidyl-1,2,3-triazole ureas as potent, selective, and in vivo-active inhibitors of alpha/beta-hydrolase domain containing 6 (ABHD6). *J. Med. Chem.* **56**, 8270-8279

261. Ran, F. A., Hsu, P. D., Wright, J., Agarwala, V., Scott, D. A., and Zhang, F. (2013) Genome engineering using the CRISPR-Cas9 system. *Nat. Protoc.* **8**, 2281-2308

262. Galligan, J. J., Kingsley, P. J., Wauchope, O. R., Mitchener, M. M., Camarillo, J. M., Wepy, J. A., Harris, P. S., Fritz, K. S., and Marnett, L. J. (2017) Quantitative Analysis and Discovery of Lysine and Arginine Modifications. *Anal. Chem.* **89**, 1299-1306

263. Zhao, Z., and Xu, Y. (2010) An extremely simple method for extraction of lysophospholipids and phospholipids from blood samples. *J. Lipid Res.* **51**, 652-659

264. Okudaira, M., Inoue, A., Shuto, A., Nakanaga, K., Kano, K., Makide, K., Saigusa, D., Tomioka, Y., and Aoki, J. (2014) Separation and quantification of 2-acyl-1-lysophospholipids and 1-acyl-2-lysophospholipids in biological samples by LC-MS/MS. *J. Lipid Res.* **55**, 2178-2192

265. Aaltonen, N., Laitinen, J. T., and Lehtonen, M. (2010) Quantification of lysophosphatidic acids in rat brain tissue by liquid chromatography-electrospray tandem mass spectrometry. *J. Chromatogr. B Analyt. Technol. Biomed. Life Sci.* **878**, 1145-1152

266. Zeng, M., and Zhou, J. N. (2008) Roles of autophagy and mTOR signaling in neuronal differentiation of mouse neuroblastoma cells. *Cell. Signal.* **20**, 659-665

267. Anghileri, E., Marconi, S., Pignatelli, A., Cifelli, P., Galie, M., Sbarbati, A., Krampera, M., Belluzzi, O., and Bonetti, B. (2008) Neuronal differentiation potential of human

adipose-derived mesenchymal stem cells. *Stem Cells Dev* **17**, 909-916

268. Palmer, T. D., Takahashi, J., and Gage, F. H. (1997) The adult rat hippocampus contains primordial neural stem cells. *Mol. Cell. Neurosci.* **8**, 389-404

269. Kim, B., Leventhal, P. S., Saltiel, A. R., and Feldman, E. L. (1997) Insulin-like growth factor-I-mediated neurite outgrowth in vitro requires mitogen-activated protein kinase activation. *J. Biol. Chem.* **272**, 21268-21273

270. Riboni, L., Prinetti, A., Bassi, R., Caminiti, A., and Tettamanti, G. (1995) A mediator role of ceramide in the regulation of neuroblastoma Neuro2a cell differentiation. *J. Biol. Chem.* **270**, 26868-26875

271. Algarni, A. S., Hargreaves, A. J., and Dickenson, J. M. (2018) Activation of transglutaminase 2 by nerve growth factor in differentiating neuroblastoma cells: A role in cell survival and neurite outgrowth. *Eur. J. Pharmacol.* **820**, 113-129

272. Sindi, R. A., Harris, W., Arnott, G., Flaskos, J., Lloyd Mills, C., and Hargreaves, A. J. (2016) Chlorpyrifos- and chlorpyrifos oxon-induced neurite retraction in pre-differentiated N2a cells is associated with transient hyperphosphorylation of neurofilament heavy chain and ERK 1/2. *Toxicol. Appl. Pharmacol.* **308**, 20-31

273. Rardin, M. J., Newman, J. C., Held, J. M., Cusack, M. P., Sorensen, D. J., Li, B., Schilling, B., Mooney, S. D., Kahn, C. R., Verdin, E., and Gibson, B. W. (2013) Label-free quantitative proteomics of the lysine acetylome in mitochondria identifies substrates of SIRT3 in metabolic pathways. *Proc. Natl. Acad. Sci. U. S. A.* **110**, 6601-6606

274. Beck, M. W., Kathayat, R. S., Cham, C. M., Chang, E. B., and Dickinson, B. C. (2017) Michael addition-based probes for ratiometric fluorescence imaging of protein S-depalmitoylases in live cells and tissues. *Chem. Sci.* **8**, 7588-7592

275. Martin, B. R., Wang, C., Adibekian, A., Tully, S. E., and Cravatt, B. F. (2012) Global profiling of dynamic protein palmitoylation. *Nat. Methods* **9**, 84-89

276. Jia, L., Chisari, M., Maktabi, M. H., Sobieski, C., Zhou, H., Konopko, A. M., Martin, B. R., Mennerick, S. J., and Blumer, K. J. (2014) A mechanism regulating G protein-coupled receptor signaling that requires cycles of protein palmitoylation and depalmitoylation. *J. Biol. Chem.* **289**, 6249-6257

277. Tulodziecka, K., Czeredys, M., and Nalecz, K. A. (2013) Palmitoylcarnitine affects localization of growth associated protein GAP-43 in plasma membrane subdomains and its interaction with Galpha(o) in neuroblastoma NB-2a cells. *Neurochem. Res.* **38**, 519-529

278. Fukata, Y., and Fukata, M. (2010) Protein palmitoylation in neuronal development and synaptic plasticity. *Nat. Rev. Neurosci.* **11**, 161-175

279. Hannoush, R. N., and Sun, J. (2010) The chemical toolbox for monitoring protein fatty acylation and prenylation. *Nat. Chem. Biol.* **6**, 498-506

280. Aderem, A. (1995) The MARCKS family of protein kinase-C substrates. *Biochem. Soc. Trans.* **23**, 587-591

281. Resh, M. D. (1999) Fatty acylation of proteins: new insights into membrane targeting of myristoylated and palmitoylated proteins. *Biochim. Biophys. Acta* **1451**, 1-16

282. Modica, G., Skorobogata, O., Sauvageau, E., Vissa, A., Yip, C. M., Kim, P. K., Wurtele, H., and Lefrancois, S. (2017) Rab7 palmitoylation is required for efficient endosome-to-TGN trafficking. *J. Cell Sci.* **130**, 2579-2590

283. Martin, B. R., Wang, C., Adibekian, A., Tully, S. E., and Cravatt, B. F. (2011) Global profiling of dynamic protein palmitoylation. *Nat. Methods* **9**, 84-89

284. Duncan, J. A., and Gilman, A. G. (1998) A cytoplasmic acyl-protein thioesterase that removes palmitate from G protein alpha subunits and p21(RAS). *The Journal of biological chemistry* **273**, 15830-15837